Studies on Chromic Behaviours and Structures of *syn*-[**PtM**] Complexes with a Dimer-of-dimer Motif

（複核二量体構造に基づく *syn*-[**PtM**]型錯体の
クロミック挙動の解明と構造化学的研究）

Graduate School of Science, Hokkaido University

Tadashi Ohba

Contents

Chapter 1

General Introduction

1-1 Introduction -2-

1-2 Vapochomism -2-

1-3 Metal-metal interactions in no metal bond -7-

1-4 Hetero metal complexes -10-

1-5 Platinum(II) dinuclear complex -12-

1-6 Purpose of this thesis -14-

1-7 Outlines of the thesis -14-

1-8 References -16-

Chapter 2

Vapour and mechanically induced chromic behaviour of platinum complexes with a dimer-of-dimer motif and the effects of hetero metal ions

2-1 Introduction -20-

2-2 Experimental -21-

2-2-1 Materials and synthesis -21-

2-2-2 Physical Measurements -22-

2-2-3 X-ray diffraction measurements and structure analyses -23-

2-3Results and Discussions -25-

2-3-1 Regioselective Syntheses of Heterodinuclear Complexes -25-

2-3-2 Crystal Structures -26-

2-3-3Vapochromic Behaviour -34-

2-3-4 Structral Transformation by Vapour -38-

2-3-4 Mechanochromic Behaviour -44-

2-4 Conclusion -46-

2-5 References -47-

Chapter 3

Vapochromic behaviour of platinum(II)-copper(II) hetero dinuclear complexes with a dimer-of-dimer motif having guest-absorption sites

3-1 Introduction -50-

3-2 Experimental -51-

3-2-1 Materials and synthesis -51-

3-2-2 X-ray diffraction measurements and structure analyses -52-

3-2-3 Other physical measurements -53-

3-3Results and Discussions -54-

3-3-1 Syntheses -54-

3-3-2 Crystal Structures -54-

3-3-3 The absorption/ desorption behaviour of *syn*-[**PtCu-G**] -61-

3-4 Conclusion -68-

3-5 References -69-

Chapter 4

Effects of counter anions on dimer-of-dimer structures of platinum(II)-copper(II) hetero dinuclear complexes

4-1 Introduction -72-

4-2 Experimental -73-

4-2-1 Materials and synthesis -73-

4-2-2 X-ray diffraction measurements and structure analyses -73-

4-3Results and Discussions -76-

4-3-1 Syntheses -76-

4-3-2 Crystal Structures -76-

4-3-3 EPR spectra -82-

4-4 Conclution -83-

4-5 References -84-

Chapter 5

Syntheses and Structures of platinum(II)-cobalt(II) and platinum(II)-nickel(II) hetero dinuclear complexes

5-1 Introduction -86-

5-2 Experimental -87-

5-2-1 Materials and synthesis -87-

5-2-2 X-ray diffraction measurements and structure analyses -87-

5-3 Results and Discussions -89-

5-3-1 Regioselective Syntheses of Heterodinuclear Complexes -89-

5-3-2 Crystal Structures -89-

5-4 Conclution -98-

5-5 References -99-

Chapter 6

General conclusion

6-1 General conclusion -102-

6-2 Acknowledgement -104-

Chapter 1

General introduction

1-1. Introduction

Gases comprise the atmosphere of the Earth and also occupy a central position of science, and technology. Oxygen is of course of great importance for living things and nitrogen is utilized in the production ammonia. On the other hand, the air pollution has been a serious problem again by the rapid development of industry in countries such as China and India. The so-called NO_x gases and SO_x emitted from the power plants, are toxic and contribute the damaging in biological tissues. The volatile organic compounds (VOCs) are also harmful at workspace. Formaldehyde, for instance, is known as the substrate of sick-house syndrome. There is, thus, an important issue of finding suitable sensors for harmful gases. Although electrochemical sensors such as semiconducting sensors are widely used, some problems remain; for example, the sensitivity, selectivity. Consequently, the detection of gases by simple means requiring only a low-cost technology is an attractive research target.

1-2. Vapochromism

As discussed above, the development of reversible chemical sensors has drawn increasing attention[1]. Vapochromism, which is reversible color change in solid state induced by solvent vapour or gases, is one of the promising phenomena to detect volatile organic compounds (VOCs). The term of ‘’vapochromism’’ was introduced in a complex salts $[Pt(CN\text{-}ph\text{-}R)_4][Pd(CN)_4]$ (Scheme 1-1, **1**) by Nagal *et al.* in 1988 and the major development came after 1990s. One of the early studies about vapochromism was reported by Gillard in 1974[2]. They found that the platinum complex $[Pt(CN)_2(bpy)]$ (**2**) exhibited the dimorphism, yellow and red forms, and these forms were reversibly converted by moisture or heating. Similarly, $[Pt(CN)_2(phen)]$ (**3**) showed the color change from yellow to red. Such chromotoropic behaviour is naked-eye perceivable. Therefore, vapochromic compounds have possible applications for chemical sensors.

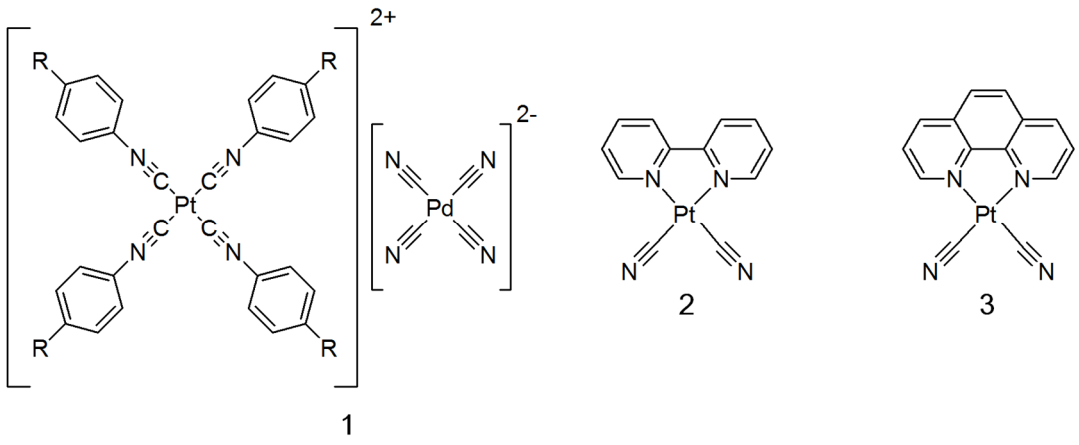

Scheme 1-1. $[Pt(CN\text{-}ph\text{-}R)_4]$ $[Pd(NC)_4]$ complex salts **1** and $[Pt(\alpha\text{-dimine})\ (CN)_2]$ complexes

For the construction of sensor systems toward VOCs, vapochromic compounds have suitable potential properties. The key factors of sensors are as follows: sensitivity, selectivity, responsive speed, responsive repeatability, and responsive range toward vapour. Vapochromism is based on chemical sorption of vapours into materials, and thus responsive properties toward VOCs and repeatability are high. Wong and co-workers studied about the sensitivity of vapochromic platinum complex. The platinum complex bearing σ-alkynyl group [Pt(*t*Bu$_2$bpy)(C≡C-Ar)$_2$] (**4**) (*t*Bu$_2$bpy = 4,4'-bis-*tert*-butyl-2,2'-bipyridine, Ar = 4-pyridyl)[3] exhibited vapochromism and enhanced emission intensity in the presence of chlorocarbon vapours (Figure 1-1). The detection limit of CH_2Cl_2 is 25 ppm and sensitivity is enough for detection in industrial environment (discharge regulation of CH_2Cl_2; 50 ppm). Kato reported that the platinum complex [Pt(CN)$_2$(dcbpy)][4] (**5**) (dcbpy = 4,4'-dicarboxy-2,2'-bipyridine) showed the colorful polymorphs depending on various vapours (Scheme 4). Moreover, the emission energy in these chromic behaviour under various vapours correlates to dielectric constant and then high selectivity was obtained (Figure 1-2). Mann discussed the time scale of vapochromism about Pt(II)-Pt(II) double salt [Pt(CN-ph-$C_{10}H_{21})_4$][Pt(CN)$_4$] (**6**)[5]. In neat **6**, the absorption maximum is at 746 nm, and on exposure of chloroform vapour, the absorption maximum was shifted to 837 nm. The time scale of this vapochromic response is ~500 ms ($t_{1/2}$). Throughout these properties, vapochromic compounds were promising materials for sensors.

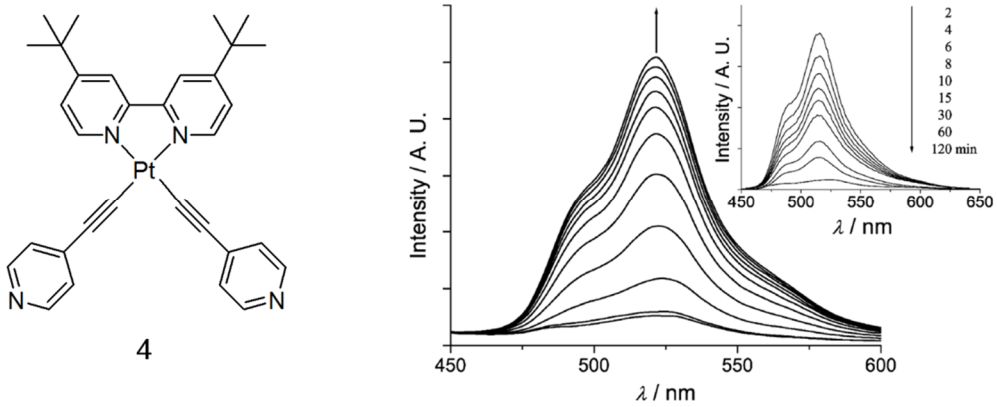

Figure 1-1. [Pt(α-dimine) (C≡C-Ar)$_2$] complex **4** and the enhancement of emission intensity in the presence of N_2 saturated with CH_2Cl_2 vapour in solid state. Inset; the attenuation of emission intensity by removal of CH_2Cl_2

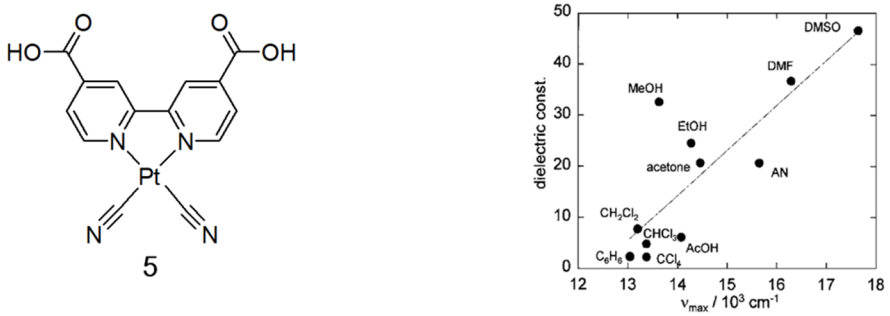

Figure 1-2. [Pt(CN)$_2$ (dcbpy)] complex **5** and relationships of **5** between electronic constant of solvent and emission energy observed in solvent vapour

A number of vapochromic compounds were reported in two decades, and they can be classified into three groups on the basis of the mechanism of their vapochromic behavior; type (i), the change of intermolecular interaction between chromophores, type(ii), the change of coordination envioronment of chromophore associated with coordination of vapour molecules, and type (iii), host-guest interactions.

Most of vapochromic compounds were included in type I which includes Pt(II), Au(I), and Ag(I) complexes as well as organic molecules with widely delocalized π electrons as chromophores

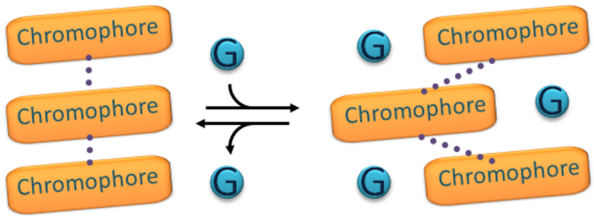

Scheme 1-2 Schematic image of mechanism of type I

In solid state, these chromophores are packed so as to close to neighbouring chromophore. When more or less subtle structural changes in crystal packing were induced by sorption/desorption of solvent molecules, the intermolecular interactions such as metallophilic interaction, π-π stacking, hydrogen bonding and C-H-π interaction, were perturbed to lead drastic color[6] and luminescence changes[7]. Eisenberg reported, for example, that gold(I) complex [Au(S$_2$CN)(C$_5$H$_{11}$)$_2$][7a] (**7**) response aprotic molecules such as acetone and acetonitrile vapour to switch color and luminescence properties. Microcrystalline **7**·solvent exhibits orange colour and intense luminescence. When **7**·solvent was dried in air or in vacuum, the solid becomes colourless and nonemissive. From X-ray diffraction analyses,

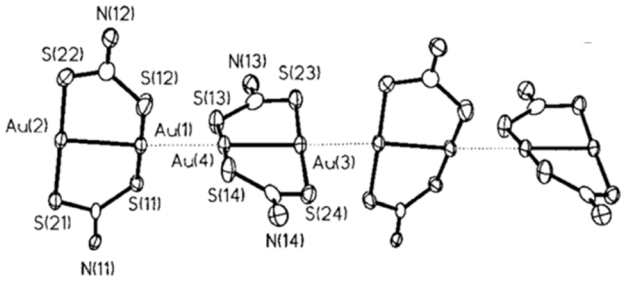

Figure 1-3. Linear chain of **7**·DMSO. The pentyl moieties have been omitted for clarify

solvent-included **7**·DMSO and **7**·CH_3CN form infinite chains of Au atoms with intermolecular Au···Au distances 2.7690(7) Å for **7**·DMSO and 3.024(1) Å for **7**·CH_3CN. In contrast, the structure of solvent-free **7** was clarified that the dimers exist as monomeric, non-interacting molecular units with shortest intermolecular Au···Au distance 8.135 Å. Therefore these results demonstrate the formation of linear Au···Au chain play an important role for orange emission.

In type II compounds, direct coordination of guest molecule to chromophore affect the electronic state of chromophore. Chromopohres, therefore, include guest-binding metal ions such as cobalt (II)[8], copper (II)[9], and platinum (II)[10] ions. One example in this type is reported by Koten et al[10]. Platinum complex with pincer ligand (**8**) have square-planar coordination mode of platinum (II) ion, and the **8** was higly selective for gaseous SO_2 to afford **8**·SO_2. It is noteworthy that in these processes the crystallinity is maintained. The X-ray structure analyses revealed that **8**·SO_2 was coordinated by SO_2 on axial site of platinum(II) ion and coordination mode of platinum ion was square-pyramidal. In characteristic, the colour of **8** was colourless while that of **8**·SO_2 was orange, and hence, the transformation was easy to detect for naked eye.

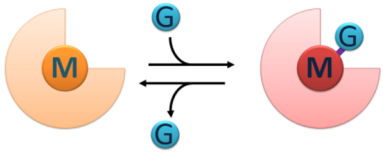

Scheme 1-3 Schematic image of mechanism of type II

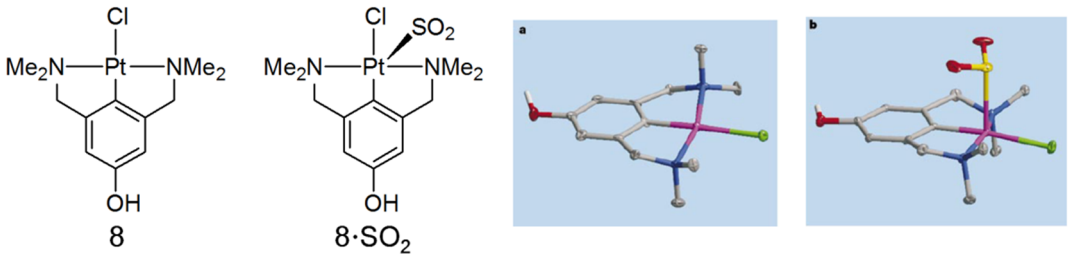

Figure 1-4. Platinum complexes **8** and **8**·SO_2, and the structures of a) **8** and b) **8** ·SO_2 from X-ray structure analyses.

The vapochromism of type III is based on the weak interaction between chromophore and guest such as π-π stacking, hydrogen bonding and C-H-π interaction, but these weak perturbation is enough to change the electronic state to give the color change[11]. Utilizing the Lewis acidity of the solvents, Shinozaki demonstrated vapochromism utilizing ruthenium(II) complex (**9**)[11a]. Ruthenium complex **9** has two

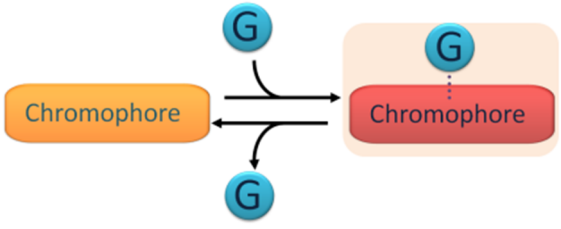

Scheme 1-4 Schematic image of mechanism of type III

cyanide ligands and exhibits the metal-to-ligand charge transfer (MLCT) emission. In solution, the MLCT emission energy depends on solvent and shows good correlation to the acceptor number (AN) as an index of the Lewis acidity of the solvents. From FTIR spectrum, the C≡N stretching absorption band also shows correlation to AN. These results suggest the local interaction of the C≡N ligand with solvent molecules enhance the Ru-C≡N back-donation, and hence the CN^- ligands stabilize the dπ(Ru) orbital to exhibit the solvatochromic behavior of the MLCT emission. In characteristic, these chromic behaviours are also observed in solid state as similar manner of in solution, and this suggests a capability for detection of organic molecules in solid state.

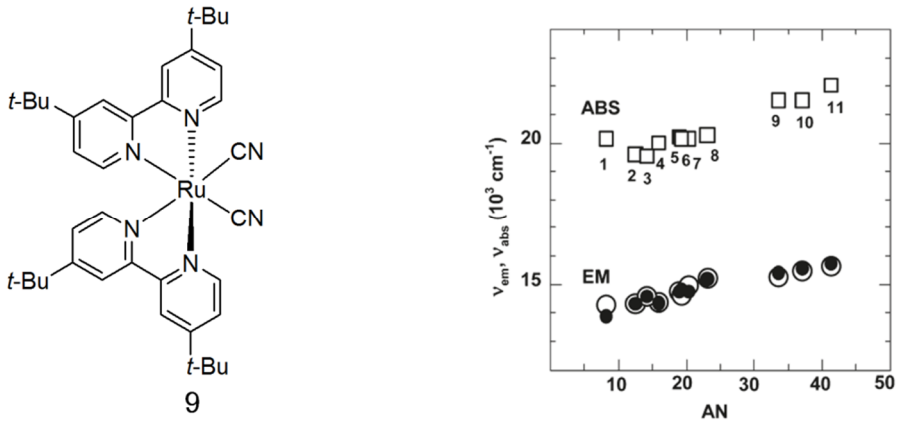

Figure 1-5. Ruthenium complex **9** and relationships of **9** between acceptor number of solvent and emission energy observed in solvent vapour

Although it is undoubtedly that vapochromic compounds are promising materials for sensors, there has been some problems for construction of sensor systems. One problem is the relationships between structure and properties. It is difficult, therefore, to "engineer" vapochromic compounds. Moreover, the crystal structure was constructed by the sum of interactions including electrostatic interaction, hydrogen bonding, C-H-π interaction and van der Waals attraction, it is even difficult to optimize the responsive ability toward VOCs. For example, the subtle substitution change leads to different responsive ability toward VOCs. Chen and co-workers reported a series of platinum complexes with phenylacetylide ligands(**9**, **10**, **11**)[12]. These complexes differ only by the fluoro substituents at the phenylacetylide ligands, and these complexes are isostructural each other in CH_2Cl_2 included crystal. In spite of these similarities of these complexes, the vapochromic behaviours of these complexes are substantially different each other; that is, **9** does not exhibit vapochromism; while **10** and **11** response toward $CHCl_3$ selectively for **10** and various vapours including halocarbone and aprotic solvents for **11**. Therefore, many efforts are invested for research on vapochromism.

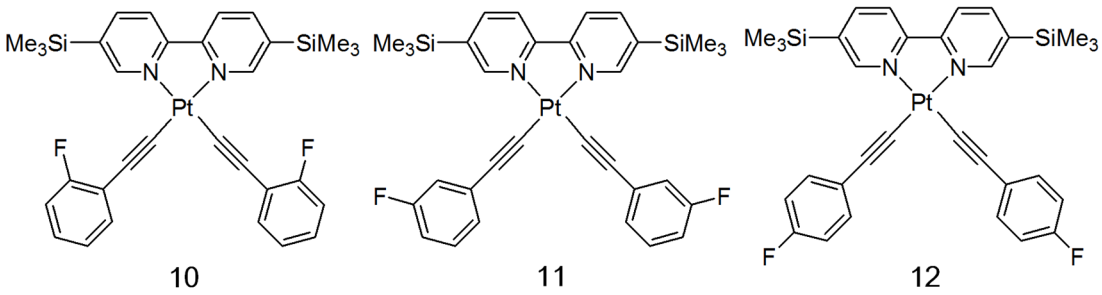

Scheme 1-5 [Pt(α-dimine) (C≡C-Ar)$_2$] complex **10**, **11**, **12**

1-3 Metal-metal interactions in no metal-metal bonds

Assembled metal complexes, which consist of two or more metal ions located nearby each other, have attracted much attraction in inorganic and biochemistry[13]. The metal ions interact each other in assembled systems, and then the characteristic properties such as catalysis, coloration properties and electric conductivity are exhibited. In particular, the dinuclear complexes are widely studied as a minimal unit of assembled complexes[14]. They can be classified into two groups on the basis of the structural properties; the complexes including multiple metal-metal bonds and no bonds between two metal ions.

The dinuclear complexes with multiple metal-metal bonds are firstly synthesized as homonuclear complex [$Cr_2(\mu$-$O_2CMe)_4(H_2O)_2$] in 19th century, and the existence of multiple metal-metal bond was reported in 1954[15]. The complexes of this type show wide bond order[16] associates with the oxidation state and characteristic reactivity[17], and thus, tremendous efforts have been invested.

On the other hand, dinuclear complexes with no metal-metal bonds provide a variety of chromotropic chemistry based on the metal-metal interaction. These complexes included the metal ions with closed shell electron configurations such as copper(I), silver(I), gold(I), palladium(II) and platinum(II) ions. In the case of platinum(II) complexes with the d^8 electron configuration, for example, platinum (II) complexes generally adopt square-planar structure. When platinum complexes are stacked with the Pt···Pt distances shorter than the sum of van der

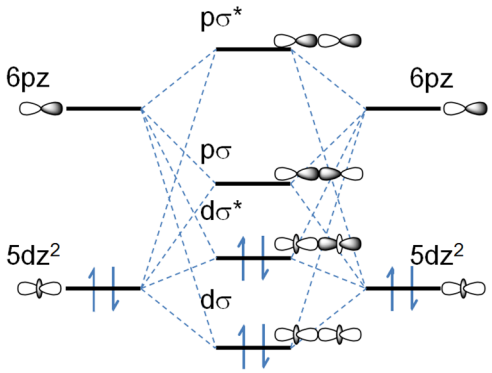

Scheme 1-6. Molecular orbital scheme for metal-metal interactions of d^8 ions

Waals radius (~ 3.5 Å), the platinum dz^2 orbitals split into the bonding dσ and the anti-bonding dσ* orbitals, the platinum dσ* orbital becomes HOMO. Due to s, p_z, and z^2 configuration mixing, the resulting the bond order becomes slightly greater than zero in these formally non-bonded platinum dimers. The platinum dinuclear complex $[Pt_2(P_2O_5H_2)_4]^{4-}$ is one of the most studied complex[18], which four pyrophosphito ligand linked two platinum(II) ions (Figure1-6a). From the X-ray structure analysis of the potassium salt, the intramolecular Pt···Pt distance is 2.925(1) Å. The $[Pt_2(P_2O_5H_2)_4]^{4-}$ exhibits absorption bands at 367 and 435 nm that are attributable to the singlet and triplet dσ* to pσ transition, respectively, and exhibit phosphorescence at 514 nm from the triplet exited state (Figure1-6b). In characteristic, the triplet excited state of the dinuclar platinum complex has a Pt-Pt bond character and exhibits redox reactions and atom transfer reactions based on this character. Therefore, the dinuclear complexes with no metal-metal bond have attracted a great deal of interests.

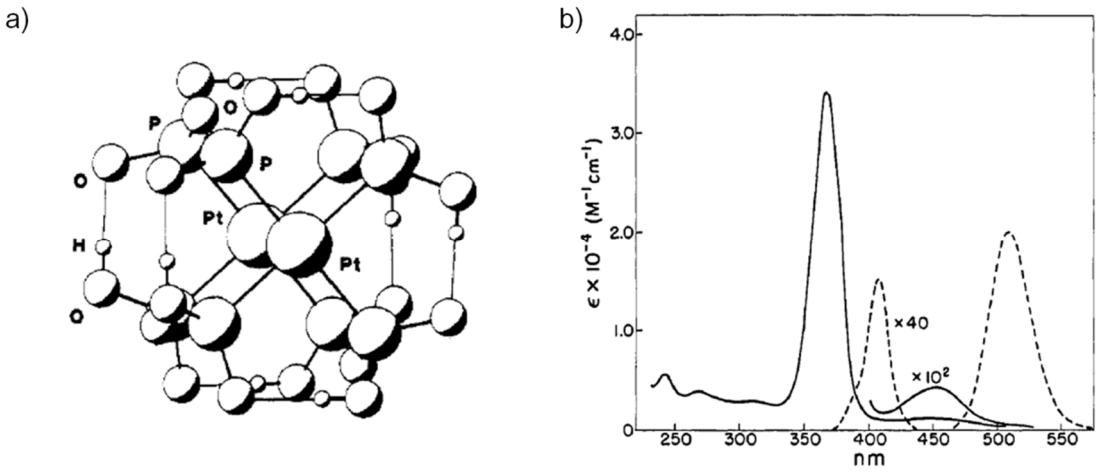

Figure 1-6. a) The structure of $[Pt_2(P_2O_5H_2)_4]^{4-}$ and b) absorption (solid line; ε scale) and emission spectra (dashed line) in aqueous solution at 25ºC.

The dinuclear complexes with no metal-metal bonds have wide design performance compared to those with multiple metal-metal bond. In Mo(III) quadruplly bridged dinuclear complexes with multiple metal-metal bond, for example, the intramolecular Mo-Mo bond distances are almost constant based on the strong Mo-Mo quadruple bond (2.037 – 2.141 Å) [14d]. In contrast, platinum(II) quadruplly bridged dinuclear complexes, the intramolecular Pt···Pt distances range from 2.680(2) Å to 2.9801(2) Å[14d]. This is due to no metal-metal bond between metal ions, however, these intramolecular bond deviations affects chemical properties such as redox and photophysical properties. Bear and co-workers reported the redox properties of two structural isomers of palladium bimetallic complex with molecular formula $Pd_2(dpb)_4$ (dpb = *N*,*N*-diphenyl-benzamidate) (Scheme 1-7)[19]. One isomer contains two palladium ions bridged by two dpb ligand with an additional dpb ion chelated to each of palladium ion ($[Pd(dpb)_2(\mu\text{-}dpb)_2]$). In another isomer, all dpb ligands

bridged two palladium ion ([Pd(μ-dpb)$_4$]). The intramolecular distances of two isomers are 2.900(1) Å for [Pd(dpb)$_2$(μ-dpb)$_2$] and 2.5769(1) Å for [Pd(μ-dpb)$_4$], respectively. The one-electron oxidation potential for [Pd(dpb)$_2$(μ-dpb)$_2$] is 370 mV higher than that for [Pd (μ-dpb)$_4$] (E_{ox} =1.02 V for [Pd(dpb)$_2$(μ-dpb)$_2$]; E_{ox} =0.65 V for [Pd(μ-dpb)$_4$]). This is consistent with differenc of intramolecular Pd···Pd distances to affect the stability of one-electron oxidation spices. The photophysical properties of dinulecar platinum complexes were discussed by Thompson and co-workers reported[20]. The complexes have the general formula *C^N*Pt(*i-pz'*)2Pt*C^N* (where *C^N*) 2-(2,4-difluorophenyl) pyridyl, *pz'*) *i*-pyrazolate (**13a**), 3,5-dimethylpyrazolate (**13b**), 3-methyl-5-*tert*-butylpyrazolate (**13c**), and 3,5-bis(*tert*-butyl)pyrazolate (**13d**)), which consist of different pyrazolate bridging ligands. Substitution of bulky groups on the 3-, 5- position of pyrazolate bridging ligands forces to the two *C^N*Pt moieties close together. From the X-ray structure analyses, the intramolecular Pt···Pt distances of platinum complexes **13a**, **13b**, **13c** and **13d** revealed 3.3763(7), 3.1914(4), 3.0457(7), 2.8343(6) Å, respectively. In platinum complexes with widely delocalized π-orbital ligands, when metal-metal interaction is effective, platinum complexes exhibit characteristic metal-metal-to-ligand charge transfer (MMLCT). In solution at 77 K, these complexes exhibit phosphorescence at 458, 468, 515, 570 nm, respectively. From the vibronic features of the emission line shapes of **13a** and **13b** at 77 K, the origin of emission state is similar to mononuclear complexes. In contrast, complex **13c** and **13d** with short intramolecular Pt···Pt distances exhibit the broad featureless emission, consistant with an assignment to a triplet metal-metal-to-ligand charge transfer (^{3}MMLCT) transition. The shortening of Pt···Pt distances, thus, affect the photophysical properties. Utilizing these design performances of dinuclear metal complexes with no metal-metal bond, therefore, dinuclear complexes with d^8-d^8, d^{10}-d^{10} and d^8-d^{10} electron configuration were studied.

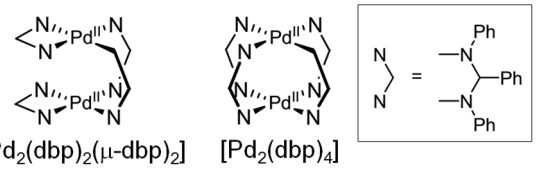

Scheme 1-7. Schematic molecular motif of Pd(II) dinuclear complexes.

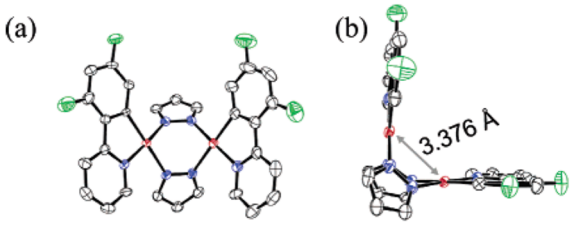

Figure 1-7. Molecular structure of **13**

The presence of metal-metal interactions can be determined by various measurements. Most common technique for identifying metal-metal interactions is metal···metal distances obtained by crystallographic studies. In other cases, the UV-vis and fluorescence spectroscopic studies reveal occupation of a σ-type molecular orbitals and NMR studies indicate change in metal valence electron density. Raman spectroscopy also can reveal directly the metal-metal interactions.

1-4 Hetero metal complexes

As discussed above, dinuclear complexes were expected to exhibit characteristic properties. In particular, hetero metal complexes containing two or more different metal ions arranged linearly, provide an opportunity to add different characters of metal ions such as coordination modes, coordination numbers, electronic configurations, and redox properties. Therefore, a number of hetero metal complexes were reported.

One of the early studies was reported by Lippert and co-workers[21]. They utilized nucleobase derivatives such as 1-methylcytocinate, 1-methyltyminate, 1-methyluracinate ion as bridging ligands, and they obtained not only hetero dinuclear complexes but also trinuclear complexes. Scheme A depicted molecular motifs of hetero metal complexes and synthetic schemes. In many cases, hetero metal complexes were synthesized by stepwise introduction of metal ions (Pd^{2+}, Cu^{2+}, Zn^{2+}, Ag^{+}, and Hg^{2+} ions) into platinum(II) precursor complexes. There are two groups of heterometal complexes with different of bridging modes; *cis*- and *trans*-coordination modes. In the heterometal complexes of the *cis*-coordination mode, the intramolecular metal···metal distances are from 2.760 to 2.929 Å. On the other hand, the metal···metal distances in the *trans* bridging mode range from 2.511 to 2.855 Å, shorter than those of the *cis*-bridging mode.

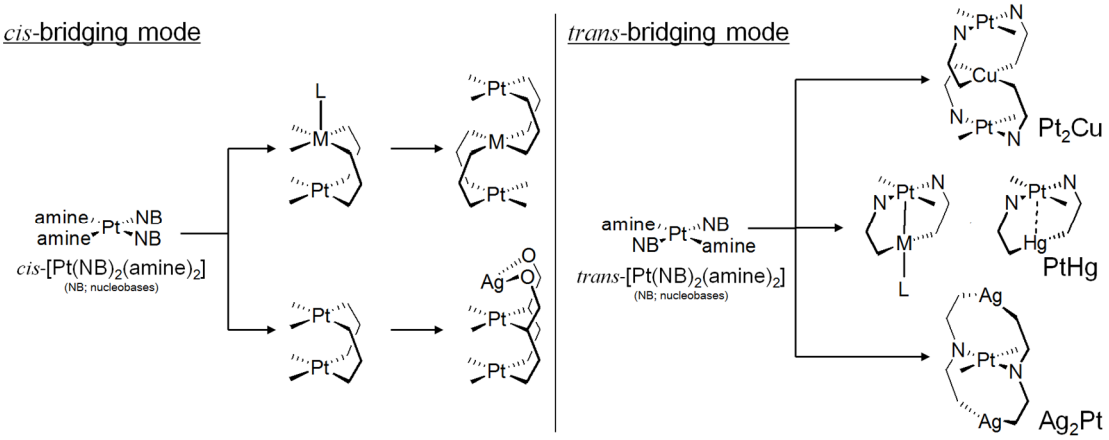

Scheme 1-8. Schematic scheme of heterometal complexes reported by Lippert and co-workers.

In the view point of molecular strings, hetero metal complexes were expected to exhibit the long range electronic interaction via metal-metal interactions in metal ions[22),23)]. Peng and co-workers reported that a trinuclear heterometal complex $[Co_2PdCl_2(dpa)_4]$ (dpa = bis(2-pyridyl)amide) exhibited the metal··metal interaction involving zero-field splitting superimposed on strong exchange coupling between two high-spin Co^{II} ion separated by a diamagnetic Pd center[22a)]. In other cases, Doerrer and co-workers reported the antiferromagnetic coupling in $[PtM(SAc)_4(L)]$ (M = Co^{II}, Ni^{II}; L = OH_2, 3-nitropyridine(3-NO_2py))[23b)]. In these complexes, the Pt ion and the metal ion were fixed by four thioacetate bridging ligands with the

intramolecular Pt-M distances 2.5682(9)-2.6347(4) Å. In the crystal structure, characteristically, two [PtM(SAc)$_4$(L)] molecules are arranged so that the Pt ions are close each other, forming the *dimer-of-dimer* structure. Antiferromagnetic coupling between 3d metal ions in the solid state through no covalent metal-metal interactions were observed in these complexes. It is noteworthy that in each case the spin coupling between terminal metal ions occurs via metal ion located between the terminal metals by metal-metal interactions.

The different coordination number and oxidation states of hetero metal ions in dinuclear complexes could utilize the reactions[24]. The photoreaction in Pt-Au hetero dinuclear complex was studied by Nocera and co-workers[4a]. The heterodinuclear complex [$Pt^{III}Au^{II}$(dppm)$_2$PhCl$_3$](PF$_6$) (1) was synthesized by the oxidation from [$Pt^{II}Au^{I}$(dppm)$_2$PhCl](PF$_6$) (2). From the X-ray analyses, the coordination mode of Pt(III) and Au(II) ions in **14** are hexagonal and square-planar, respectively, while those of Pt(II) and Au(I) ions in **15** are linear and square-planar, respectively (Figure 1-8a), b)). In acetonitrile solution, **14** exhibits two absorption bands at 278 and 391 nm that are attributable to the dσ to dσ* and dπ* to dσ* transition, respectively. The light irradiation at 405 nm of **14** in acetonitrile solution with 2,3-dimethyl-1,3-butadiene induce the extinction of absorption band at 391 nm and emerge of new absorption band at 338 nm. The final absorption spectrum is co-incident wih that independently **15**, and therefore **14** exhibits the metal-halide bond photoactivation (Figure 1-8)

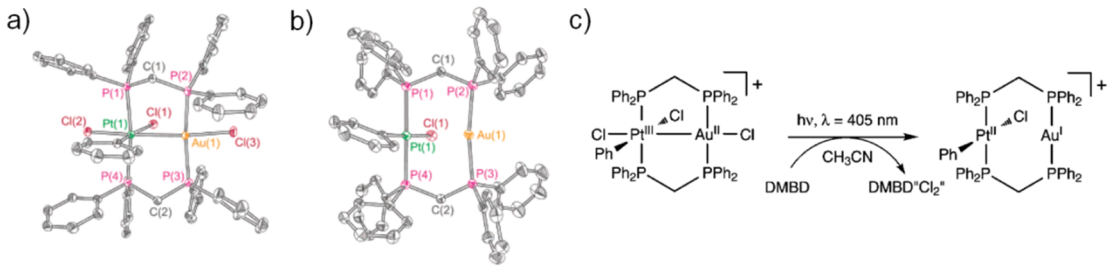

Figure 1-8. Structure of a) **14** and b) **15,** and c) photoreaction of **14**

1-5 Platinum(II) dinuclear complex

A number of vapochromic complexes have been reported to date. However, the vapochromic dinuclear complexes are not so many. In particular, the compounds which exhibit both intra- and inter- metal-metal interactions are still limited.

Kato and co-workers reported the platinum(II) dinuclear complex *syn*-[$Pt_2(bpy)_2(\mu\text{-pyt})_2](PF_6)_2$ (pyt = 2-pyridine-thiolate; *syn*-[**PtPt**]$(PF_6)_2$, Scheme A)[25]. In *syn*-[**PtPt**], two pyt ligands have N,S-coordinating atoms, providing different coordination environment and two platinum(II) ions were bridged by two pyt ligands in *syn*-coordination mode, adopting *head-to-head* orientation. From the X-ray analysis, dark red cryatals of *syn*-[**PtPt**]$(PF_6)_2 \cdot CH_3CN$ obtained by recrystallization from CH_3CN/Et_2O include the acetonitrile molecule, and the intramolecular Pt···Pt distance is 2.997(1) Å, suggesting the intramolecular metal-metal interaction (Figure 1-9). In hexafluorophosphate salt, interestingly, two *syn*-[**PtPt**] form the *dimer-of-dimer* structure so that two platinum(II) ions with S-coordination of pyt ligands arranged to close each other. The intermolecular Pt···Pt distance is 3.3884(1) Å, suggesting metal-metal interaction between two *syn*-[**PtPt**] motifs, and therefore, *syn*-[**PtPt**] exhibit not only intra- but also inter-molecular metal-metal interactions. The emission maximum of dark red crystal is 766 nm, which is attributable to ^{3}MMLCT transition reflecting the intra- and inter-molecular metal-metal interactions. In characteristic, *syn*-[**PtPt**]$(PF_6)_2$ exhibits drastic colour change and the vapoluminescence behavior. Crystals of the *syn* isomer are initially dark-red in appearance, and appear to become light-red in color upon standing in air for several hours at room temperature The emission maxima shifted from 766 nm to 644 nm, which is attributable to ^{3}MMLCT transition based on the intramolecular Pt···Pt interaction. From IR spectra, the C≡N stretching band corresponding to acetonitrile molecule was disappeared in light-red form, while dark-red form possesses the C≡N stretching band corresponding to acetonitrile. Therefore, the origin of the chromic behaviour was thought to be induced by acetonitrile vapour.

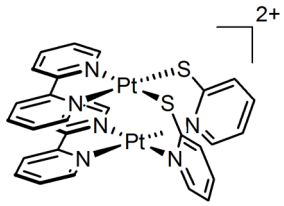

Scheme 1-9. Molecular motif of *syn*-[**PtPt**]

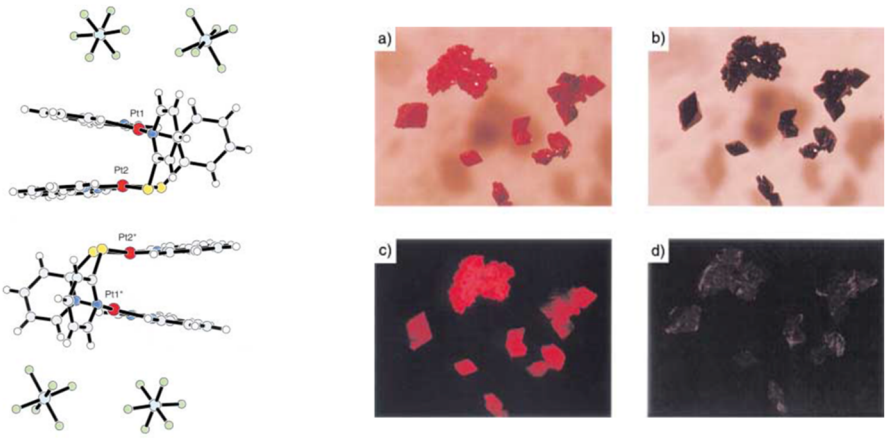

Figure 1-9. Dimer-of-dimer structure of hexafluorophospheta salts of *syn*-[**PtPt**] (left) and photographic images of crystals of the syn isomer, illustrating vapochromic effects(right): a)the light-red (desolvated) form in air and b)the dark-red form after exposure of (a)to acetonitrile vapor. Luminescence images of c)the light-red and d) dark-red forms.

The *syn*-[**PtPt**] has promising characters for sensors, however, some problems are remained. One problem is the simple preparation. In the one-step synthesis of platinum dinuclear complexes by the reaction of [$PtCl_2$(bpy)] and Hpyt (Scheme 1-10), the *syn* and *anti* geometrical isomers were produced as a mixture and the isolation of the *syn* isomer of the minor component was troublesome in this method. Second, the mechanisms of vapochromic behaviours were unclear and needed to elucidate.

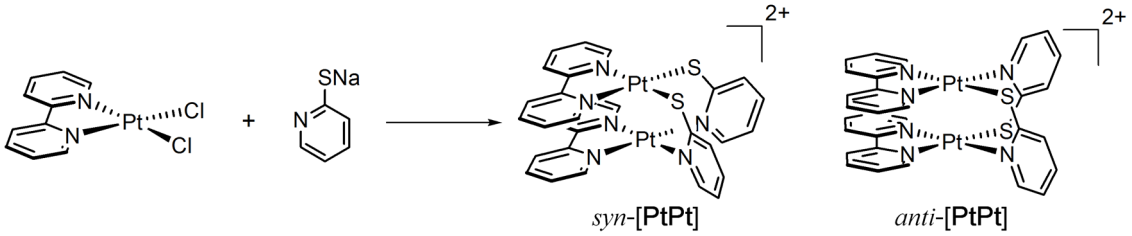

Scheme 1-10. Synthetic scheme of platinum(II) dinuclear complex

1-6 Purpose of the thesis

A number of studies of vapochromic complexes have been reported until now. Although many derivatives were synthesized for modulation of vapochromism by ligand modification such as introduction of substitution groups, it is still difficult to engineer vapochromic behaviour due to the difficulty of the control of assembled structures of their derivatives. On the other hand, the studies of the introduction of hetero metal ions in the same molecular motif were limited in spite of their advantages of small structural influence for molecular motif and the ease of perturbation of electron configurations. In *syn*-[**PtPt**], two platinum(II) ions have different coordination environment by *head-to-head* orientation of two pyt ligands and exhibit the intra- and intermolecular interactions based on the *dimer-of-dimer* structure in crystal state. The structural features of syn-[**PtPt**], therefore, strongly suggest that the molecular framework would be a good candidate for the incorporation of two different metal ions to affect the intra and intermolecular metal-metal interactions.

In this thesis, a series of the hetero metal dinuclear complexes *syn*-[**PtM**] containing heterometal ions and the effects of metal ion to vapochromic behavior were discussed. Firstly, the palladium(II) and gold(III) ions, which have d^8 electron configuration as same as platinum(II) ion were introduced to study the influence toward packing structure by the charge of metal ion and the effect of metal-metal interaction of metal ion. In addition, incorporation of 3d metal ions in *syn*-[**PtM**] motif were investigated for the use of 3d metal ions as an guest binding site to obtain the selectivity toward the vapour.

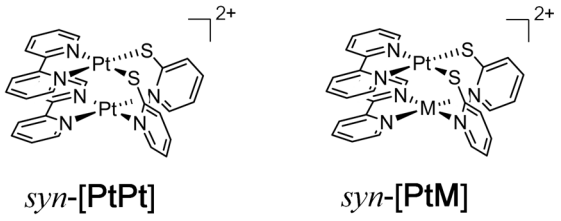

syn-[PtPt] *syn*-[PtM]

Scheme1-11. Schematic motif of *syn*-[**PtM**]

1-7 Outlines of the thsis

This thesis consists of 5 chapters as briefly described below.

In chapter I, the research background and purpose of the thesis are described. As key aspects into the present study, the essence of the chemistry of vapochromism, metal-metal interaction, hetero dinuclear complxes are overviewed

In chapter II, the syntheses, structures and properties of two heterodinuclear metal complexes using d^8 metal ions, *syn*-$[MPt(\mu\text{-pyt})_2(bpy)_2]^{n+}$ (*syn*-[**PtM**]; M = Pd^{2+} (*n* = 2), M = Au^{3+} (*n* = 3)) are described. In order to achieve stereoselective syntheses of hetero metal complexes, the metal ions were introduced in stepwise method utilizing the different affinity (-N and -S atoms) of pyt ligand toward metal ion. *Syn*-[**PtPd**] which was found to be isostructural with *syn*-[**PtPt**] exhibited vaposhcomic behaviour, and the mechanism were discussed in detail as well as *syn*-[**PtPt**].

In chapter III, the sturctures and absorption / desorption behaviors of hexafluorophosphate salts of copper(II)-platinum(II) heterodinuclear complex *syn*-[PtCu(Guest)(μ-pyt)$_2$(bpy)$_2$](PF$_6$)$_2$ (*syn*-[**PtCu-G**]) are described (guest = CH_3CN for *syn*-[**PtCu-CH$_3$CN**]; acetone for *syn*-[**PtCu-acetone**]; MeOH for *syn*-[**PtCu-MeOH**]). The introduction of copper(II) ion into *syn*-[**PtM**] motif provide the *syn*-[**PtCu-G**] motifs including one solvent molecule as additional ligands at the axial site of copper ion. In spite of additional ligands, each complex forms the dimer-of-dimer structure and provide different intermolecular Pt···Pt distances. Absorption / desorption behaviour of *syn*-[**PtCu-G**] were found to be reversible but the chromic shift of each *syn*-[**PtCu-G**] were completely different each other.

In chapter IV, the structures and the effect of counter ion on copper(II)-platinum(II) hetero dinuclear complexes *syn*-[PtCuX(μ-pyt)$_2$(bpy)$_2$]X (*syn*-[**PtCu-X**]) were described (X = Cl-, SCN^-, PF_6^-). The introduction of different counter anions into *syn*-[**PtM**] motif provide the *syn*-[**PtCu-X**] motifs including one of counter anions as additional ligands at the axial site of copper ion. In spite of additional ligands, each complex forms the dimer-of-dimer structure and the donating abilities of counter anions affect the intermolecular Pt···Pt distances, indicating that the intermolecular Pt···Pt interaction affect the axial ligand of counter anion even separated by copper(II) ion.

In chapter V, the structures of 3d metal ion-platinum(II) heterodinuclear which have solvent molecule as axial ligands are described. The stepwise introduction of 3d metal ion into *syn*-[**PtM**] motif afford dimorphism of *syn*-[**PtCo-CH$_3$CN**] and *syn*-[**PtNi-CH$_3$CN**]. In two forms of *syn*-[**PtM-CH$_3$CN**], the structure is similar; that is, coordination of one of acetonitrile molecules in crystal as axial ligand of 3d metal ios and formation of dimer-of-dimer structure. In α-form, the the π-π stackings of bpy ligand with adjacent dimer-of-dimer structure formed, while in β-forms. no π-π stackings of bpy ligand with adjacent dimer-of-dimer structure formed. The intermolecular Pt···Pt distances of α-forms are shorter than that of β-form which does not have π-π stacking of the bpy ligand, suggesting that the intermolecular π-π stacking of bpy ligands with adjacent dimer-of-dimer structure forces the tight packing to shorten the intermolecular Pt···Pt distances.

In chapter VI, general conclusion and future perspectives of the study are summarized.

1-8 References

1) a)A. P. De Silva, D. B. Fox, A. J. M. Huxley, and T. S. Moody, *Coord. Chem. Rev.*, 2000, **205**, 41-57, b) L. E. Kreno, K. L.eong, M. O. K. Farha, M. Allendorf, R. P. V. Duyne, and J. T. Hupp, *Chem. Rev.*, 2012, **112**, 1105-1125.

2) E. Bielli, P. M. Gidney, R. D. Gillard, and B. T. Heaton, *J. Chem. Soc. Dalton Trans.* **1974**, 2133.

3) W. Lu, M. C. Chan, N. Zhu, C.-M. Che, Z. He, and K.-Y. Wong, Chem. Eur. J., 2003, **9**, 6155-6166.

4) M. Kato, Bull. Chem. Soc. Jpn. 2007, **80**, 287-294, M. Kato, S. Kishi, Y. Wakamatsu, Y. Sugi, Y. Osamura, T. Koshiyama, and M. Hasegawa, Chem. Lett., 2005, **34**, 1368-1369.

5) C. A. Daws, C. L. Exstrom, J. R. Sowa, and K. R. Mann, 1997, **9**, 303-368.

6) a) E. Takahashi, H. Takaya, T. Naota, *Chem. Eur. J.*, 2010, **16**, 4793-4802.

7) a)M. A. Mansour, W. B. Connick, R. J. Lachiocotte, H. J. Gysling and R. Eisenberg, *J. Am. Chem. Soc.*, 1998, **120**, 1329-1330.

8) D. Bradshaw, J. E. Warren, M. J. Rosseinsky, *Science*, 2007, **315**, 977-980, J. Lefebvre, J. L. Korčok, M. J. Katz, D. B. Leznoff, *Sensors*, 2012, **12**, 3669-3692.

9) a) C. E. Strasser, V. J. Catalano, *J. Am. Chem. Soc.*, 2010, **132**, 10009-10011, b) J. Lefebvra, R. J. Batchelor, D. B. Lezeoff, *J. Am. Chem. Soc.*, 2004, **126**, 16117-16125.

10) M. Albrecht, M. Lutz, A. L. Spek, G. van Koten, *Nature*, 2000, **406**, 970-974.

11) a) T. Abe, T. Suzuki, K. Shinozaki, *Inorg. Chem.*, **49**, 1794-1800, b) Z. Fei, N. Kocher, C. J. Molurshladt, H. Ihmels, D. Stalke, *Angew. Chem. Int. Ed.*, 2003, **42**, 783-787 c) Z. M. Hudson, C. Sun, K. J. Harris, B. E. G. Lucier, R. W. Schurko, S. Wang, *Inorg. Chem.*, 2011, **50**, 3447-3457, d) C. –S. Lee, R. R. Zhuang, S. Sabiah, J. –C. Wang, W. –S. Hwang, I. J. B. Lin, *Organomet.*, 2011, **30**, 3897-3900, e) C. E. Buss, C. E. Anderson, M. K. Pomije, C. M. Lutz, D. Britton, K. R. Mann, *J. Am. Chem. Soc.*, 1998, **120**, 7783-7790, f) M. A. Rawhdeh-Omary, M. D. Rashdan, S. Dharanipathi, O. Elbjeirami, P. Ramesh, H. V. R. Dias, *Chem. Commun.*, 2011, **47**, 1160-1162, g) T. Abe, K. Shinozaki, *Inorg. Chem.*, 2005, **44**, 849-851, h) Z. Kiu, Z. Bian, J. Bian, Z. Li, D. Nie, C. Huang, *Inorg. Chem.*, 2008, **47**, 8025-8030.

12) J. Ni, Z. Zhang, Y. –H. Wu, L. –Y. Zhang, Z. –N. Chen, *Chem. Eur. J*, 2011, **17**, 1171-1183.

13) a) L. H. Doerrer, Dalton trans., 2010, **39**, 3343-3553, b) I. P. –C. Liu, W. –Z. Wang. S. –M. Peng, Chem. Commun. , 2009,4323-4331.

14) a) D. C. Powers, T. Riter, *Acc. Chem. Res.*, 2012, **45**, 840-850, b) J. P. Collman, R. Boulatoy, Angew. Chem. Int. Ed., 2012, 41, 3948-3961, c) E. Zangando, F. Pichierri, L. Randaccio, B. Lippert, *Coord. Chem. Rev.*, 1996, **156**, 275-332, d) K. Umakoshi, Y. Sasaki, Adv. *Inorg. Chem.*, 1993, 40,187-239, c) H. –C. Chang, K. Mochizuki, S. Kitagawa, *Inorg. Chem.*, 2005, **44**, 3810-3817.

15) B. N. Tiggis, R. L. Martin, *J. Chem. Soc.*, **1956**, 3837-3846.

16) a) M. H. Chisholm, Acc. Chem. Res., 1990, **23**, 419-425, b) U. Radius, F. Breher, *Angew. Chem. Int. Ed.*, 2006, **45**, 3006-3010.

17) M. Nippe, S. M. Goodman, C. G. Fry, J. F. Berry, *J. Am. Chem. Soc.*, 2011, **132**, 2856-2859.

18) D. M. Roundhill, H. B. Gray, C. M. Che, *Acc. Chem. Res.*, 1989, **22**, 55-61.

19) C. –L. Yao, L. –P. He., J. D. Korp, J. L. Bear, *Inorg. Chem.*, 1988, **27**, 4389-4395.

20) B. Ma, J. Li. P. I. Djurovich, M. Yousufuddin, R. Bau, M. E. Thompson, *J. Am. Chem. Soc.*, 2005, **127**, 28-29..

21) a) Ennio Zangrando, Fabio Picherri, Lucio Randaccio, Bernhard Lippert, *Coord. Chem. Rev.*, 1996, **156**, 275-332, b) Jorge, A. R. Navarro, Bernhard Lippert, *Coord. Chem. Rev.*, 1999, **185**, 653-667.

22) a) M.-M. Rohmer, I. P. -C. Liu, J. -C. Lin, M. -J. Chiu, C. -H. Lee, G. -H. Lee, M. Bènard, X. López, S. -M. Peng, *Angew. Chem. Int. Ed.*, 2007, **46**, 3533-3536, b) I. P. -C. Liu, C. -H. Chen, C. -F. Chen, G. -H. Lee, S. -M. Peng, *Chem. Commun.*, **2009**, 577-579, c) I. P. -C. Liu, G. -H. Lee, S. -M. Peng, *Inorg. Chem.*, 2007, **46**, 9602-9608.

23) a) E. W. Dald, F. G. Raddour, S. R. Fiedler, W. A. Hoffert, M. P. Shores, G. T. Yee., J. -P. Djukic, J. W. Bacon, A. L. Rhingold, L. H. Doerrer, *Chem. Sci.*, 2012, **3**, 602-609, b) F. G. Raddour, S. R. Fiedler, M. P. Shores, J. A. Golen, A. L. Rhingold, L. H. Doerrer, *Inorg. Chem.*, ASAP, doi: 10.1021/ic302531t

24) a) T. R. Cook, A. J. Esswein, D. G. Nocera, *J. Am. Chem. Soc.*, 2007, **129**, 10094, b) A. J. Esswein, J. L Dempsey, D. G. Nocera, *Inorg. Chem.*, 2007, **46**, 2362-2364

25) M. Kato, A. Omura, A. Toshikawa, S. Kishi, Y. Sugimoto, *Angew. Chem. Int. Ed.*, 2002, **41**, 3183-3185

Chapter 2

Vapour and mechanically induced chromic behaviour of platinum complexes with a dimer-of-dimer motif and the effects of hetero metal ions

2-1 Intoduction

There has been considerable interest in recent years in the development of vapochromic sensor materials for the detection of volatile organic compounds (VOCs).[1] In particular, assembled platinum(II) complexes with d^8 configurations provide rich chromotropic chemistry on the basis of changes in intermolecular interactions such as π-π, donor-acceptor, and metal-metal interactions induced by the absorption/desorption of vapour molecules.[2] Thus, they are promising materials for naked-eye perceivable chemosensors for small molecules. However, vapochromic systems with clearly elucidated mechanisms are still limited despite the increasing numbers of reported systems, and detailed investigation is necessary to achieve their rational design.

Kato *et al.* previously reported a homometallic dinuclear platinum(II) complex, $[Pt_2(\mu\text{-pyt})_2(bpy)_2]^{2+}$ (pyt = pyridine-2-thiolate, bpy = 2,2′-bipyridine),[3] which has two geometrical isomers, the *syn*- and *anti*-isomers (*syn*-[**PtPt**] and *anti*-[**PtPt**]), corresponding to the case of M = Pt^{2+} in Scheme 1. The hexafluorophosphate salt of *syn*-[**PtPt**] exhibits an interesting vapour-induced colour change between dark-red and light-red on the absorption/desorption of acetonitrile (CH_3CN) molecules.

Concomitantly, a remarkable luminescence switching occurs for the dinuclear complex. The dark-red form (CH_3CN-included form) of the *syn*-isomer crystal adopts a dimer-of-dimer structure, wherein the four Pt ions of two *syn*-[**PtPt**] cations are arranged so as to generate an intermolecular metal–metal interaction (Scheme 2-1). Similar dimer-of-dimer structures are known for mixed-valence platinum complexes (*i.e.* platinum blues).[4] Though there is no chemical bond between intermolecular divalent platinum ions for *syn*-[**PtPt**], the expansion of the electronic metal-metal interactions from the dimer to the dimer-of-dimer structure could lower the energy of the metal-metal-to-ligand charge transfer (MMLCT) transition.[3] Thus, I proposed that the vapochromic behaviour for this system would occur by the change of the Pt···Pt electronic interactions between the dinuclear complexes. To explore the electronic effects of the metal-metal interactions on the vapochromic behaviour, it would be effective to introduce different metal ions into the same dinuclear motif. Fortunately, the structural features of *syn*-[**PtPt**] strongly suggest that the molecular framework would be

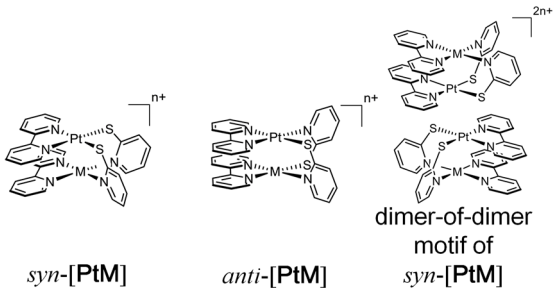

Scheme 2-1. Homo (M = Pt^{2+}) and heterodinuclear motif

a good candidate for the incorporation of two different metal ions because the bridging ligand (pyt) provides two different coordination environments.

In this chapter, newly synthesized two heterodinuclear metal complexes using d^8 metal ions, *syn*-$[MPt(\mu\text{-pyt})_2(bpy)_2]^{n+}$ (*syn*-[**PtM**]; M = Pd^{2+} (*n* = 2), M = Au^{3+} (*n* = 3)), as well as *anti*-$[PdPt(\mu\text{-pyt})_2(bpy)_2]^{2+}$ (*anti*-[**PtPd**]) were discussed. The hexafluorophosphate salt of *syn*-[**PtPd**] exhibited vapochromic behaviour with different colour changes from that of *syn*-[**PtPt**], while *syn*-[**PtAu**] and *anti*-[**PtPd**] did not show any vapochromic behaviour. I also succeeded in the direct observation of the structural transformation induced by the absorption/desorption of vapour molecules for *syn*-[**PtPt**] and *syn*-[**PtPd**] on the basis of X-ray diffraction studies. Herein, the particular mechanism of the vapochromism and the effects of hetero metal ions based on the metal-metal interactions for these dinuclear systems are discussed, considering other findings by UV-vis spectroscopy and thermal analysis.

2-2 Experimental

2-2-1 Materials and synthesis. All starting materials were used as received from commercial sources, and the solvents were used without purification. 2,2′-Bipyridine (bpy), pyridine-2-thiol (Hpyt) and $PdCl_2$ were purchased from Wako. K_2PtCl_4 and $HAuCl_4$ were purchased from Tanaka Holdings. $[PtCl_2(bpy)]$,[5] $[PdCl_2(bpy)]$,[6] $[AuCl_2(bpy)](NO_3)$,[7] $[Pt(pyt)_2(bpy)]$,[8] and *syn*-$[Pt_2(\mu\text{-pyt})_2(bpy)_2](PF_6)_2$[3] were prepared according to methods previously reported.

***Syn*-[PtPd (μ-pyt)$_2$(bpy)$_2$](PF$_6$)$_2$** (*syn*-[**PtPd**]$(PF_6)_2$). To a suspension of $[PdCl_2(bpy)]$ (33.3 mg, 0.1 mmol) in H_2O (6 mL) was added silver nitrate (34.0 mg, 0.2 mmol) in H_2O (4 mL). The reaction mixture was stirred for 2 h in the dark at 60°C, and then filtered to remove silver chloride. The pale yellow filtrate was treated with $[Pt(pyt)_2(bpy)]$ (57.1 mg, 0.1 mmol) in H_2O (2 mL). The resulting red solution was allowed to stir for 30 min and NH_4PF_6 (81.5 mg, 0.5 mmol) in H_2O (2 mL) was added. An orange precipitate was immediately deposited, which was then filtered and dried under reduced pressure. Yield: 103.5 mg (92.1%). Red polyhedral crystals (*syn*-isomer) suitable for X-ray diffraction were obtained as an CH_3CN-solvated form by the diffusion method using Et_2O/ CH_3CN at 4°C. ^{1}H NMR (DMSO-d_6): δ 7.30 (t, 2H), 7.39 (td, 2H), 7.44 (d, 2H), 7.59 (t, 2H), 7.69 (t, 2H), 7.82 (d, 2H), 8.15 (d, 2H), 8.18 (td, 2H), 8.27 (t, 2H), 8.35 (d, 2H), 8.87 (d, 2H), 9.07 (d, 2H). Anal. Calcd. for $C_{30}H_{24}F_{12}N_6P_2PdPtS_2$: C, 32.05; H, 2.15; N, 7.48; S, 5.71. Found: C, 32.00; H, 2.26; N, 7.46; S, 5.87.

***Anti*-[PtPd (μ-pyt)$_2$(bpy)$_2$](PF$_6$)$_2$** (*anti*-[**PtPd**]$(PF_6)_2$). The powder of the *syn*-[**PtPd**] complex (98.3

mg, 87 μmol) was dissolved in CH_3CN (1 mL) and allowed to stand for 1 day at room temperature (RT). After 1 day, a crystal suitable for X-ray diffraction was obtained as an CH_3CN-solvated form by the diffusion method using Et_2O/CH_3CN at RT. Yield: 45.2 mg (46.0%). ^{1}H NMR (DMSO-d_6): δ 7.21–7.35 (m, 4H), 7.55 (d, 1H), 7.46 (t, 4H), 7.77 (t, 1H), 7.90 (t, 1H), 8.38 (d, 2H), 8.74 (d, 2H), 8.83 (d, 2H). Anal. Calcd. for $C_{30}H_{24}F_{12}N_6P_2PdPtS_2$: C, 32.05; H, 2.15; N, 7.48. Found: C, 31.83; H, 2.30; N, 7.47.

***Syn*-[PtAu (μ-pyt)$_2$(bpy)$_2$](PF$_6$)$_3$** (*syn*-[**PtAu**]$(PF_6)_3$). $[AuCl_2(bpy)](NO_3)$ (72.7 mg, 0.15 mmol) was suspended in H_2O (10 mL) and silver nitrate (50.4 mg, 0.3 mmol) in H_2O (5 mL) was added. The reaction mixture was stirred for 3 days in the dark at RT and then filtered to remove silver chloride. The pale yellow filtrate was treated with $[Pt(pyt)_2(bpy)]$ (57.1 mg, 0.1 mmol) in H_2O (2.5 mL). The resulting solution was stirred for 30 min at room temperature. NH_4PF_6 (81.5 mg, 0.5 mmol) in H_2O (2 mL) was added and the resulting red precipitate was filtered. The red filtrate was allowed to stand for ca. 10 days and a red crystalline solid was obtained (yield: 22.6 mg (17%)). Dark red crystals suitable for X-ray diffraction were obtained as an CH_3CN -solvated form via the diffusion of EtOH into a CH_3CN solution of the crude material. ^{1}H NMR (DMSO-d_6) for $[AuPt(pyt)_2(bpy)_2](PF_6)_3$: δ 7.45 (m, 2H), 7.70 (t, 2H), 7.84 (d, 2H), 7.86 (d, 2H), 8.11 (t, 2H), 8.24 (d, 2H), 8.33 (d, 4H), 8.53 (t, 2H), 8.64 (d, 2H), 9.02 (d, 2H), 9.10 (d, 2H). Anal. Calcd. for $C_{30}H_{24}AuF_{18}N_6P_3PtS_2$: C, 26.50; H, 1.78; N, 6.18; S, 4.72. Found: C, 26.38; H. 1.90; N, 5.92; S, 4.67.

2-2-2 Physical measurements

^{1}H NMR spectra were recorded on a JEOL JNM-EX270 FT-NMR system. Elemental analyses were performed by a Micro Corder JM 10 analyser at the Analysis Centre, Hokkaido University. UV–vis spectra in solution were recorded on a Shimadzu MultiSpec-1500 spectrophotometer. UV–vis diffuse reflectance spectra were obtained on a Hitachi U-3000 spectrometer equipped with an integrating sphere apparatus. Thermogravimetry and differential thermal analysis were performed using a Rigaku ThermoEvo TG8120 analyzer.

2-2-3 X-ray diffraction measurements and structure analyses

A summary of the crystallographic data of the single-crystal X-ray diffraction for the *syn*-[**PtPd**], *anti*-[**PtPd**], and *syn*-[**PtAu**] complexes is given in Table 2-1. Each crystal was mounted on a glass fibre with silicon grease. All measurements for the three crystals were made on a Rigaku

AFC-7R diffractometer with Mercury CCD area detector, graphite monochromated Mo-$K\alpha$ radiation (λ = 0.71069 Å) and a rotating anode generator. The data were corrected for Lorentz and polarization effects. Diffraction data were collected and processed using CrystalClear.[9] The structures were solved using direct methods (SIR92)[10] and expanded using Fourier techniques (DIRDIF99).[11] Full-matrix least-squares structural refinement based on F^2 was employed. The non-hydrogen atoms were refined anisotropically. The hydrogen atoms were refined using a riding model. For *anti*-[**PtPd**], the Pt and Pd atoms were found to be completely disordered. They were placed on same site at each of the two metal centres with a half occupancy, and their positions were refined. All calculations were performed using CrystalStructure,[12] a crystallographic software package except for refinement, which was performed using SHELXL97.[13] Full crystallographic data have been deposited with the Cambridge Crystallographic

Table 2-1 Crystallographic data of hexafluorophosphate salts of [PtM]

	syn-[**PdPt**]$(PF_6)_2$·1.5CH_3CN	*anti*-[**PdPt**]$(PF_6)_2$·CH_3CN	*syn*-[**PtAu**]$(PF_6)_3$·2CH_3CN
Formula	$C_{33}H_{28.5}N_{7.5}F_{12}P_2PdPtS_2$	$C_{32}H_{27}N_7F_{12}P_2PdPtS_2$	$C_{34}H_{30}N_8AuF_{18}P_3PtS_2$
Formula weight	1185.68	1165.15	1441.73
Crystal system	Orthorhombic	Monoclinic	Monoclinic
Space group	*Pbcn* (#60)	$P2_1/c$ (#14)	$C2/c$ (#15)
a (Å)	27.586(4)	24.774(2)	22.673(3)
b (Å)	13.543(2)	11.1858(8)	13.050(2)
c (Å)	21.015(3)	14.211(1)	30.037(5)
α (°)	90	90	90
β (°)	90	92.3480(8)	100.1920(5)
γ (°)	90	90	90
V (Å^3)	7851(2)	3934.7(5)	8747(2)
Z	8	4	8
T (K)	150	150	150
D_{calcd} (g cm^{-3})	2.006	1.967	2.189
μ (Mo $K\alpha$) (cm^{-1})	42.87	42.74	68.66
R_1 [a] ($F^2>2\sigma(F^2)$)	0.0605	0.0477	0.0504
wR_2 [b] (all data)	0.1087	0.1186	0.1169

[a] $R_1 = \Sigma||F_o| - |F_c||/\Sigma|F_o|$. [b] $wR_2 = [\Sigma w(F_o^2 - F_c^2)/\Sigma w(F_o)^2]^{1/2}$, $w = [\sigma_c^2(F_o^2) + (xP)^2 + yP]^{-1}$, $P = (F_o^2 - 2F_c^2)/3$.

2-3 Results and discussion

2-3-1 Regioselective synthesis of heterodinuclear complexes.

Kato *et al.* previously reported the one-step synthesis of homodinuclear platinum complexes *syn*- and *anti*-[**PtPt**] by the reaction of [$PtCl_2$(bpy)] and Hpyt.[3] The *syn* and *anti* geometrical isomers were produced as a mixture and the isolation of the *syn* isomer of the minor component was troublesome in this method. For the regioselective synthesis of the *syn* isomer, a stepwise complexation as shown in Scheme 2-2 should be favourable, in particular, it should be a good way to prepare heterodinuclear complexes. Recently, Lippert et al. reported that the stepwise synthesis of a *syn* isomer of heterodinuclear complex of Pd(en) (en = ethylenediamine) and Pt(bpy) units by using two cytosinato bridges. However, they could not obtained the corresponding heterodinuclear complex from Pd(bpy) and Pt(bpy) units but a Pd-Pt-Pd trinuclear motif with an *anti*-configration.[14] I succeeded in the formation of the *syn* isomer of heterodinucler complex comprising Pd(bpy) and Pt(bpy) units by using the pyt bridging ligand. The different affinities of the coordinating atoms (N and S) in the pyt ligand to Pd^{2+} and Pt^{2+} ions would be more advantageous for the regioselective synthesis. In the first step, the mononuclear complex [$Pt(pyt)_2$(bpy)] including S-coordinated pyt ligands was selectively prepared. In the second step, the Pd^{2+} ion was introduced by the coordination of nitrogen atoms of the pyt ligands. Applying this stepwise synthesis, the *syn*-[**PtAu**] complex was also obtained.

In solution at room temperature, the isomerisation from *syn*- to *anti*-isomer is very slow for [**PtPt**]. In the case of the palladium–platinum mixed complex, [**PtPd**], however, the isomerization was faster than that for the dinuclear platinum complex, and *syn*-[**PtPd**] was almost completely converted to *anti*-[**PtPd**] within a day at RT (Figure. 2-1). The crystal of *anti*-[**PtPd**] was thus isolated from the solution. On the other hand, isomerization of *syn*-[**PtAu**] was not observed, but a precipitate due to decomposition was deposited after one day in CH_3CN.

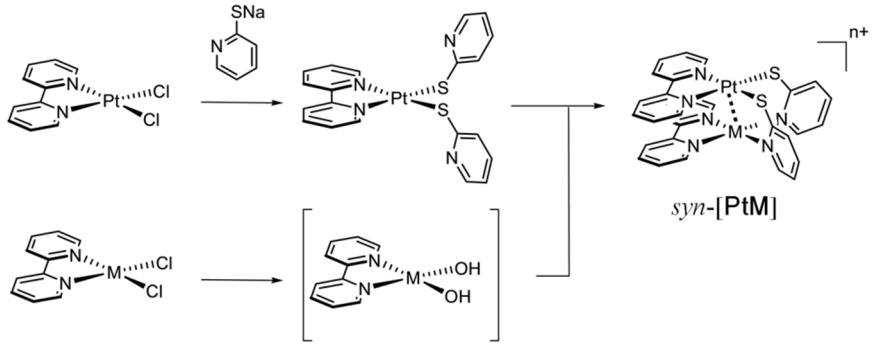

Scheme 2-2 Regioselective synthesis of *syn*-[**PtM**] motif.

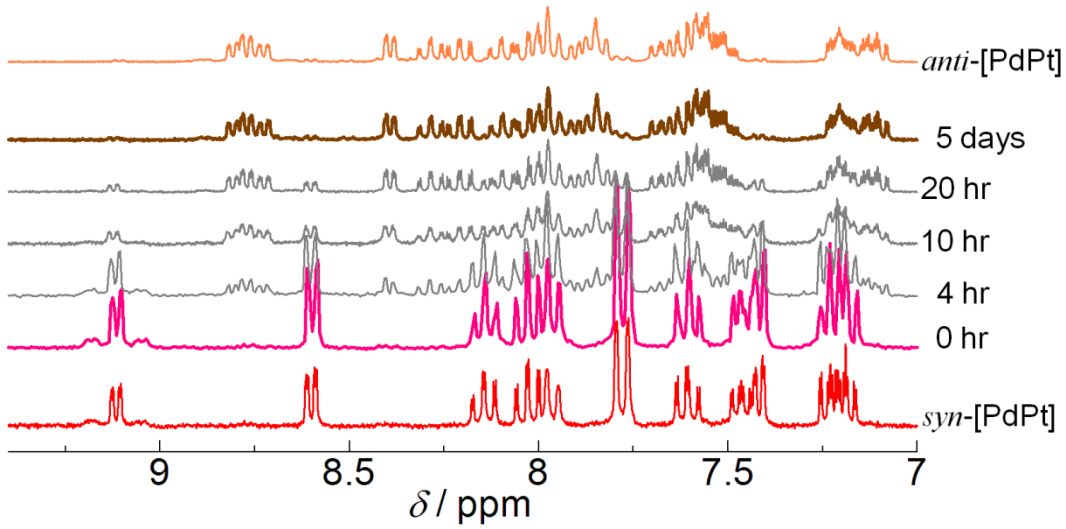

Figure 2-1. ^{1}H NMR spectral changes showing the isomerization from *syn*-[**PtPd**] to *anti*-[**PtPd**] in CD_3CN (0 h – 5 d). The spectra at the top and bottom were those of crystalline samples used for X-ray analysis, *anti*-[**PtPd**] and *syn*-[**PtPd**], respectively.

2-3-2 Crystal structures.

The selected interatomic distances and dihedral angles are shown in Table 2-2 as well as those of *syn*-[**PtPt**]. The hexafluorophosphate salt of *syn*-[**PtPd**] was found to be isostructural with that of *syn*-[**PtPt**].[3] As shown in Figure. 2-2a, the Pd^{2+} ion in *syn*-[**PtPd**] was surrounded by four nitrogen atoms while the Pt^{2+} ion was coordinated by two nitrogen atoms and two sulphur atoms. Reasonable values for the thermal factors for Pt and Pd supported the assignment in this structure, indicating no disorder between the two metal ions. Observed Pd-N, Pt-S, and Pt-N bond distances are typical values. The dihedral angle between the Pd-bpy and Pt-bpy planes (the least-square planes defined by the metal ion and non-hydrogen atoms of the bpy ligand) is about 15° which is similar to that of *syn*-[**PtPt**]. The intramolecular Pd···Pt distance (2.9084(4) Å) is also comparable to that of the *syn*-[**PtPt**] complex (2.9240(8) Å), and shorter than the sum of the van der Waals radii of Pt and Pd (3.38 Å), suggesting that a metal–metal interaction is in effect in the heterodinuclear complex. Interestingly, two *syn*-[**PtPd**] units were arranged so that the Pt ions are closely located, as shown in Fig. 1b. This dimer-of-dimer structure is nearly the same as that of *syn*-[**PtPt**]. The intermolecular distance between the two Pt ions for *syn*-[**PtPd**] (3.3757(3) Å) is shorter than twice the van der Waals radius of Pt (3.50 Å), as in the case of *syn*-[**PtPt**] (3.3839(3) Å),[3] strongly suggesting a metal-metal interaction between two *syn*-[**PtPd**]. Interestingly, a dimer-of-dimer structure for $[PtPd(bpy)_2(DMGI)_2]$ (DMGI = 3,3-dimethylglutarimidate) adopted an arrangement which faced two Pd^{2+} coordination sites instead of the Pt^{2+} sites, and the Pd···Pd distance was very long (3.829(2) Å), suggesting no intermolecular metal-metal interaction.[15]

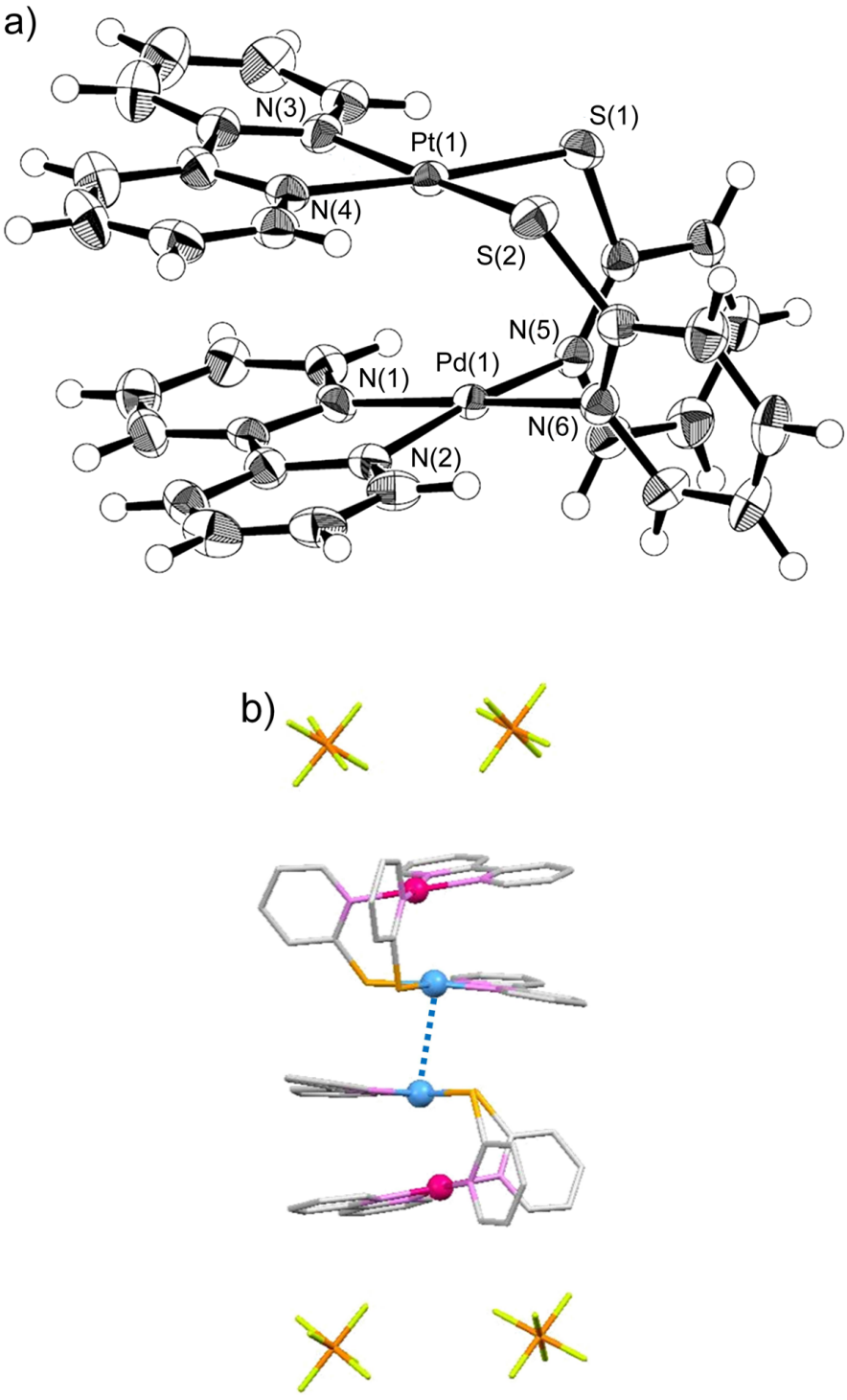

Figure 2-2. a) Molecular structure of *syn*-**[PtPd]** (50% probability ellipsoids). b) The dimer-of-dimer structure of *syn*-**[PtPd]**. The PF_6^- ions located at the top and bottom of the dimer-of-dimer motif are also included. The intermolecular Pt···Pt contact is shown by the dotted line.

Figure 2-3 depicts the structure of *anti*-[**PtPd**]. Each metal ion is surrounded by three nitrogen atoms and one sulphur atom. In contrast with *syn*-[**PtPd**], the Pt and Pd ions for *anti*-[**PtPd**] were found to be completely disordered at the two metal sites. The heterodinuclear structure was confirmed by the FAB-MS spectrum of the crystalline sample which gave only the peaks originating from the heterodinuclear complex [**PtPd**] (*m/z* = 977.1 for $\{[\mathbf{PtPd}]\cdot PF_6\}^+$, Figure. 2-4). The intramolecular Pd···Pt distance for *anti*-[**PtPd**] was 2.9765(3) Å, which also suggests the existence of a metal-metal interaction, although it is slightly longer than that of *syn*-[**PtPd**]. Considering that the torsion angle between the bpy ligands about the Pd-Pt axis (N1–M···M'–N3 = 40.3° av.) is much larger for *anti*-[**PtPd**] than for *syn*-[**PtPd**] (N1-Pd···Pt–N3 = 17.8° av.), as well as the smaller dihedral angles between the bpy and pyt ligands for *anti*-[**PtPd**] than for *syn*-[**PtPd**] (Table 2), the longer Pd···Pt distance of *anti*-[**PtPd**] is attributable to the larger deformation of the dinuclear framework compared with that of *syn*-[**PtPd**]. In the crystal, *anti*-[**PtPd**] forms a columnar structure with intermolecular π-π stacking (3.35 Å) between the bpy ligands (Figure. 2-3b), in which the stack is a rather shifted arrangement to avoid the steric hindrance of the pyt ligand. The deformation of the dinuclear framework in *anti*-[**PtPd**] could be due to adjustment of the packing structure. As a result, the intermolecular metal-metal distance (4.3 Å) in the column is too long for a metal-metal interaction.

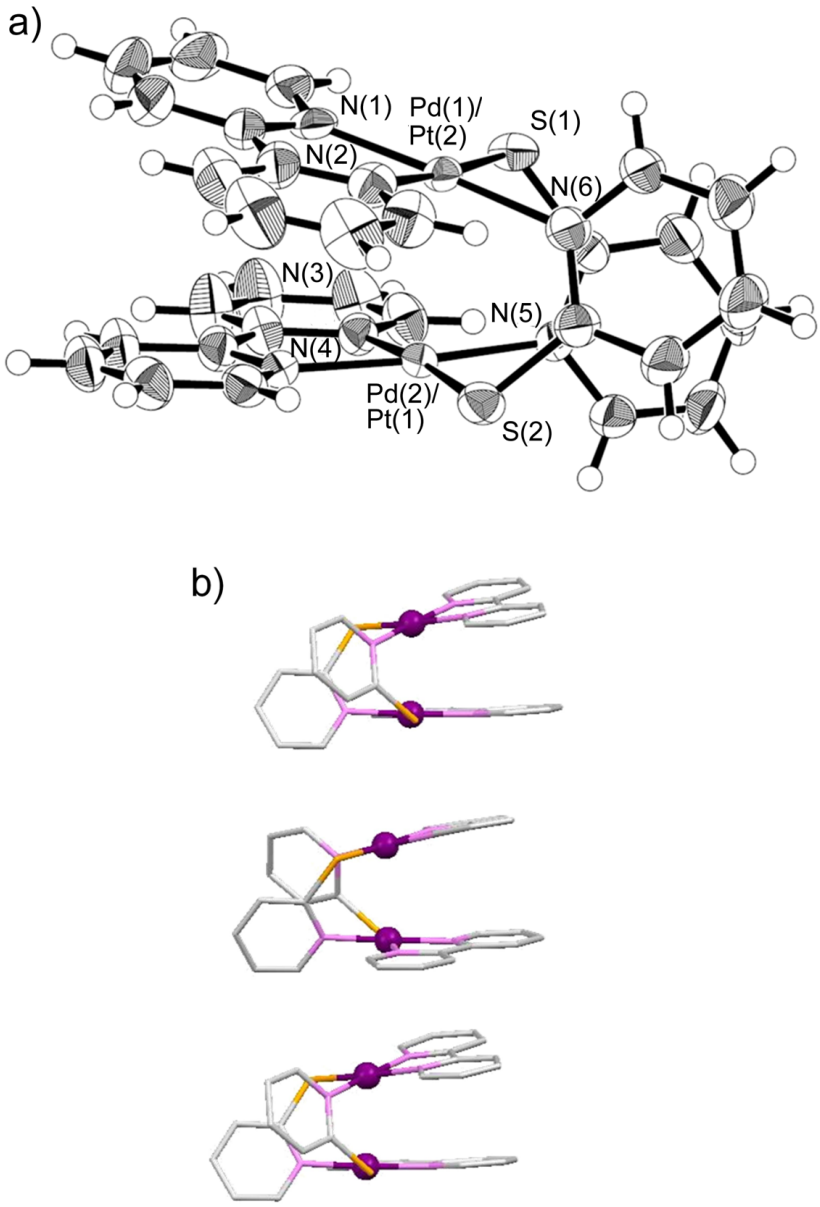

Figure 2-3. a) Molecular structure of *anti*-**[PtPd]** (50% probability ellipsoids). The Pt and Pd atoms are disordered with half occupancies. b) The loose stacked structure of *anti*-**[PtPd]**.

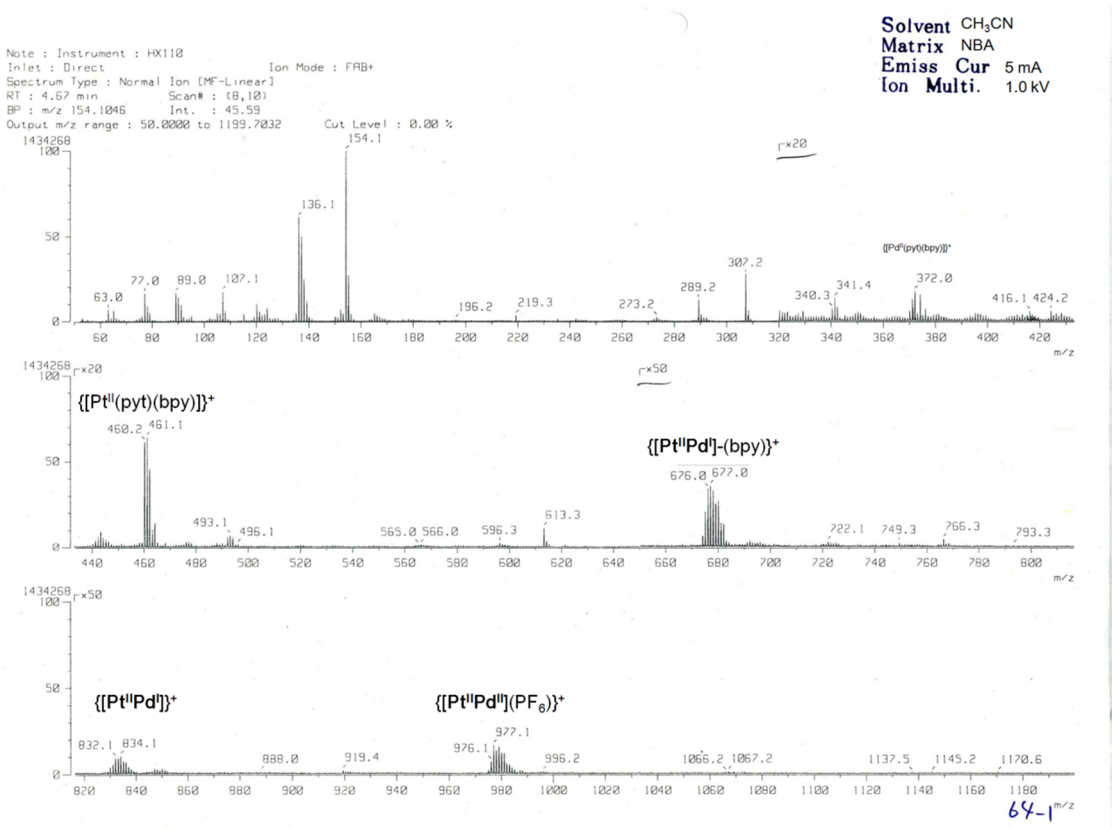

Figure 2-4.. FAB-MS spectra of *anti*-[**PtPd**]$(PF_6)_2$.

Figure 2-5a shows the molecular structure of *syn*-[**PtAu**]. As in the case of *syn*-[**PtPd]**, the introduced Au^{3+} ion occupies the N_4 coordination site while the Pt ion is coordinated by two sulphur and two nitrogen atoms. The intramolecular Au···Pt distance (2.9292(3) Å) is comparable to the Pt···Pt distance of the *syn*-[**PtPt**] complex and shorter than the sum of the van der Waals radii (3.41 Å), suggesting that a metal-metal interaction is in effect in the Pt(II)-Au(III) dinuclear complex. Although the stacking structure of Pt^{2+} and monovalent Au^{+} ions is well known,[16] assembled systems of Au(III) complexes have not often been reported. The dimeric structure of $[Au(C^N^N\text{-dpp})Cl]^{+}$ (C^N^N-dppH = 2,9-diphenyl-1,10-phenanthroline) was reported to provide a long Au···Au distance (3.6 Å).[17] A π-π stacking structure was found for a Au(III) complex, [Au(C^N^C)(C≡CPh)] (HC^N^CH = 2,6-diphenylpyridine), where Au···Au was 5.003(1) Å.[18] Bosnich et al. reported that the interaction between Pt^{2+} and Au^{3+} was unfavourable on the basis of experiments carried out for the adduct formation of a Pt(II) dinuclear complex with a terpyridine derivative, and a Au(III) complex, [Au(C^N^C)CN].[19] To the best of our knowledge, *syn*-[**PtAu**] is the first example that includes Au^{3+} and Pt^{2+} ions in close arrangement. The key point for *syn*-[**PtAu**] is that no intermolecular interactions could be observed between adjacent dinuclear complexes (Pt···Pt = 5.1899(3) Å) in contrast to the cases for *syn*-[**PtPd**] and *syn*-[**PtPt**] (Figure. 2-3b). This is due to the higher positive charge (3+) of *syn*-[**PtAu**]. There are three PF_6^{-} anions per one [**PtAu**] cation in the crystal, which prevents the complexes from forming the dimer-of-dimer structure with a short intermolecular Pt···Pt contact.

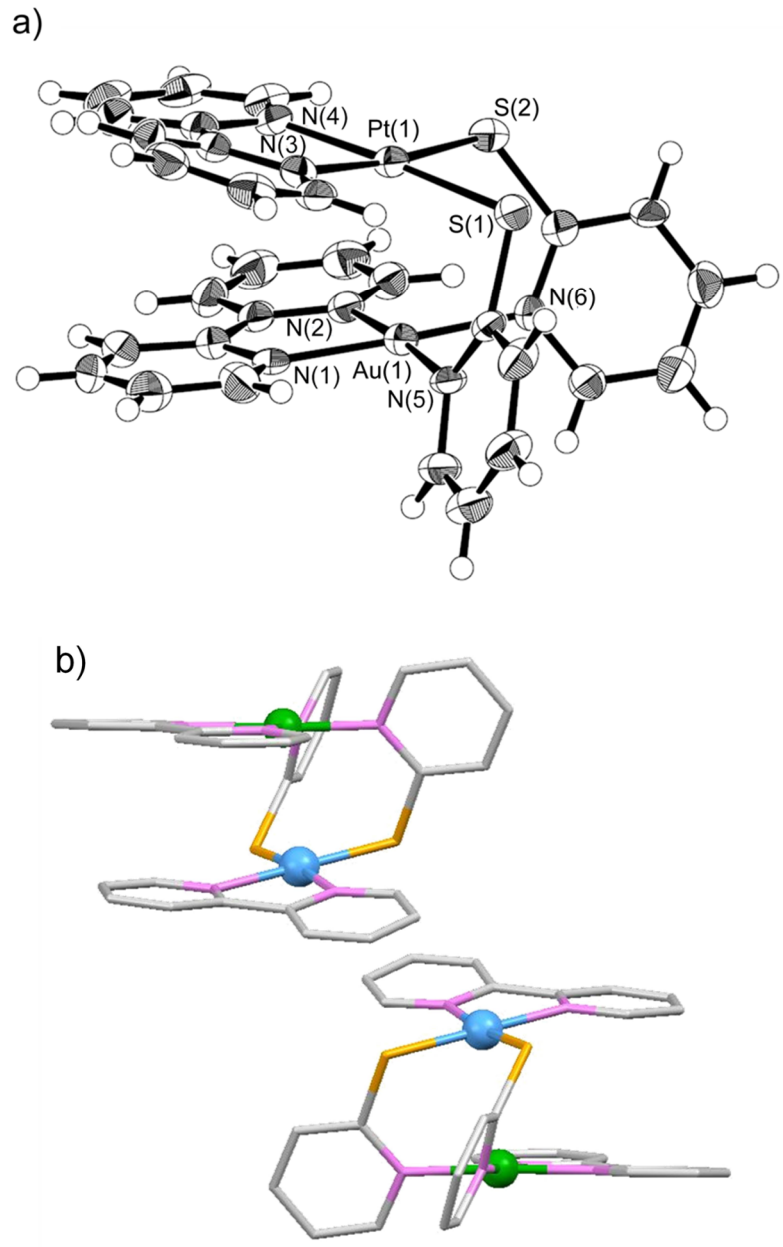

Figure 2-5. a) Molecular structure of *syn*-**[PtAu]** (50% probability ellipsoids). b) No interactive arrangement of two adjacent complexes for *syn*-**[PtAu]**.

Table 2-2 Selected interatomic distances (Å) and dihedral angles (°) for three *syn*-[PtM]$(PF_6)_n$ complexes and *anti*-[**PdPt**]$(PF_6)_2$.

	syn-[**PtPt**]$(PF_6)_2$ [a]	*syn*-[**PdPt**]$(PF_6)_2$	*syn*-[**PtAu**]$(PF_6)_3$	*anti*-[**PdPt**]$(PF_6)_2$
Selected distance(Å)	M = Pt	M = Pd	M = Au	M = Pd
Pt–S	2.288(2), 2.281(2)	2.293(2), 2.282(2)	2.299(2), 2.318(2)	2.297(2), 2.309(2)
Pt–N(bpy)	2.066(8), 2.076(6)	2.070(5), 2.060(5)	2.099(5), 2.097(5)	2.018(6), 2.045(6)
M–N(bpy)	2.020(6), 2.017(6)	2.023(5), 2.012(5)	2.016(5), 2.024(5)	2.058(6), 2.026(5)
M–N(pyt)	2.038(6), 2.033(6)	2.040(5), 2.034(5)	2.029(5), 2.030(5)	2.023(5), 2.032(5)
M···Pt (intramolecular)	2.9240(8)	2.9084(4)	2.9292(3)	2.9767(5)
Pt···Pt (intermolecular)	3.3839(3)	3.3757(3)	5.1899(3)	4.2893(3)
Dihedral angles(°)				
bpy(M)/bpy(Pt)	15.07(9)	14.54(6)	13.93(7)	13.3(1)
bpy(Pt)/pyt	63.3(1), 85.1(1)	71.9(1), 88.1(1)	72.9(1), 81.0(1)	65.5(1), 71.1(1)
bpy(M)/pyt	70.7(1), 96.4(1)	79.9(1), 98.06 (8)	67.1(1) ,70.8(1)	74.3(1), 72.1(1)

[a] ref. 3.

2-3-3 Vapochromic behaviour.

The *syn*-[**PtPd**] salt exhibits vapochromic behaviour, similarly to the isomorphous *syn*-[**PtPt**] salt. Characteristically, *syn*-[**PtPd**] exhibited a quite different colour change compared with the *syn*-[**PtPt**] salt (Figure. 2-6). For *syn*-[**PtPd**], the CH_3CN-included form is red in colour and air-stable at room temperature (Figure. 2-6A). However, a colour change from red to orange was observed upon moderate heating (50°C) under dry Ar atmosphere or vacuum (Fig. 6B). Upon exposure to CH_3CN vapour, the orange colour reverted to the original red colour in a few minutes. Such colour changes occurred reversibly by the absorption and desorption of CH_3CN vapour as proven by an adsorption isotherm and thermogravimetric analyses for *syn*-[**PtPd**] (Figures. 2-7 and 2-8). The absence of CH_3CN molecules in the orange form was also confirmed by ^1H NMR measurements (Figure. 2-9).

Figure 2-6. Photographs of powder samples: A and D) vapour-included forms; B and E) desorbed forms; and C and F) ground forms, for *syn*-[**PtPd**] and *syn*-[**PtPt**], respectively.

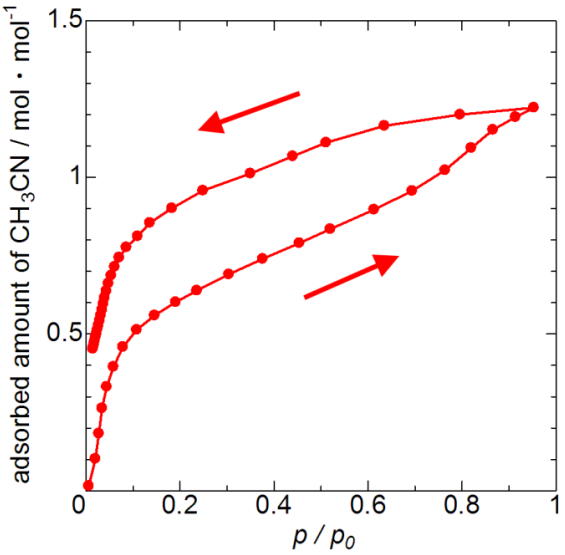

Figure 2-7. CH_3CN vapour-adsorved isotherm of *syn*-[**PtPd**] at 298 K.

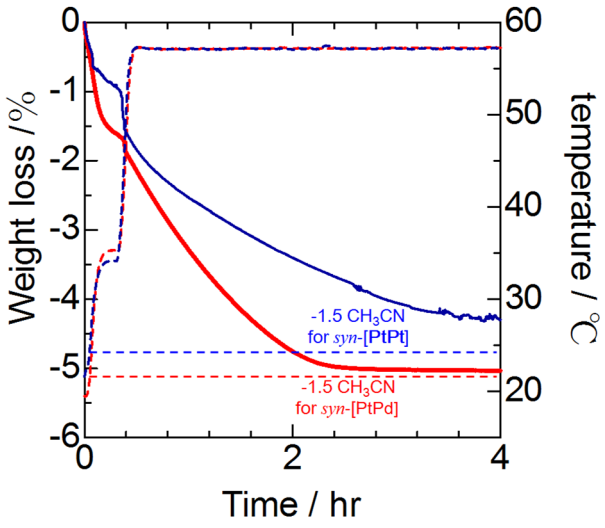

Figure 2-8. Thermogravimatric analyses for the CH_3CN-included forms of *syn*-[**PtPd**] (blue) and *syn*-[**PtPt**] (red).

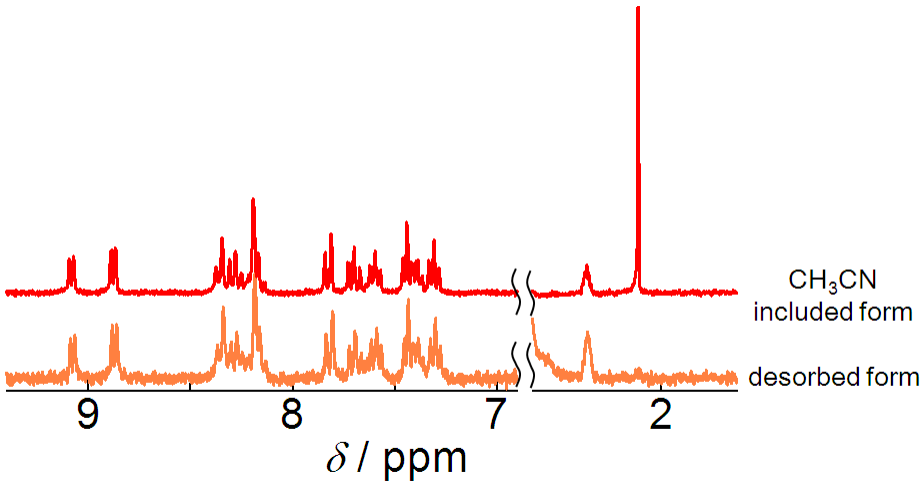

Figure 2-9. ^1H NMR spectra of the red CH_3CN-included form and orange desorbed form of *syn*-[**PtPd**] in DMSO-d_6.

For comparison of the vapour response of the *syn*-[**PtM**] complexes, UV-vis diffuse reflectance spectra of the solid samples are shown in Figure 2-10. For both *syn*-[**PtPd**] and *syn*-[**PtPt**] salts, distinct spectral changes were confirmed on exposure of the samples after heat treatment to CH_3CN vapour (Figures 2-10a and 10b). In contrast, the *syn*-[**PtAu**] salt exhibits no chromic behaviour and the solid state spectrum is essentially the same as that in solution (Figure. 2-10c). The blue-shifted spectra of the desorbed forms for the *syn*-[**PtPd**] and *syn*-[**PtPt**] salts are close to those in solution. Considering the short intermolecular Pt···Pt distances for the CH_3CN-included forms in the *syn*-[**PtPd**] and *syn*-[**PtPt**] salts (ca. 3.37 Å), the red-shifts for the vapour-included forms were attributable to the lowering of the MMLCT transition energy due to the *inter*molecular Pt···Pt interactions between the two dinuclear motifs. The conceptual MO energy diagram is shown in Scheme 2-3. It is also interesting to note that the spectral change for the *syn*-[**PtPd**] salt occurs in a high-energy region compared with that of the *syn*-[**PtPt**] salt. This indicates that the chromic region is controlled by the *intra*molecular metal-metal interaction. Additionally, taking into account that the vapochromic shift is larger for *syn*-[**PtPt**] (Δ = 2,340 cm^{-1}) than for *syn*-[**PtPd**] (Δ = 1,680 cm^{-1}), where Δ denotes the energy difference in wavenumbers of the vapour-included and desorbed spectra at the positions with half intensity, the intramolecular metal-metal interaction could affect the intermolecular metal-metal interaction.

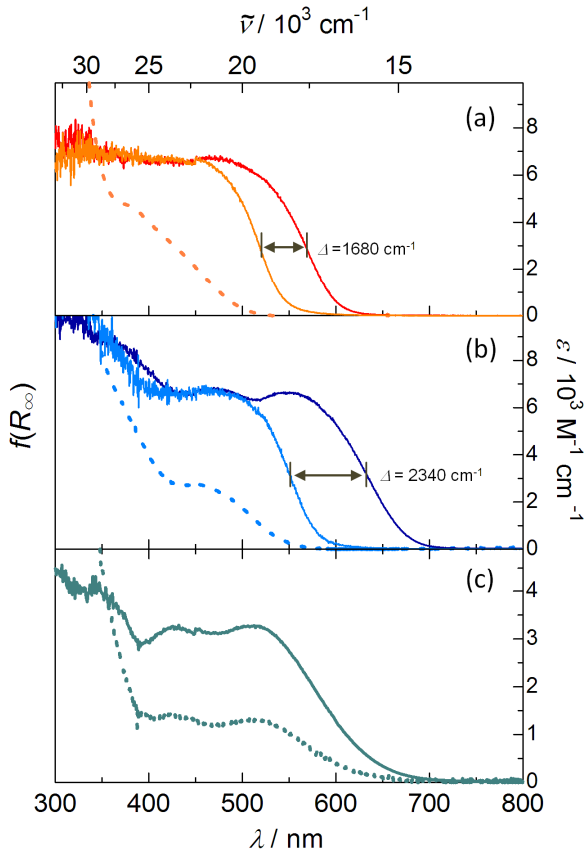

Figure 2-10. Diffuse reflectance spectra for hexaflurophosphate of (a) *syn*-[**PtPd**], (b) *syn*-[**PtPt**], and (c) *syn*-[**PtAu**]: orange and light blue solid lines are for the desorbed forms, B and E in Fig. 6, and red blue, and blue solid lines are those under exposure to CH_3CN vapour, respectively. The dotted lines exhibit the solution spectra in CH_3CN with the scale on the right.

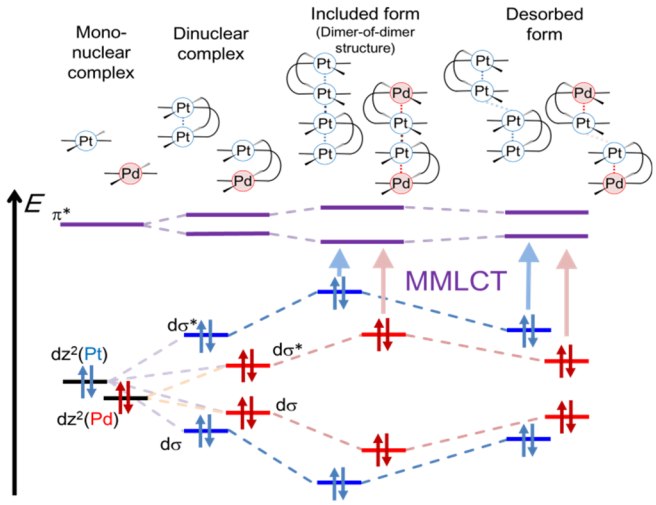

Scheme 2-3. Conceptual MO energy diagram for *syn*-[**PtPd**] and *syn*-[**PtPt**].

Structural transformation induced by vapour.

To clarify the structural factors of the colour change induced by the absorption/desorption of vapour molecules, I next carried out single-crystal diffraction measurements at various temperatures. Figure 6 shows the changes in the lattice constants of the dark-red form of *syn*-[**PtPt**] with increasing temperature from −180°C under nitrogen gas flow. A drastic change in the lattice parameters occurred at 0°C while retaining the same orthorhombic crystal system. Concomitantly, a clear colour change in the crystal was also observed from dark-red to light-red (Figure 2-11, inset photos). By using a thus-obtained single crystal of the light-red form, I succeeded in determining the crystal structure of the light-red form. Though the quality of the diffraction data for the light-red form was not very high, it was sufficient to determine the arrangement of the light-red form of *syn*-[**PtPt**]. As a result, a significantly shifted arrangement of the dimer-of-dimer structure was elucidated (Figures 2-12 and 2-13). For the light-red form, the intermolecular Pt···Pt contact that has been observed in the crystal of the dark-red form is completely broken and replaces by the π-π stacking of the bpy ligands. Although the dimer structure of the complex unit was essentially the same for both forms, the intramolecular Pt···Pt distance (2.876(2) Å) is slightly shorter compared to that of the dark-red form (2.9168(3) Å), which could be due to the breaking of the intermolecular Pt···Pt interaction (Pt···Pt (intermolecular) = 5.508(2) Å). The transformation of the dimer-of-dimer structure is induced by the release of CH_3CN molecules included in the dark-red form, followed by sliding so as to fill the void space.

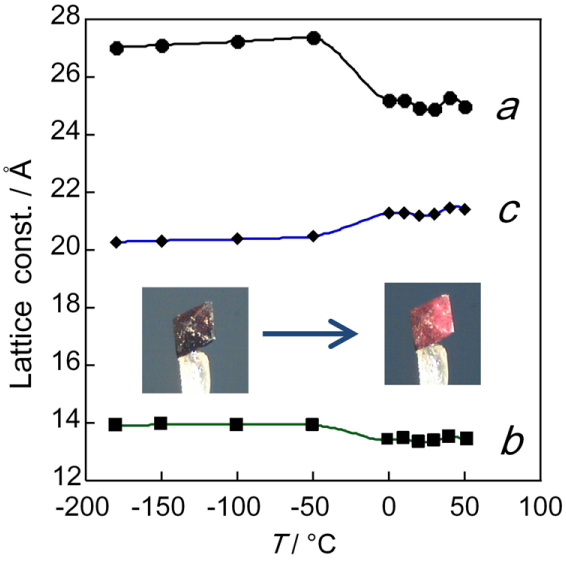

Figure 2-11. Plots of the lattice constants (*a*, *b*, and *c*) of *syn*-[**PtPt**]$(PF_6)_2$-1.5 CH_3CN at various temperatures upon heating from −180 to 50°C. Inset: Photographs of the sample crystal before and after a series of measurements.

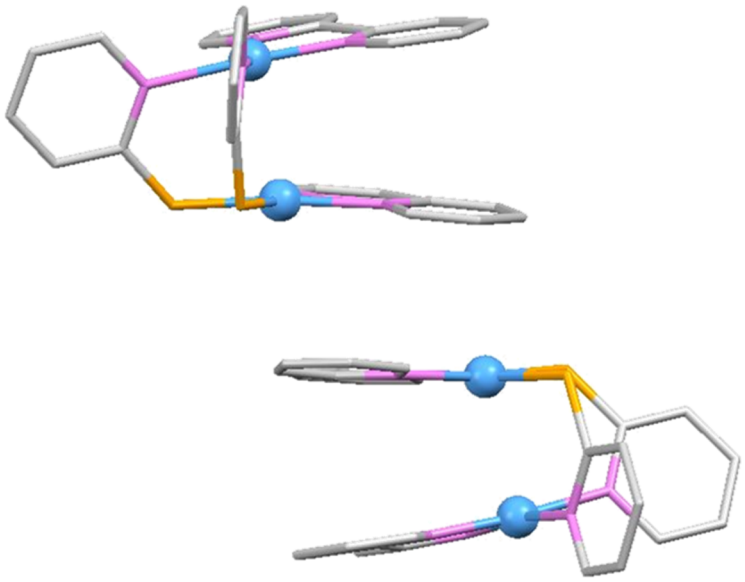

Figure 2-12. Shifted dimer-of-dimer structure for the light-red form of *syn*-[**PtPt**]. The nearest Pt···Pt distance between the two dinuclear units is 5.508(2) Å.

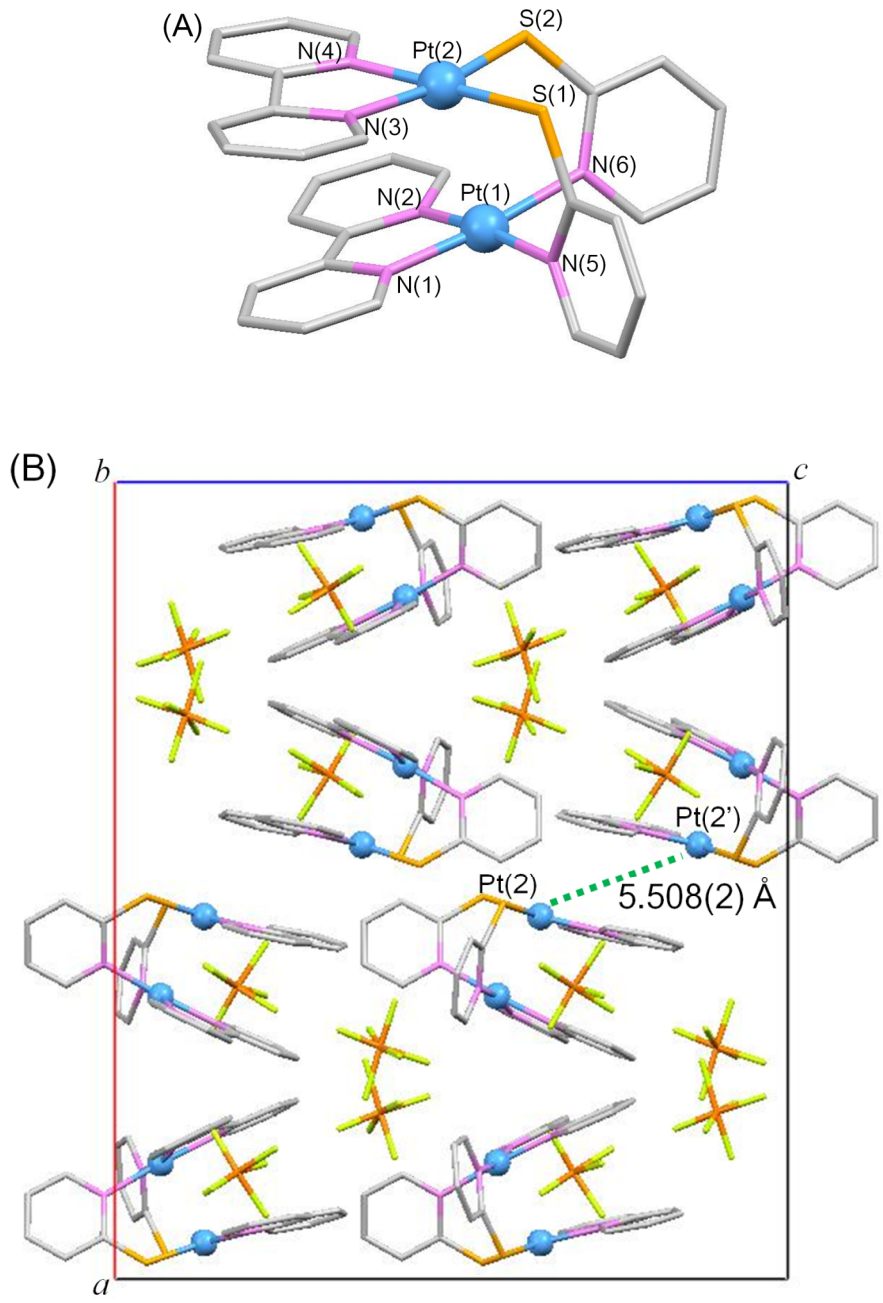

Figure 2-13. (A) Molecular and (B) packing structures of the light-red form of *syn*-[PtPt](PF$_6$)$_2$.

Crystal data: Formula = $C_{30}H_{24}F_{12}N_6P_2S_2Pt_2$, fw = 1212.79, crystal system = orthorhombic, space group = *Pbcn* (#60), a = 25.22(2), b = 13.43(1), c = 21.32(2) Å, V = 7219(11) Å^3, T = 273 K, Z = 8, D_{calc} = 2.232 g cm^{-3}, R_1 = 0.222 (I > 2□(I)). Pt2–S1 = 2.25(1), Pt2–S2 = 2.27(1), Pt1–N1 = 1.999(1), Pt1–N2 = 2.041(2), Pt1–N5 = 2.041(2), Pt1–N6 = 2.148(2), Pt2–N3 = 2.218(2), Pt2–N4 = 1.938(2), Pt1···Pt2 (intramolecular) = 2.876(2), Pt2···Pt2′ (intermolecular) = 5.508(2) Å

The reversible structural transformations driving the vapochromic behaviours of *syn*-**[PtPt]** and *syn*-**[PtPd]** were confirmed by powder X-ray diffraction (PXRD). As shown in Figure 2-14, the PXRD pattern of *syn*-**[PtPt]** changed between the vapour-included and desorbed forms repeatedly, corresponding to the changes in the diffuse reflectance spectra upon repeated heating at 50°C and CH_3CN vapour exposure. Essentially the same changes of the PXRD pattern as those for *syn*-**[PtPt]** were observed for the isomorphous *syn*-**[PtPd]** (Figure. 2-15). These results clearly indicate that the vapochromism of *syn*-[**PtPt**] and *syn*-**[PtPd]** occurs essentially by the same mechanism, which is based on the structural transformation of the intermolecular Pt···Pt interaction between the dinuclear units, i.e. an ON-OFF switch. The fact that *syn*-[**PtAu**], which lacked the dimer-of-dimer structure, exhibited no vapochromic behaviour also supports this mechanism.

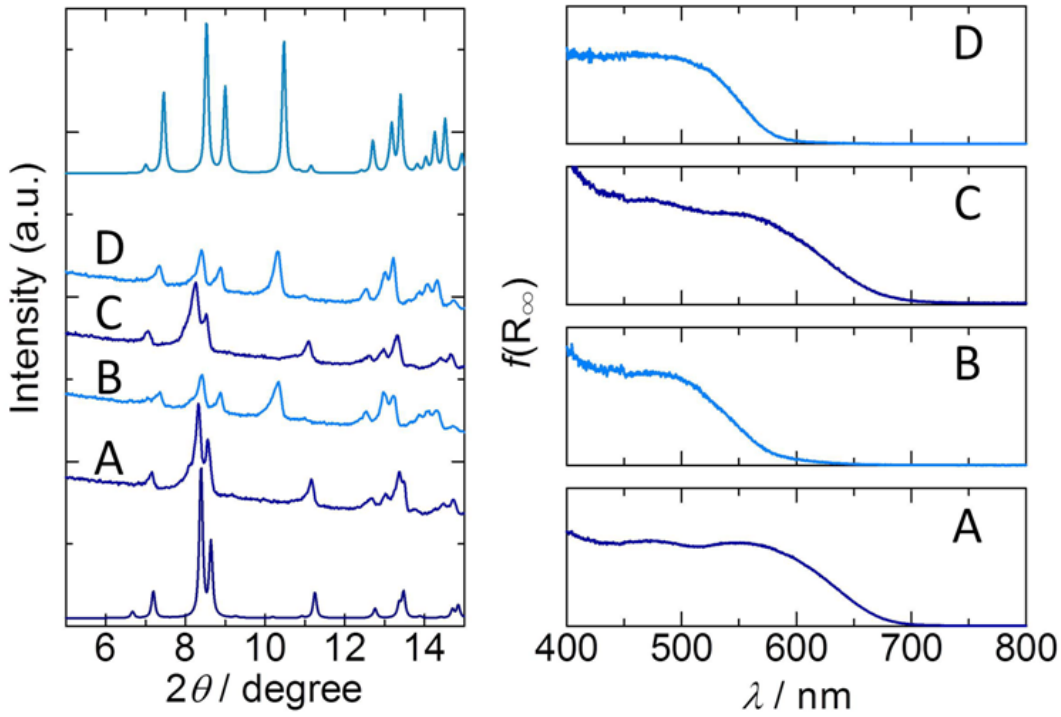

Figure 2-14. Reversible vapochromic response of *syn*-**[PtPt]**. Left: The PXRD pattern changes in the repeated cycles of CH_3CN vapour exposure (A and C) and after heating at 80°C (B and D). Top and bottom patterns are the calculated ones on the basis of the single-crystal structures of the light-red and dark-red forms, respectively. Right: The diffuse reflectance spectra of the samples corresponding to the PXRD data.

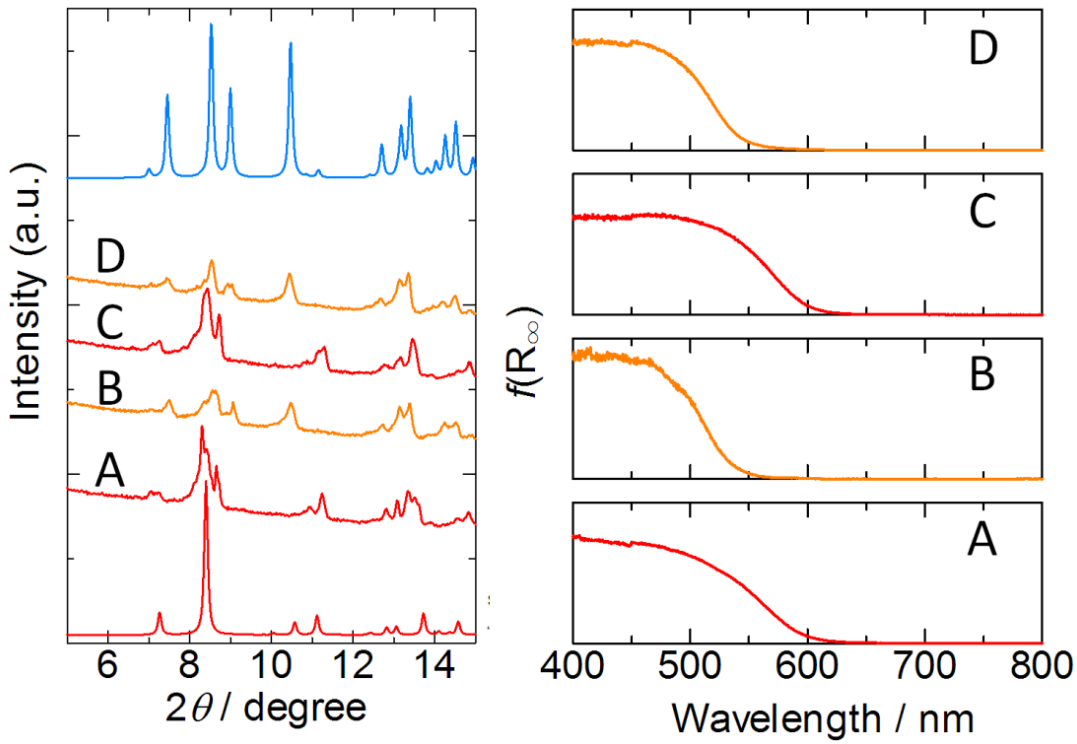

Figure 2-15. Reversible vapochromic response of *syn*-**[PtPd]**. Left: The PXRD pattern changes in the repeated cycles of CH_3CN vapour exposure (A and C) and after heating at 50°C (B and D). The pattern at the bottom is for the calculated one on the basis of the single-crystal structures of the red form of *syn*-**[PtPd]** and the top pattern shows that of the light-red form of *syn*-**[PtPd]** for comparison. Right: The diffuse reflectance spectra of the samples corresponding to the PXRD data.

In addition, the responses of *syn*-[**PtPd**] and *syn*-[**PtPt**] to other organic vapours were investigated. As shown in Fig. 16, similar spectral changes were observed on exposure to vapours of small organic molecules such as methanol, acetone, tetrahydrofuran (THF), and formaldehyde, while no changes occurred for vapours with relatively lower polarity, such as chloroform, *n*-hexane, and carbon tetrachloride. The samples which underwent colour changes by the former vapours exhibited the PXRD patterns of the vapour-included forms (Figure 2-17). These results suggest that the structural transformations due to vapour sorption of these complexes generated essentially the same dimer-of-dimer structure with short Pt···Pt contacts as that found for the CH_3CN vapour. On the other hand, there are no changes in the PXRD patterns of the desorbed forms in the cases of hexane and carbon tetrachloride vapours. It is interesting to note that some structural transformation occurred in the presence of chloroform vapour, resulting in another structure with no Pt···Pt close contactbetween the dinuclear motifs. These results suggest that the vapochromic response of these complexes depends on whether the dimer-of-dimer structure with the Pt···Pt close contact can be formed by taking up the vapour. Such vapochromic dinuclear systems are quite unique; most

vapochromic systems consist of mononuclear complexes assembled by metallophilic interactions. Only a few examples of dinuclear complexes whose chromic origins are π-π interactions and halogens have been reported.[2m-o]

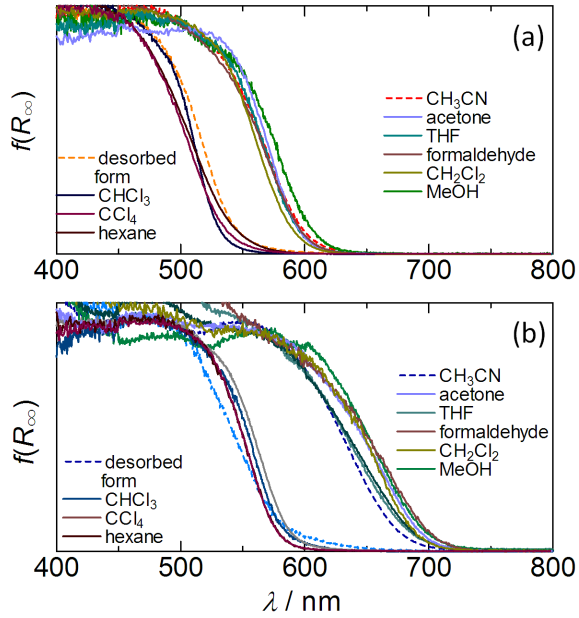

Figure 2-17. Diffuse reflectance spectra for (a) *syn*-[**PtPd**] and (b) *syn*-[**PtPt**] under various solvent vapours.

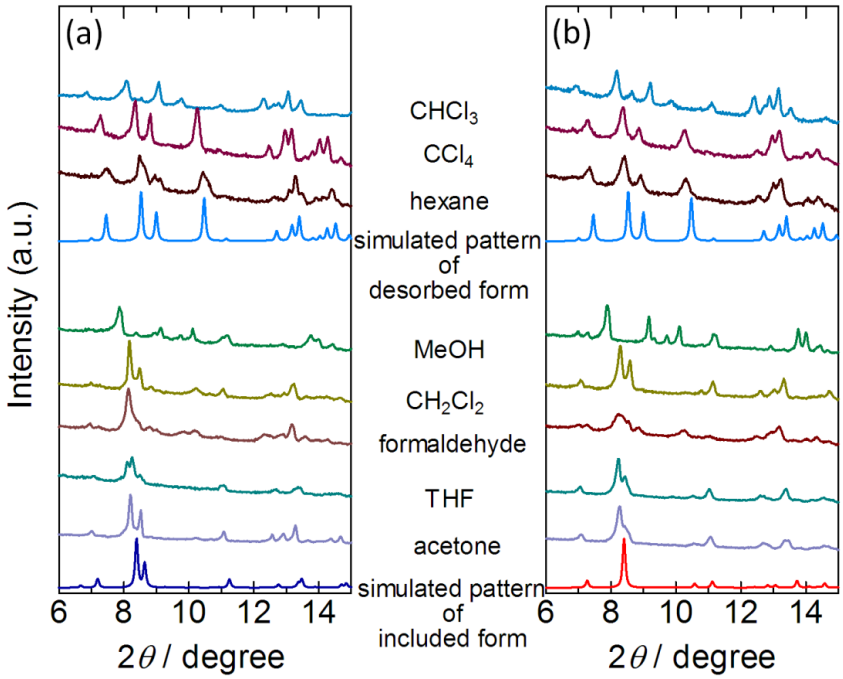

Figure 2-18. PXRD patterns of (a) *syn*-[**PtPt**] and (b) *syn*-[**PtPd**] under various vapours. Exposure times were in the minutes to days range, depending on the species.

2-3-4 Mechanochromic behaviour.

In the course of the investigation of the vapochromic response, I also found that the complexes exhibited mechanochromic behaviour. The desorbed forms of *syn*-[**PtPt**] and *syn*-[**PtPd**] are air-stable at room temperature. However, when they were ground in agate mortars, distinct colour changes occurred even in the absence of vapour, from orange to red for *syn*-[**PtPd**], and from light-red to dark-red for *syn*-[**PtPt**] (Figures 2-6C and 6F, respectively). The diffuse reflectance spectra of the ground samples exhibited large red shifts compared with those of the desorbed forms, extending to slightly longer wavelengths than those of the corresponding vapour-included forms (Figure 2-19). The samples after grinding did not exhibit any diffraction peaks (Figure 2-20), indicating that the desorbed crystalline forms of *syn*-[**PtPt**] and *syn*-[**PtPd**] were transformed to amorphous forms by grinding. The amorphous states were also obtained by grinding the vapour-included forms. Such mechanochromic behaviours based on a crystalline-to-amorphous transformation by grinding were reported recently.[20] For example, Ito et al.[20*a*] found that the Au(I) complex, $[(C_6F_5Au)_2(\mu\text{-}1,4\text{-diisocyanobenzene})]$ exhibited mechanochromic luminescence due to the formation of a Au···Au interaction by grinding, and Chen et al.[20*b*] reported the case of platinum(II) complexes containing 5-trimethylsilylethynyl-2,2′-bipyridine and phenylacetylide. Kato et al. also reported a coordination polymer with the formula $[Mg(H_2O)_5][Pt(CN)_2(4,4'\text{-dcbpy})]$ (4,4′-dcbpy = 4,4′-dicarboxy-2,2′-bipyridine) which exhibited multichromic behaviour by grinding and vapour exposure.[2*i*] These results suggest that metal-metal interactions often occur in the amorphous state by grinding, forming short, local metal-metal contacts. Interestingly, the vapour-included forms were reconstructed on exposure to CH_3CN vapour, as shown by the recovered PXRD patterns and absorption spectra for both *syn*-[**PtPd**] and *syn*-[**PtPt**] systems (Figure 2-20). Therefore, taking into account the relatively stable dinuclear framework of *syn*-[**PtM**] in the solid, it would be reasonable that the intermolecular Pt···Pt interaction between the dinuclear motifs could also occur mechanically by the collapse of the crystal structure. It is noteworthy that structural reconstruction was not observed by heating to 50°C, at which the structural transformations occurred from the included to the desorbed forms. This indicates that vapour molecules play an essential role to control the structural construction and transformation.

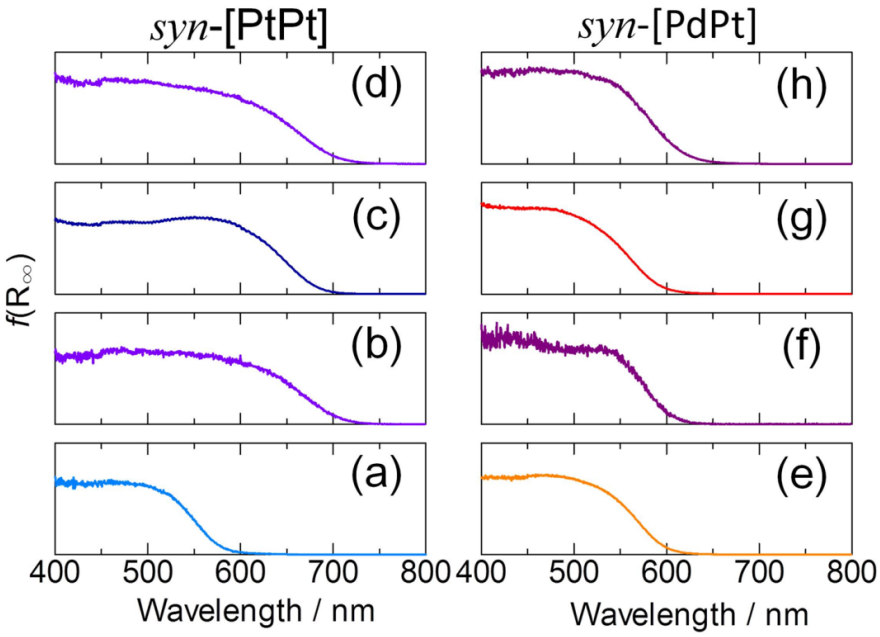

Figure 2-19. UV–vis diffuse reflectance spectral changes by grinding the samples for *syn*-[**PtPt**] (a–d) and *syn*-[**PtPd**] (e–h): (a) and (e) desorbed forms (starting materials), (b) and (f) after grinding, (c) and (g) after exposure of acetonitrile vapour to ground samples, (d) and (h) re-grinding.

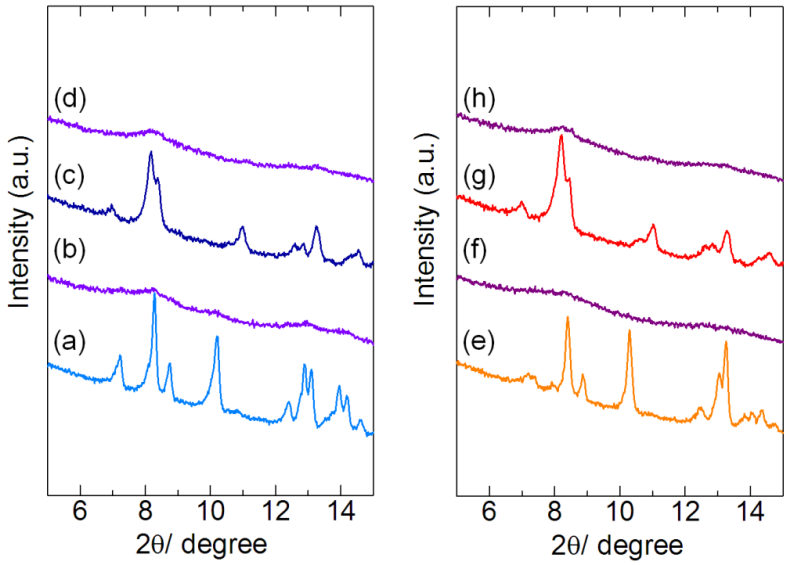

Figure 2-20. Changes in PXRD patterns by grinding the samples for *syn*-[**PtPt**] (a–d) and *syn*-[**PtPd**] (e–h): (a) and (e) desorbed forms (starting materials), (b) and (f) after grinding, (c) and (g) after exposure of acetonitrile vapour to ground samples, (d) and (h) re-grinding.

2-4 Conclusion

In addition to homometallic platinum dinuclear complexes bridged by pyridinethiolate ligands, a series of heterodinuclear complexes by stepwise complexation were synthesized. The mechanism of the vapochromism characteristic of *syn*-[**PtPd**]$(PF_6)_2$ and *syn*-[**PtPt**]$(PF_6)_2$ was clarified on the basis of X-ray diffraction studies, including a single-crystal to single-crystal transformation and powder diffraction. The vapochromic behaviour arises by the formation and breaking of the intermolecular Pt···Pt interaction induced by the absorption and desorption of the vapour molecules. It is noteworthy that the energy region of the colour change can be controlled by the introduction of different metal ions, from red to orange for *syn*-[**PtPd**] and from dark-red to light-red for *syn*-[**PtPt**]. The vapochromic mechanism was also supported by the facts that neither *syn*-[**PtAu**] having a discrete dimer structure nor *anti*-[**PtPd**] with only loose stacking exhibited such vapochromic responses. Furthermore, these complexes were found to exhibit mechanochromic behaviour, through the crystal-to-amorphous transformation, by grinding. The overall chromic behaviour of these dinuclear complexes is summarized in Scheme 2-4.

The dinuclear complexes constructed using a planar ligand (bpy) and two bridging ligands containing two different coordinating atoms (pyt) constituted a good molecular motif through which to assemble metal ions and control both *intra*- and *inter*molecular metal-metal interactions. Taking advantage of the regioselective introduction of the heterometal ions into the same molecular motif, further investigations of *syn*-[**PtM**] complexes including 3d metal ions are now in progress.

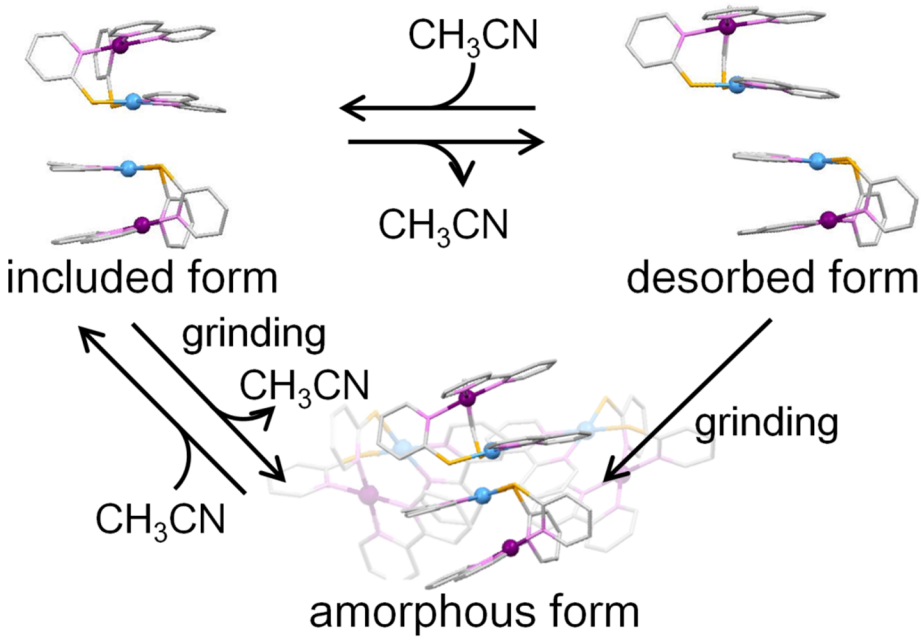

Scheme 2-4 Structural transformations of the dimer-of-dimer motif of *syn*-**[PtM]** (M = Pd^{2+} and Pt^{2+}) induced by vapour and grinding.

2-5 References

1) (*a*) X. Zhang, B. Ki, Z.-H. Chen, and Z.-N. Chen, *J. Mater. Chem.*, 2012, **22**, 11427; (*b*) M. A. Moansour, W. B. Connick, R. J. Lachicotte, H. J. Grysling, and R. Eisenberg, *J. Am. Chem. Soc.* 1998, **120**, 1329; (*c*) E. Cariati, X. Bu, and P. C. Ford, *Chem. Mater.*, 2000, **12**, 3385; (*d*) L. G. Beauvais, M. P. Shores, and J. R. Long, *J. Am, Chem. Soc.,* 2000, **122**, 2763; (*e*) E. J. Fernandez, J. M. Lopez-de-Luzuriaga, M. Monge, M. E. Olomos, R. C. Puelles, A. Laguna, A. A. Mohamed, and J. P. Fackler, *Inorg. Chem.*, 2008, **47**, 8069; (*f*) M. Albrecht, M. Lutz, A. L. Spek, and G. Koten, *Nature*, 2000, **406**, 970; (*g*) A. Kobayashi, M. Dosen, M. Chang, K. Nakajima, S. Noro, and M. Kato, *J. Am. Chem. Soc.*, 2010, **132**, 15286; (*h*) Z. Fri, N. Koche, C. J. Mohrschladt, H. Ihmels, and D. Stalke, *Angew. Chem. Int. Ed.*, 2003, **42**, 783.

2) (*a*) M. Kato, *Bull. Chem. Soc. Jpn.*, 2007, **8**, 287; (*b*) S. M. Drew, D. E. Janzen, C. E. Buss, D. I. MacEwan, K. M. Dublin, and K. R. Mann, *J. Am. Chem. Soc.*, 2001, **123**, 8418; (*c*) T. J. Wadas, Q.-M. Wang, Y. J. Kim, C. Flaschenreim, T. N. Blaton, and R. Eisenberg, *J. Am. Chem. Soc*., 2004, **126**, 16841; (*d*) L. J. Grove, J. M. Rennekamp, H. Jude, and W. B. Connick, *J. Am. Chem. Soc*., 2004, **126**, 1594; (*e*) M. L. Muro, C. A. Daws, and F. N. Castellano, *Chem. Commun*., **2008**, 6134; (*f*) A. Kobayashi, Y. Fukuzawa, H.-C. Chang, and M. Kato, *Inorg. Chem.*, 2012, **51**, 7508; (*g*) Z. M. Hudson, C. Sun, K. J. Harris, B. E. G. Lucier, R. W. Schurko, and S. Wang, *Inorg. Chem.*, 2011, **50**, 3447; (*h*) J. Ni, Y.-H. Wu, X. Zhang, B. Li, L.-Y. Zhang, and Z.-N. Chen, *Inorg. Chem.*, 2009, **48**, 10202; (*i*) A. Kobayashi, H. Hara, T. Yonemura, H.-C. Chang, and M. Kato, *Dalton. Trans*., 2012, **41**, 1878; (*j*) A. Kobayashi, H. Hara, S. Noro, and M. Kato, *Dalton. Trans*., 2010, **39**, 3400; (*k*) H. Hara, A. Kobayashi, S. Noro, H.-C. Chang, and M. Kato, *Dalton. Trans.*, 2011, **40**, 8012; (*l*) P. Du, J. Schneider, W. W. Brennessel, and R. Eisenberg, *Inorg. Chem.*, 2008, **47**, 69; (*m*) I. Mathew, Y. Li, Z. Li, and W. Sun, *Dalton. Trans.*, 2010, **39**, 11201; (*n*) S. C. F. Kui, S. S.-Y.Chui, C.-M Che, and N. Zhu, *J. Am. Chem. Soc.*, 2006, **128**, 8297; (*o*) H. Mastuzaki, H. Kishida, H. Okamoto, K. Takizawa, S. Matsunaga, S. Takaishi, H. Miyasaka, K. Sugiura and M. Yamashita, *Angew. Chem., Int. Ed*., 2005, **44**, 3240.

3) M. Kato, A. Omura, A. Toshikawa, S. Kishi, and Y. Sugimoto, *Angew. Chem. Int. Ed.,* 2002, **41**, 3183.

4) (*a*) J. K. Barton, H. N. Rabinowitz, D. J. Szalda, and S. J. Lippard, *J. Am. Chem. Soc.*, 1977, **99**, 2827; (*b*) J. P. Laurent, P. Lepage, and F. Dahan, *J. Am. Chem. Soc.*, 1982, **104**, 7335; (*c*) L. S. Hollis and S. J. Lippard, *J. Am, Chem. Soc.*, 1981, **103**, 1230; (*d*) K. Matsumoto and M. Ochiai, *Coord. Chem. Rev.*, 2002, **231**, 229; (*e*) K. Sakai, M. Takeshita, Y. Tanaka, T. Ue, M. Yanagisawa, M. Kosaka, T. Tsubomura, M. Ato, and T. Nakano, *J. Am. Chem. Soc.*, 1998, **120**, 11353.

5) T. J. Egan, K. R. Koch, P. L. Swan, C. Clarkson, D. A. V. Schalkwyk, and P. J. Smith, *J. Med. Chem.,* 2004, **47**, 2926.

6) M. Noskowska, E. Śliwińska, and W. Duczmal, *Transition Met. Chem.,* 2003, **28**, 756.
7) J. K. Bjernemose, P. R. Raithby, and H. Toftlund, *Acta Cryst.*, 2004, **E60**, m1719.
8) B.-C. Tzeng, W.-F Fu, C.-M. Che, H.-Y. Chao, K.-K. Cheung, and S.-M. Peng, *J. Chem. Soc., Dalton Trans.,* **1999**, 1017.
9) *CrystalClear*, Molecular Structure Corporation, Orem, UT, 2001.
10) *SIR92*: A. Altomare, G. Cascarano, C. Giacovazzo, A. Guagliardi, M. Burla, G. Polidori, and M. Camalli, *J. Appl. Cryst.,* 1994, **27**, 435.
11) *DIRDIF99*, P. T. Beurskens, G. Admiraal, G. Beurskens, W. P. Bosman, R. de Gelder, R. Israel, and J. M. M. Smits (1999).
12) *CrystalStructure 3.8*, Crystal Structure Analysis Package, Rigaku and Rigaku/MSC (2000-2006), 9009 New Trails Dr., The Woodlands, TX 77381 USA.
13) *SHELX97*, G. M. Sheldrick, *Acta Crystallogr., Sect. A*, 2008, **64**, 112.
14) L. Yin, P. J. S. Miguel, W. Hiller, and B. Lippert, *Inorg. Chem.*, 2012, **51**, 6784.
15) K. Matsumoto, and H. Urata, *Chem. Lett.,* **1993**, 2061.
16) (*a*) R. Hayoun, D. K. Zhong, A. L. Rheingold, and L. H. Doerrer, *Inorg. Chem.* 2006, **45**, 6120; (*b*) L. H. Doerrer, *Dalton Trans.*, 2010, **39**, 3543; (*c*) M. Stender, R. L. White-Morris, M. M. Olmstead, and A. L. Balch, *Inorg. Chem.,* 2003, **42**, 4504.
17) C.-W. Chan, W.-T. Wong, and C.-M. Che, *Inorg. Chem.,* 1994, **33**, 1266.
18) V. W.-W. Yam, K. M.-C. Wong, L.-L. Hung, and N. Zhu, *Angew. Chem. Int. Ed.,* 2005, **44**, 3107.
19) J. D. Crowley, and B. Bosnich, *Inorg. Chem.,* 2005, **44**, 2989.
20) (*a*) H. Ito, T. Saito, N. Oshima, N. Kitamura, S. Ishizaka, Y. Hinatsu, M. Wakeshima, M. Kato, K. Tsuge, and M. Sawamura, *J. Am. Chem. Soc.*, **2008**, 130, 10044; (*b*) J. Ni, X. Zhang, N. Qiu, Y.-H. Wu, L.-Y. Zhang, J. Zhang, and Z.-N. Chen, *Inorg. Chem*., 2011, **50**, 9090; (*c*) Y. Sagara, T. Mutai, I. Yoshikawa, and K. Araki, *J. Am. Chem. Soc.*, 2007, **129**, 1520; (*d*) M. Osawa, I. Kawata, S. Igawa, M. Hoshino, T. Fukunaga, and D. Hashizume, *Chem. Eur. J*., 2010, **16**, 12114; (*f*) Y. Sagara, and T. Kato, *Nature Chem.*, 2009, **1**, 605; (*g*) Y.-A. Lee, and R. Eisenberg, *J. Am. Chem. Soc.*, 2003, **125**, 7778.

Chapter 3

Vapochromic behaviour of platinum(II)-copper(II) hetero dinuclear complexes with a dimer-of-dimer motif having guest absorption sites

3-1 Introduction

There has been much attention to chemosensors[1]. Vapochromism, which is reversible color change in solid state induced by solvent vapours or gases, is one of the promising phenomena. In particular, assembled platinum(II) complexes provide a variety of chromotropic chemistry based on the interactions between neighboring molecules such as hydrogen bonding and Coulombic interactions[2]. These chromic behaviors are naked-eye perceivable, and thus they are promising materials for chemosensors.

In previous chapter, homo- and hetero- dinuclear complexes, *syn*-$[PtM(\mu\text{-pyt})_2(bpy)_2]^{n+}$ complexes (pyt = pyridine-2-thilate, bpy = 2,2'-bipyridine, *syn*-[**PtM**], *syn*-[**PtPt**]; M = Pt^{2+} (*n* = 2), *syn*-[**PtPd**]; M = Pd^{2+} (*n* = 2), *syn*-[**PtAu**]; M = Au^{3+} (*n* = 3)) are described. These complexes have two pyt ligands, adopting a *head-to-head* orientation, and thiolate ion and nitorogen atoms of pyt ligands coordinate to platinum(II) ion and another metal ion, respectively. The structures of hexafulorophosphate salts of *syn*-[**PtPt**] and *syn*-[**PtPd**] as CH_3CN included form are isostructural each other and form the dimer-of-dimer structure so as to close platinum ion of two *syn*-[**PtM**] motifs (Scheme 3-1), while that of *syn*-[**PtAu**] is monomeric structure.

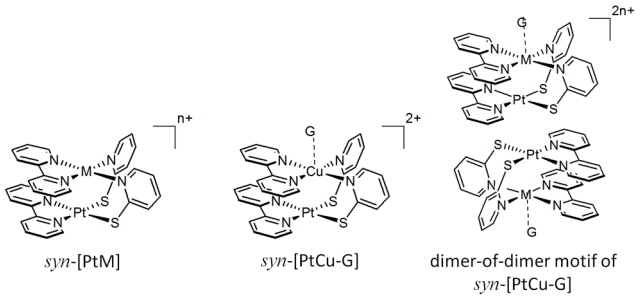

Scheme 3-1 Schematic motif of heterodinuclear motif

Concomitantly, the hexafulorophosphate salts of *syn*-[**PtPt**] and *syn*-[**PtPd**] exhibit the vapochromic behaviors in a similar manner to each other on the basis of the formation/disruption of dimer-of-dimer structure induced by absorption/desorption of solvent molecules. Though there is no chemical bond berween intermolecular divalent platinum ions for *syn*-[**PtPt**] and *syn*-[**PtPd**], the expansion of the electtromic metal-metal interactions from the dimer to the dimer-of-dimer structure could lowere the energy of the metal-metal-to-ligand charge transfer (MMLCT) transition. However, the spectral changes of vapochromism toward solvent molecules are similar, suggesting that the structural transformation due to vapour sorption generate essentially the same dimer-of-dimer structure.

Copper(II) ion, on the other hand, provide unique axial Jahn–Teller effect, which leads to extraordinary optical properties and host-guest interactions[3), 4)]. Noro and co-workers reported that

the coordination polymer {[Cu(bpetha) (bpy)(MeOH)]$(PF_6)_2$}$_n$ (bpethe = 1,2-bis-(4-pyridyl)ethane) exhibits smooth absorption for EtOH, MOH and H_2O utilizing wide coordination space at the axial site of copper(II) ion[5]. A combination of copper(II) ion and *syn*-[**PtM**] motif, thus, could be effective to form different structure utlizing the coordination of solvent molecule on the axial site of copper ion to afford the different spectral changes.

In this chapter, I newly synthesized heterodinuclear platinum-copper complexes *syn*-[PtCu-(guest)(μ-pyt)$_2$(bpy)$_2$]$^{2+}$, *syn*-[**PtCu-G**] (guest = CH_3CN for *syn*-[**PtCu-CH_3CN**]; acetone for *syn*-[**PtCu-acetone**]; MeOH for *syn*-[**PtCu-MeOH**]). Under various recrystallization conditions, I obtained three crystals which include solvent molecule as an axial ligand of copper ion and found that these complexes formed dimer-of-dimer structures in different crystal packings. The absorption/desorption behaviors are reversible, but the structural transformations are different each other and the chromic shift in the cource of absorption/desorption behaviour for these complexes were completely different. I also investigate the guest exchange properties of each *syn*-[**PtCu-G**] complexes. Herein, the structure of syn-[**PtCu-G**] complexes and the structural transoformation of absorption/desorption behavior were discussed, considering other findings by UV-vis spectroscopy and thermal analysis.

3-2 Experimental Section

3-2-1 Materials and Syntheses.

All starting materials were used as received from commercial sources, and the solvents were used without any purification. 2,2'-bipyridine (bpy), pyridine-2-thiol (Hpyt), and $CuCl_2$ were purchased from Wako. K_2PtCl_4 was purchased from Tanaka Kikinzoku. [$PtCl_2$(bpy)][6], [$CuCl_2$(bpy)][7] and [Pt(pyt)$_2$(bpy)][8] were prepared according to the method previously reported. Elemental analyses were performed by a MICRO CORDER JM 10 analyzer at the Analysis Center, Hokkaido University.

[PtCu (μ-pyt)$_2$(bpy)$_2$]$(PF_6)_2 \cdot 3H_2O$ (*syn*-[**PtCu**]): [$CuCl_2$(bpy)] (29.0 mg, 0.1 mmol) was dissolved in 10 mL of H_2O and [Pt(pyt)$_2$(bpy)] (57.1 mg, 0.1 mmol) in 5 mL of H_2O was added. The reaction mixture was stirred for 2 h at room temperature, and then filtered off to remove unreacted compounds. The resulting brown filtrate was allowed to stir for 30 min and NH_4PF_6 (81.5 mg, 0.5 mmol) in 2 mL of water was added. The brown precipitate produced immediately was filtered and

dried under reduced pressure. Yeild 78.9 mg (84.0%). Anal. Calcd. for $C_{30}H_{30}CuF_{12}N_6O_3P_2PtS_2$: C, 31.74; H, 2.66; N, 7.40. Found: C, 31.80; H, 2.49; N, 7.43.

[PtCu(CH_3CN)(μ-pyt)$_2$(bpy)$_2$](PF_6)$_2$·2CH_3CN ([**PtCu**-CH_3CN](PF_6)$_2$·2CH_3CN) Single crystals suitable for X-ray analysis were obtained by diffusion method using Et_2O/CH_3CN at 4°C. IR (ATR, cm^{-1}): 2248m (C≡N), 825s (PF_6). The powder dried at 125°C was used for elemental analysis as a monohydrate where the acetonitrile molecules were completely removed. Anal. Calcd for $C_{30}H_{26}CuF_{12}N_6S_2OP_2Pt$: C, 32.78; H, 2.38; N, 7.65. Found: C, 32.67; H, 2.59; N, 7.69.

[PtCu(C_3H_6O)(μ-pyt)$_2$(bpy)$_2$](PF_6)$_2$·0.5Acetone ([**PtCu**-Acetone](PF_6)$_2$·0.5Acetone) Single crystals suitable for X-ray analysis were obtained by diffusion method using hexane/acetone at RT. IR (ATR, cm^{-1}): 1712m, 1689s (C=O), 829s (PF_6). The powder dried at 125°C was used for elemental analysis as a monohydrate where the acetone molecules were completely removed. Anal. Calcd for $C_{30}H_{26}CuF_{12}N_6S_2OP_2Pt$: C, 32.78; H, 2.38; N, 7.65. Found: C, 32.86; H, 2.50; N, 7.69.

[PtCu(μ-pyt)$_2$(bpy)$_2$(MeOH)][PtCu(μ-pyt)$_2$(bpy)$_2$](PF_6)$_4$·MeOH ([**PtCu-MeOH**] (PF_6)$_2$·MeOH) Single crystals suitable for X-ray analysis were prepared from crude *syn*-[**PtCu**] by diffusion method using Et_2O/MeOH at RT. IR (ATR, cm^{-1}): 2952w (O-H), 829s (PF_6). The powder dried at 125°C was used for elemental analysis as a monohydrate where the methanol molecules were completely removed. Anal. Calcd for $C_{30}H_{26}CuF_{12}N_6S_2OP_2Pt$: C, 32.78; H, 2.38; N, 7.65. Found: C, 32.92; H, 2.62; N, 7.72.

3-2-2 X-ray diffraction measurements and structure analyses

A summary of the crystallographic data of the single-crystal X-ray diffraction for the [**PtCu-CH_3CN**], [**PtCu-Acetone**], [**PtCu-MeOH**] complexes is given in Table 3-1. Each crystal was mounted on a glass fibre with silicon grease. All measurements for the three crystals were made on a Rigaku AFC-7R diffractometer with Mercury CCD area detector, graphite monochromated Mo-*K*α radiation (λ = 0.71069 Å) and a rotating anode generator. The data were corrected for Lorentz and polarization effects. Diffraction data were collected and processed using CrystalClear[9]. The structures were solved using direct methods (SIR92)[10] and expanded using Fourier techniques (DIRDIF99)[11]. Full-matrix least-squares structural refinement based on F^2 was employed. The non-hydrogen atoms were refined anisotropically. The hydrogen atoms were refined using a riding model.

Powder X-ray diffraction measurements were carried out with Cu *K*α radiation using a Rigaku SmartLab diffractometer.

3-2-3 Other physical measurements

UV–vis spectra in solution were recorded on a Shimadzu MultiSpec-1500 spectrophotometer. UV–vis diffuse reflectance spectra were obtained on a Hitachi U-3000 spectrometer equipped with an integrating sphere apparatus. IR spectra were recorded on Thermo Nicolet 6700 FT-IR spectrophotometer by ATR method. Thermogravimetry and differential thermal analysis were performed using a Rigaku ThermoEvo TG8120 analyzer.

Table 3-1 . Crystallographic data of hexafluorophosphate salts of [**PtCu-G**]

	syn-[**PtCu-CH$_3$CN**](PF$_6$)$_2$ ·2CH$_3$CN	*syn*-[**PtCu-Acetone**](PF$_6$)$_2$ ·0.5C$_3$H$_6$O	*syn*-[**PtCu-MeOH**](PF$_6$)$_2$·MeOH
Formula	$C_{36}H_{33}CuN_9F_{12}P_2PtS_2$	$C_{34.5}H_{33}CuF_{12}N_6O_{1.5}P_2PtS_2$	$C_{33}H_{28}CuF_{12}N_6OP_2PtS_2$
Formula weight	1204.39	1113.24	1145.33
Crystal system	Monoclinic	Triclinic	Monoclinic
Space group	$P2_1/n$ (#14)	P-1 (#2)	$P2_1/c$ (#14)
a (Å)	11.918(2)	12.6129(2)	19.730(5)
b (Å)	13.510(3)	13.9481(9)	16.764(5)
c (Å)	27.418(6)	14.8775(2)	24.633(7)
α (°)	90	63.09(1)	90
β (°)	101.3720(8)	87.69(1)	102.042(4)
γ (°)	90	64.18(1)	90
V (Å^3)	4328.0(1)	2060.6(4)	7968(4)
Z	4	2	8
T (K)	150	150	150
D_{calcd} (g cm^{-3})	1.793	1.883	1.909
μ (Mo $K\alpha$) (cm^{-1})	39.666	41.66	43.08
R_1 [a] ($F^2>2\sigma(F^2)$)	0.0615	0.0334	0.0785
wR_2 [b] (all data)	0.2278	0.0814	0.2375

[a] $R_1 = \Sigma||F_o| - |F_c||/\Sigma|F_o|$. [b] $wR_2 = [\Sigma w(F_o^2 - F_c^2)/\Sigma w(F_o)^2]^{1/2}$, $w = [\sigma_c^2(F_o^2) + (xP)^2 + yP]^{-1}$, $P = (F_o^2 - 2F_c^2)/3$.

3-3 Results and Discussions

3-3-1 Syntheses

The synthetic procedure of *syn*-[**PtCu**] is shown in Scheme 3-2. A number of hetero metal complexes containing platinum and copper ions are reported to date, and many complexes were synthesized by stepwise syntheses[12]. Most of complexes contain N,O- or N,N-bidentate ligands as bridging ligands, however, hetero metal complexes linked by N,S-bidentate ligands have not been reported. In previous chapter, the systematic introduction of hetero metal ion into *syn*-[**PtM**] motif utilizing the affinity of metal ions to coordinating atoms were discussed. The use of a platinum complex containing 2-pyridinethiolate ligand, which is N,S-bidentate bridging ligand, should be favourable of *syn*-[**PtCu**]. First, thiolate ion of pyt ligand was introduced to Pt^{2+} ion to obtain $[Pt(pyt)_2(bpy)]$, and then copper ion was introduced into the nitrogen of pyt ligand. Using different counter anions, hexafluorophospate, thiocyanate and chloride ions, three salts of *syn*-[**PtCu-X**] were obtained. In hexafluorophospate salt, characteristically, four crystals of *syn*-[**PtCu-X**] including different axial ligand were obtained from recrystallizations utilizing various conditions. According to this synthetic approach, we have succeeded in the syntheses of hetero dinuclear complexes *syn*-[**PtPd**], *syn*-[**PtAu**], however, the removal of Cl^- ion from by adding Ag^+ ion into starting compounds $[MCl_2(bpy)]^{n+}$ was needed. In this work, we can get the *syn*-[**PtCu-X**] by mixing the $[Pt(pyt)_2(bpy)]$ and $[CuCl_2(bpy)]$ without any pretreatment. These result implies the labile of copper ions increase the reactivity for introduction of copper ion into *syn*-[**PtM**] motif.

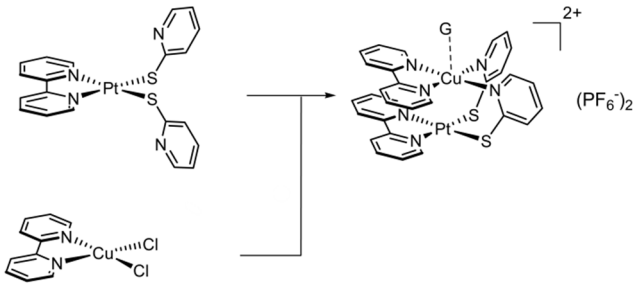

Scheme 3-2. Systematic introductions of *syn*-[**PtCu-G**]

3-3-2 Crystal structure

The selected bond distances and angles of *syn*-**[PtCu-G**] are shown in Table 3-2. All of cations have similar structural motifs *syn*-[**PtM**] basically. Platinum (II) ion and copper (II) ions are bridged by two pyt ligands adopt a *head-to-head* orientation. Two pyt ligands coordinate to the platinum ion with the thiol ion and to the copper ion with the nitrogen atom. The coordination spheres of platinum ion and copper ion in plane were completed by bpy ligand respectively. Except for independent unit A in *syn*- [**PtCu-MeOH**] (vide infra), copper ion had an additional guest molecule on axial site. Therefore the coordination mode of platinum ion and copper ion is N_2S_2 for platinum ion and N_4X for copper ion. Although there have been a number of copper (II) complexes which include solvent

molecules as ligands to date, copper(II) complexes which include various solvent molecules in the same molecular motif were scarce[13]. In all *syn*-[**PtCu-G**] crystals, interestingly, two *syn*-[**PtCu**] units are arranged so that the Pt ions are closely located to adopt the dimer-of-dimer structure.

In *syn*-[**PtCu-MeOH**] crystal, which crystallized in monoclinic $P2_1/c$ space group, two independent units of *syn*-[**PtCu**] motif were obsereved and two copper ions of these units had different coordination environment. Figure 3-2a shows one of independent unit (unit A). In unit A, a MeOH molecule coordinates to copper ion on the axial site with bond distance 2.537(6) Å. The Cu-O-C bond angle 129.2 ° is similar to the values for previous reported copper (II) complexes[5),14)] . On the other hand, copper ion in unit B had no axial ligand (Figure 3-2b). Although PF_6^- anion located at a nearby site of copper ion, the Cu···F distance 3.33(2) Å is longer than the sum of Van der Waals radius of Cu and F (2.87 Å), and thus, the copper ion had square-planar geometry (Figure 3). The Cu···Pt distances of unit A and unit B are 2.8032(8) Å and 2.7545(8) Å, respectively. The dimer-of-dimer structure was constructed by unit A and unit B (Figure 3-2c), and the intermolecular Pt···Pt distance is 3.4300(3) Å, suggesting the Pt···Pt interaction.

Figure 3-4a shows the cation of *syn*-[**PtCu**-acetone]. Single crystal of *syn*-[**PtCu**-acetone] was obtained by slow diffusion method with hexane/acetone. *Syn*-[**PtCu**-acetone] crystallized in *P*1 space group. On the axial site of copper ion, the acetone molecule coordinates to Cu ion with the Cu-O-C bond angle 153.2°. The Cu-O distance 2.748(7) Å is longer than that of unit A in *syn*-[**PtCu**-MeOH]. This elongation of Cu-O bond is thought to be due to the steric hinderance between methyl group and pyridine of pyt ligand. The intramolecular Cu···Pt distance is 2.7889(8) Å and intermolecular Pt···Pt distance of 3.4964(3) Å (Figure 3-4b).

An ORTEP view of cation of *syn*-[**PtCu**-CH_3CN] is depicted in Figure 3-5a. In *syn*-[**PtCu**-CH_3CN] crystal, copper ion has an acetonitrile molecule on the axial site. The acetonitrile molecule coordinates linearly toward the Cu···Pt axis with the Cu-N-C bond angle 173.7°, and Cu-N bond distance is 2.558(8) Å. Intramolecular Cu···Pt bond distance is 2.8084(8) Å. In the dimer-of-dimer structure, intermolecular Pt···Pt distance is 3.5109(3) Å, slightly longer than twice the van der Waals radius of Pt (3.50 Å), suggesting no Pt-Pt interaction between two *syn*-[**PtCu-CH_3CN**] (Figure 3-5b).

It is noteworthy that three *syn*-[**PtCu-G**] complexes have completely different structures. In *syn*-[**PtPt**], *syn*-[**PtPd**], the spectral changes in vapochromic behaviour are similar on expousure of CH_3CN, acetone and MeOH vapour each other, suggesting that the structural transformation due to vapour sorption generate essentially the same dimer-of-dimer structure. It is also noted that no additional axial ligands were observed in *syn*-[**PtPt**], *syn*-[**PtPd**], *syn*-[**PtAu**], whereas each complexes include CH_3CN in crystal structure in void space. In contrast, the diemer-of-dimer structures in *syn*-[**PtCu-G**] complexes are different to afford various intermolecular Pt···Pt distances. This implies, therefore, that the coordination of guest molecules on copper ion affects the crystal

structures. In characteristic, moreover, the coordinating atoms of guest molecules have different character; that is, sp^3 oxygen atom for MeOH, sp^2 oxygen atom for acetone and sp nitrogen atom for CH_3CN. This is thought to be due to the wide coordination space on the axial site of Cu ion by bpy plane[2)].

Table 3-2 Selected interatomic distances (Å) and dihedral angles (°) for three *syn*-[**PtCu-G**] complexes.

	syn-[**PtCu-CH_3CN**]$(PF_6)_2 \cdot 2CH_3CN$	*syn*-[**PtCu-acetone**]$(PF_6)_2 \cdot 0.5C_3H_6O$	*syn*-[**PtCu-MeOH**]$(PF_6)_2$
Selected distance(Å)	G = CH_3CN	G = Acetone	G = MeOH
Pt–S	2.293(2), 2.272(2)	2.281(1), 2.267(1)	2.278(2), 2.279(2), 2.292(2), 2.275(2)
Pt–N(bpy)	2.067(6), 2.061(7)	2.066(4), 2.071(3)	2.062(6), 2.068(5), 2.066(6), 2.075(5)
Cu–N(bpy)	2.026(6), 2.011(7)	2.016(3), 2.001(4)	2.017(6), 2.015(5), 2.007(6), 2.007(6)
Cu–N(pyt)	2.029(7), 2.020(6)	1.999(4), 2.021(3)	2.016(5), 1.979(6), 1.994(5), 2.007(6)
Cu-G	2.558(8)	2.693(4)	2.537(6)
Cu···Pt (intramolecular)	2.8084(8)	2.7838(7)	2.8032(8), 2.7545(8)
Pt···Pt (intermolecular)	3.5109(3)	3.4772(4)	3.4300(3)

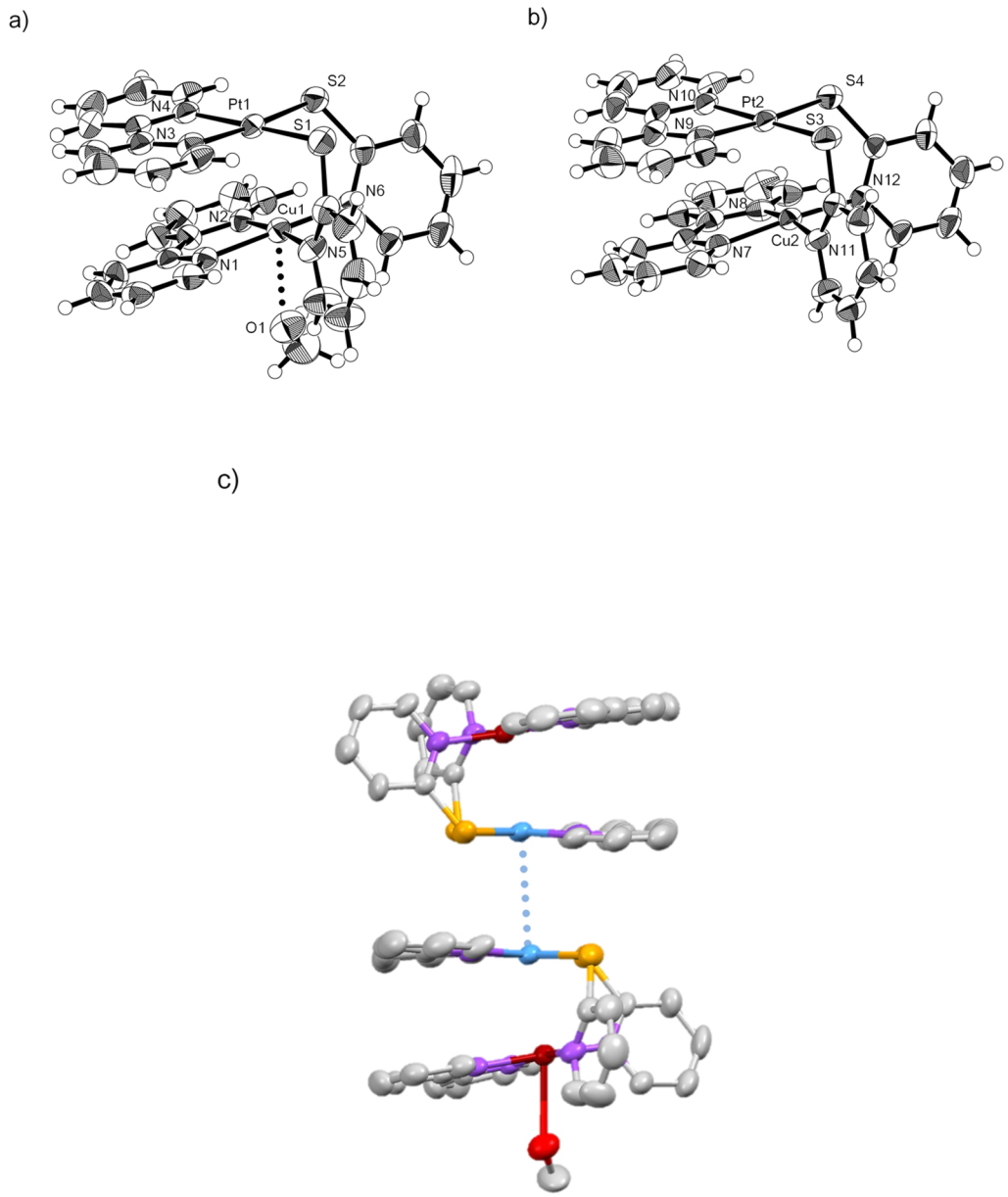

Figure 3-2. Molecular structure of a) unit A and b) unit B in *syn*-**[PtCu-MeOH]** (50% probability ellipsoids). c) The dimer-of-dimer structure of *syn*-**[PtCu-MeOH]**. The intermolecular Pt···Pt contact is shown by the dotted line.

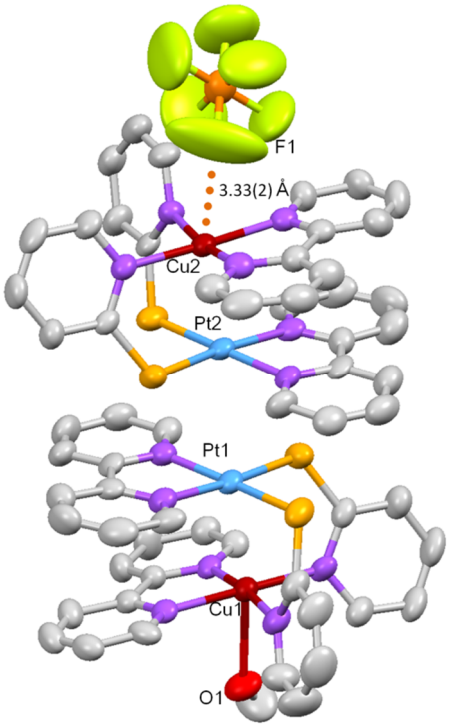

Figure 3-3. Molecular structure in *syn*-**[PtCu-MeOH]** of unit A and unit B with PF_6^- anion located at a nearby site of copper ion

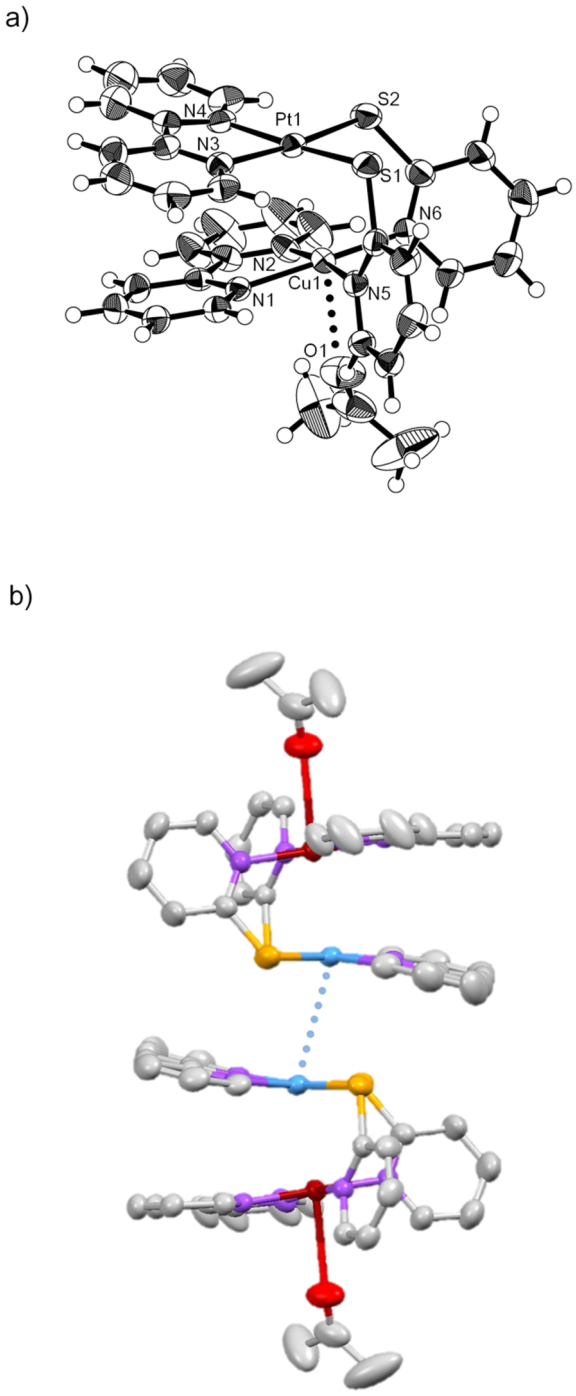

Figure 3-4. a) Molecular structure of *syn*-**[PtCu-acetone]** (50% probability ellipsoids). b) The dimer-of-dimer structure of *syn*-**[PtCu-acetone]**. The intermolecular Pt···Pt contact is shown by the dotted line

a)

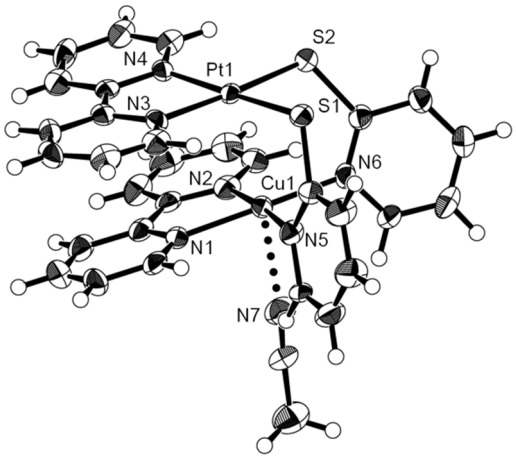

b)

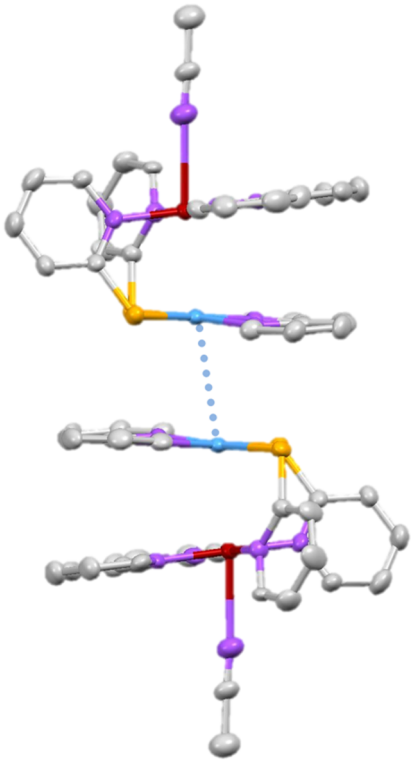

Figure 3-5. a) Molecular structure of *syn*-**[PtCu-CH$_3$CN]** (50% probability ellipsoids). b) The dimer-of-dimer structure of *syn*-**[PtCu- CH$_3$CN]**. The intermolecular Pt···Pt contact is shown by the dotted line.

3-3-3 The absorption/desorption behaviour of *syn*-[PtCu-G]

In previous chapter, the vapochromism of homo- and hetero dinuclear complexes *syn*-[**PtPt**] and *syn*-[**PtPd**] based on the absorption/desorption of solvent molecules were discussed. In *syn*-[**PtCu-G**] complexes, solvent molecules coordinates to copper(II) ion at the axial site, which was and then, absorption / desorption behaviours of these complexes were examined. In the course of absorption/desorption behaviours, interestingly, each complex exhibits different chromic shift. The colour of each complex was ocher, light-brown and reddish brown for *syn*-[**PtCu-CH_3CN**], *syn*-[**PtCu-acetone**] and *syn*-[**PtCu-MeOH**], respectively (Figures 3-6, A, B, C). When these crystals were heated to 125 ºC, solvent molecules were released to afford desorbed forms. Thermogravimetric analyses and differential thermal analyses revealed that transition point of desorption is about 43 ºC, 123 ºC, and 85 ºC for *syn*-[**PtCu-CH_3CN**], *syn*-[**PtCu-acetone**] and *syn*-[**PtCu-MeOH**], respectively (Figure 3-7). As shown in Figure 3-6, the color of each complexes were changed by desorption of solvent molecules from ocher to reddish brown for *syn*-[**PtCu-CH_3CN**], from light brown to light brown for *syn*-[**PtCu-acetone**], and from reddish brown to light brown; that is, red-shift for *syn*-[**PtCu-CH_3CN**], no shift for *syn*-[**PtCu-acetone**] and blue shift for *syn*-[**PtCu-MeOH**] by desorption of solvent molecules. Figure 3-8 and Figure 3-9 depicts UV-vis diffuse reflectance spectra of the solid samples as well as those in solution. In solvent included form of *syn*-[**PtCu-G**] crystals, the absorption shoulder were observed in the order of *syn*-[**PtCu-MeOH**], *syn*-[**PtCu-acetone**] and *syn*-[**PtCu-CH_3CN**] from lower energy region (Figure 9). In these solutions, *syn*-[**PtCu**] complex does not exhibit solvatochromic behaviour, suggesting that solvent molecules coordinated at the axial site of *syn*-[**PtCu**] in the crystals do not affect these color differences. On the other hand, considering the intermolecular Pt···Pt distances in the dimer-dimer structres, it is suggested that the intermolecular Pt···Pt interactions affect the absorption band; that is, the metallophilic interaction would be effective to lower the MMLCT transition energy in the order of *syn*-[**PtCu-MeOH**] (Pt···Pt = 3.4300(3) Å), *syn*-[**PtCu-acetone**] (Pt···Pt = 3.4964(3) Å), whereas it would be less effective for *syn*-[**PtCu-CH_3CN**] (Pt···Pt = 3.5109(3) Å). In desorbed form of *syn*-[**PtCu-G**] obtained by heating , the absorption shoulders shows red-shift for *syn*-[**PtCu-CH_3CN**], no shift for *syn*-[**PtCu-acetone**], blue-shift for *syn*-[**PtCu-MeOH**], and therefore, each *syn*-[**PtCu-G**] complex exhibits different chromic shift. In order to elucidate structural information, powder X-ray diffractions (PXRD) were measured (Figure 3-10). The patterns of the solvent included form in each crystal is essentially the same as the corresponding simulation patterns calculated from the crystal structures of *syn*-[**PtCu-G**], indicating that the structures were maintained in the powder samples. In contrast, the patterns of the desorbed form obtained from each crystal were completely different each other although the desorbed forms have the same compositions. Unfortunately, I could not determine any structures of the desorbed forms, but considering no solvatochromic behaviour in solutions, these results imply that desorption

of solvent molecules from *syn*-[**PtCu-G**] induce different alignment to afford different intermolecular Pt···Pt distances and differences of metallophilic interaction. The structural transformations from the desorbed form to the solvent-included *syn*-[**PtCu-G**] were observed on exposure of corresponding solvent vapours (Figure 3-11), indicating that these structural transformations were reversibly occur by vapour molecules. In addition, I investigated the structural transformations with guest exchanges by organic vapours. On exposure of solvent vapours to *syn*-[**PtCu-G**], the structural transformations were obsereved, suggesting that the different alignments of *syn*-[**PtCu**] motif coordinated by solvent molecules were reversibly occurred (Figure 3-12).

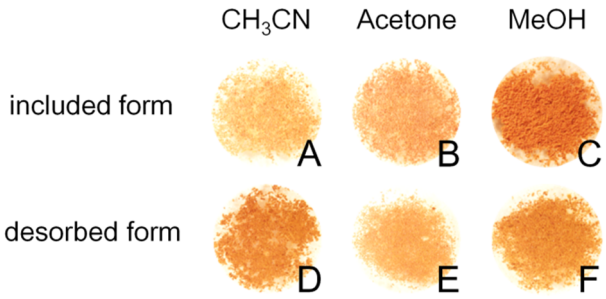

Figure 3-6. Photographs of powder samples. (A, B and C) vapour-included form, (D, E and F) desorbed forms for *syn*-[**PtCu-CH$_3$CN**], *syn*-[**PtCu-acetone**] and *syn*-[**PtCu-MeOH**], respectively.

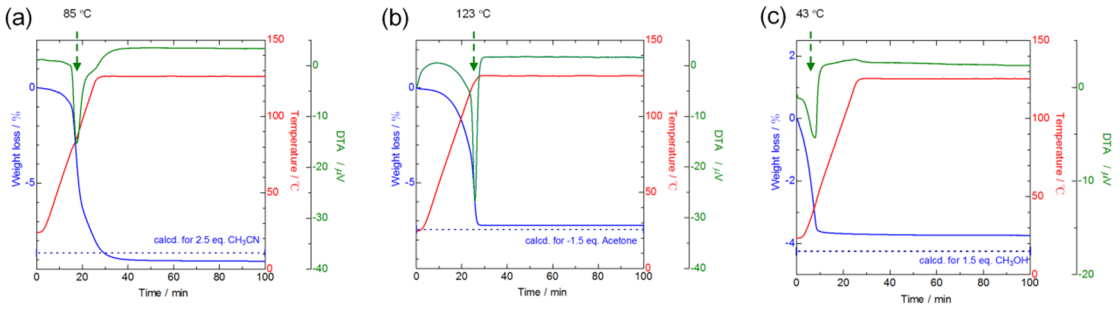

Figure 3-7. Thermogravimatric analyses for the solvent-included forms of (a) *syn*-[**PtCu-CH$_3$CN**], (b) *syn*-[**PtCu-acetone**] and (c) *syn*-[**PtCu-MeOH**].

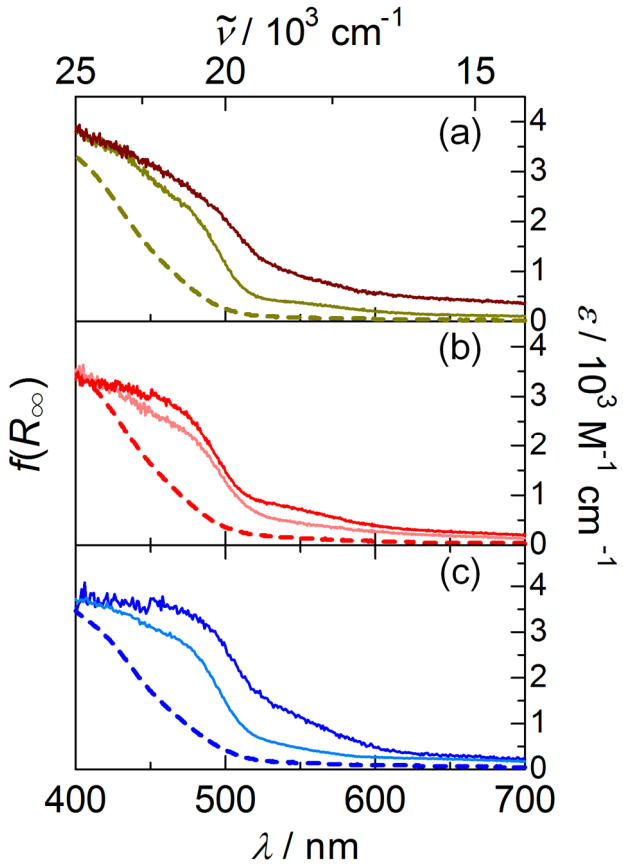

Figure 3-8. UV-vis Diffuse-reflectance spectra for (a) *syn*-[PtCu-CH_3CN], (b) *syn*-[PtCu-acetone] and (c) *syn*-[PtCu-MeOH]: ocher, red, blue solid lines are for the solvent-included form A, B, and C in Figure A, and brown, pink and cyan solid lines are for desorbed form D, E and F in Figure A, respectively. The dotted lines exhibit the solution spectra in (a) CH_3CN, (b) acetone and (c) MeOH with the scale on the right.

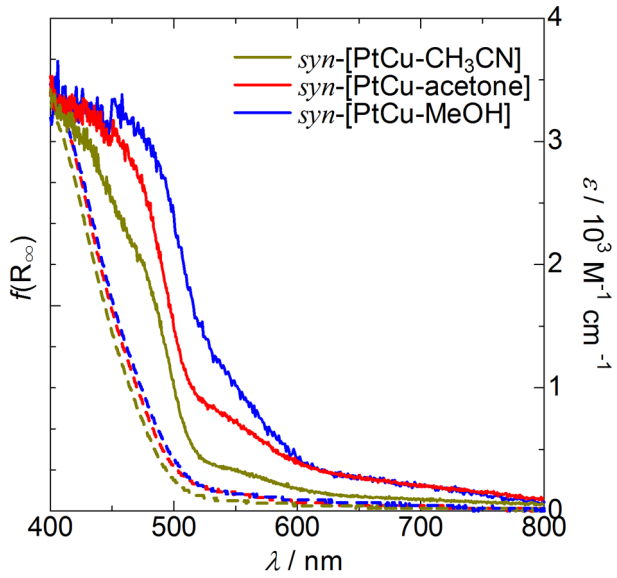

Figure 3-9. UV-vis Diffuse-reflectance spectra (solid line) for *syn*-[**PtCu-CH$_3$CN**] (ocher), (b) *syn*-[**PtCu-acetone**] (red) and (c) *syn*-[**PtCu-MeOH**] (blue) The dotted lines exhibit the solution spectra in CH_3CN (ocher), acetone (red) and MeOH (blue) with the scale on the right.

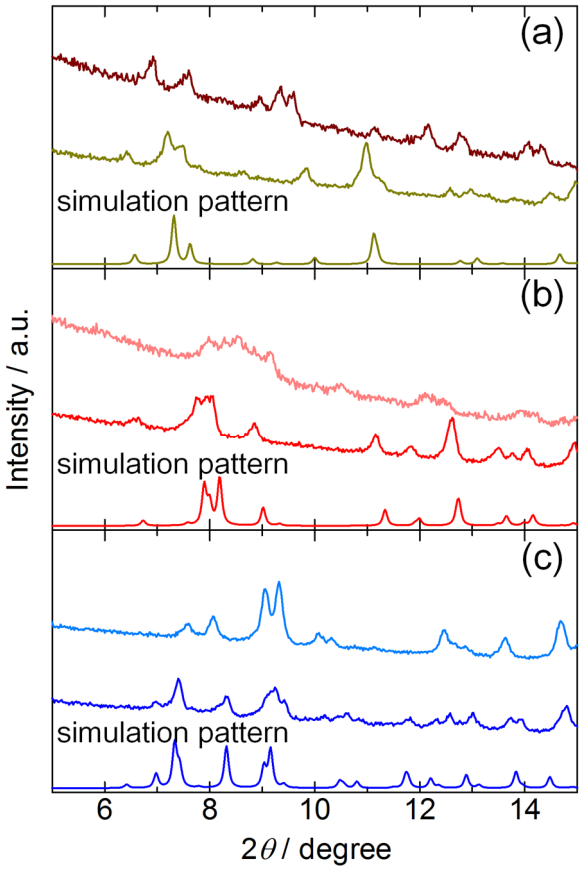

Figure 3-10. The PXRD patterns of solvent-included and desorbed forms of (a) *syn*-[**PtCu-CH_3CN**], (b) *syn*-[**PtCu-acetone**] and (c) *syn*-[**PtCu-MeOH**]: ocher, red, blue solid lines are for the solvent-included form A, B, and C in Figure A, and brown, pink and cyan solid lines are for desorbed form D, E and F in Figure A, respectively. The bottom patterns in graph are the calculated ones on the basis of the single crystal strutures of (a) *syn*-[**PtCu-CH_3CN**], (b) *syn*-[**PtCu-acetone**] and (c) *syn*-[**PtCu-MeOH**] respectively.

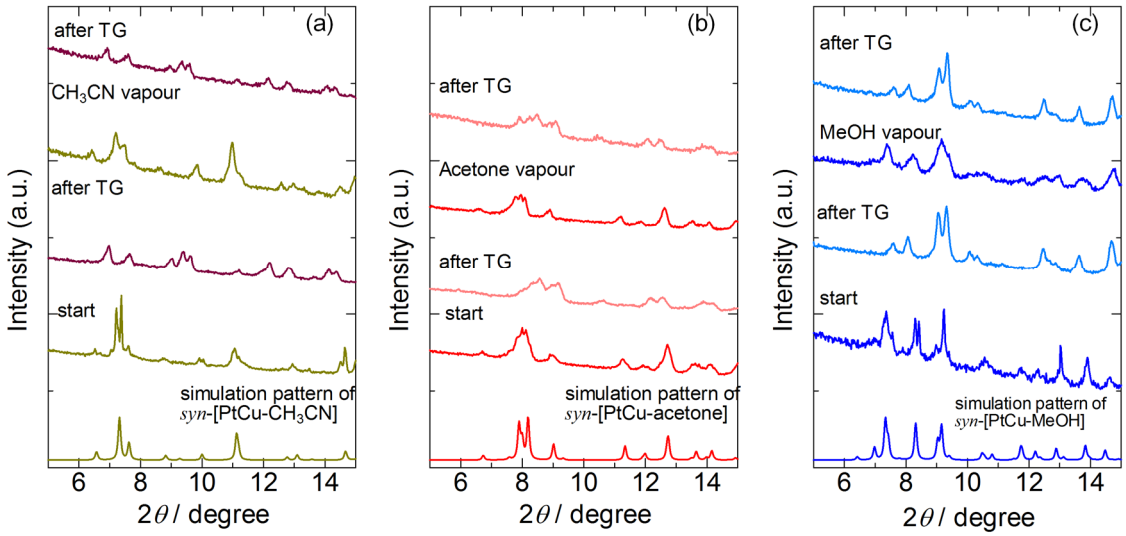

Figure 3-11. Reversible structural transformations by absorption/desorption behaviour of solvent molecules in PXRD patterns of (a) *syn*-[**PtCu-CH$_3$CN**], (b) *syn*-[**PtCu-acetone**] and (c) *syn*-[**PtCu-MeOH**].

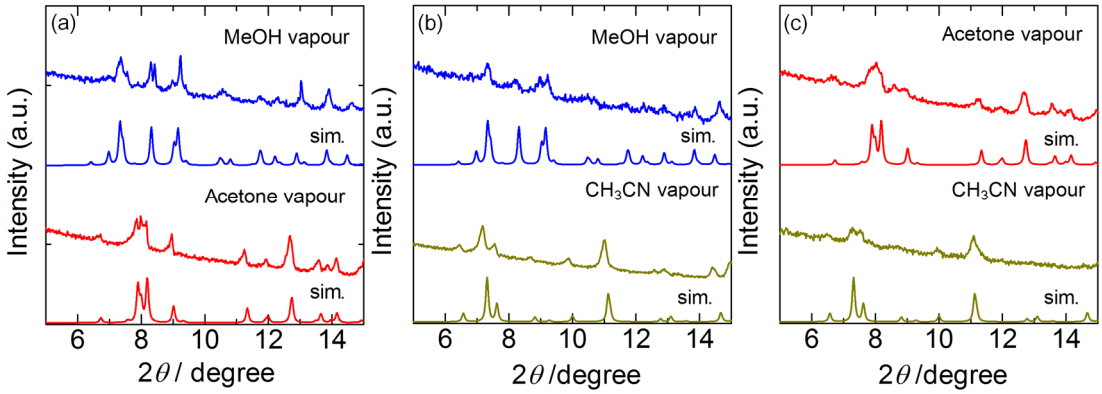

Figure 3-12. Reversible structural transformations by guest exchange of solvent molecules in PXRD patterns from (a) *syn*-[**PtCu-CH$_3$CN**], (b) *syn*-[**PtCu-acetone**] and (c) *syn*-[**PtCu-MeOH**].The calculated pattern obtained from *syn*-[**PtCu-G**] corresponding to exposing vapours are also shown.

3-4 Conclusion

Utilizing platform of systematic introduction of *syn*-[**PtM**] molecular motif, I have synthesized the coppr(II)-platinum(II) hetero dinuclar complexes *syn*-[**PtCu-CH$_3$CN**], *syn*-[**PtCu-Acetone**], *syn*-[**PtCu-MeOH**]. The introduction of copper(II) ion into *syn*-[**PtM**] motif afford an additional solvent molecule on the axial site of copper(II) ion except for one of the independent unit of *syn*-[**PtCu-MeOH**]. These complexes form dimer-of-dimer structures with differenc crystal packing. The absorption/desorption behaviour of solvent molecules including axial coordinating molecule of these complexes were reversibly occured but the chromic shift are different each other, while the compositions of desorbed compounds of these complexes are essentially same each other. The overall these structural transformation and chromic behaviours are summaraized in shcme 3-3. This result suggests that axial coordinating solvent molecule arranged their packing structre in not only included form but also desorbed form.

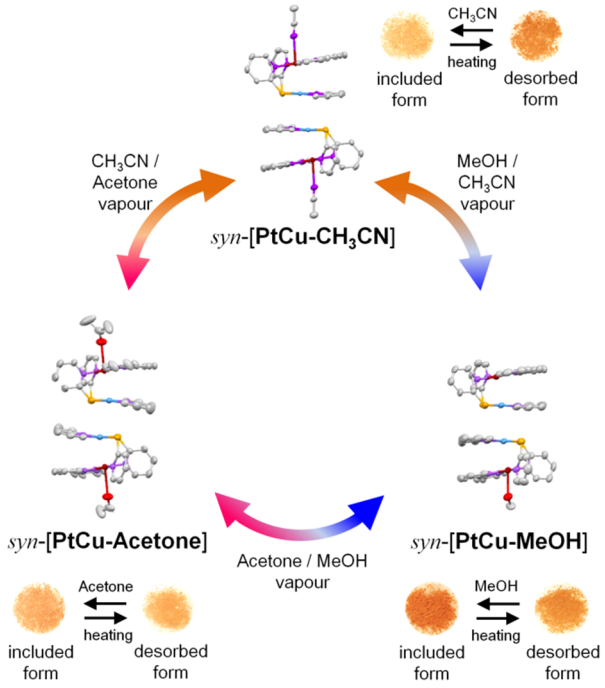

Scheme 3-3. Structural transformation of dimer-of-dimer structure of *syn*-[**PtCu-G**] motifs induced by vapours and chromic behaviours induced by absorption/desorption behaviour of *syn*-[**PtCu-G**].

3-5 Refernces

1) a)A. P. De Silva, D. B. Fox, A. J. M. Huxley, and T. S. Moody, *Coord. Chem. Rev.*, 2000, **205**, 41-57, b) L. E. Kreno, K. L.eong, M. O. K. Farha, M. Allendorf, R. P. V. Duyne, and J. T. Hupp, *Chem. Rev.*, 2012, **112**, 1105-1125.

2) a) O. S. werger, *Chem. Rev.*, 2013, **113**, 3686–3733, b) Kato, *Bull. Chem. Soc. Jpn.*, 2007, **80**, 284-294, c) X.Zhang, B. Li. Z.-H. Chen, Z.-N. Chen, *J. Mat. Chem.*, 2012, **22**, 11427-11441

3) a) W. Kinrt, Y. Fukuda, A. Camard, *Coord. Chem. Rev.*, 2001, **128**, 113-152, b) S.-I. Noro, N. Yanai, S. Kitagawa, T. Akutagawa, T. Nakamura, *Inorg. Chem.*, 2008, **47**,7360-7365, c) J. Lefebvre, R. J. Batchelor, D. B. Lenzoff, *J. Am. Chem. Soc.*, 2004, **126**, 16117-16125.

4) a) S.-I. Noro, *Phys. Chem. Chem. Phys.*, 2010, **12**, 2519-2531, b)

5) S.-I. Noro, K. Fukuhara, K. Kubo, T. Nakamura, *Cryst. Growth. Des.*, 2011, **11**, 2379-2385.

6) T. J. Egan, K. R. Koch, P. L. Swan, C. Clarkson, D. A. V. Schalkwyk, and P. J. Smith, *J. Med. Chem.,* 2004, **47**, 2926.

7)M. Hernández-Molina, J. Gonzálaias-Platas, C. Ruiz-Pérez, F. Llore and M. Julve, Inorg. Chim. Acta, 1999, **284**, 258-265.

8) B.-C. Tzeng, W.-F Fu, C.-M. Che, H.-Y. Chao, K.-K. Cheung, and S.-M. Peng, *J. Chem. Soc., Dalton Trans.,* **1999**, 1017.

9) *CrystalClear*, Molecular Structure Corporation, Orem, UT, 2001.

10) *SIR92*: A. Altomare, G. Cascarano, C. Giacovazzo, A. Guagliardi, M. Burla, G. Polidori, and M. Camalli, *J. Appl. Cryst.,* 1994, **27**, 435.

11) *DIRDIF99*, P. T. Beurskens, G. Admiraal, G. Beurskens, W. P. Bosman, R. de Gelder, R. Israel, and J. M. M. Smits (1999).

12) a)A. Schreiber, O. Krizanovic, E. C. Fusch. B. Lippert, F. Lianza, A. Albinati, S. Hill, D. M. L. Goodgame, H. Stratemeier, M. A. Hitchman, *Inorg. Chem.*, 1994, 33, 6101-6110, b) C. Chen, H. Qiu, F. Liu, W. Chen, *J. Chem. Crystallogr.*, 2007, **37**, 619-622, c) W. Chen, F. Liu, T. Nishioka, K. Matsumoto, *Eur. J. Inorg. Chem.*, 2003, 4234-4243, d) G. Fusch, E. C. Fusch, A. Erxleben, J. Hüttermann, H. –J. Scholl, B. Lippert, Inorg. Chim. Acta, **1996**, 252, 167-168 e) D. Neugebaur, B. Lippert, *J. Am. Chem. Soc.*, 1982, 104, 6596-6601

13) F. P. W. Agterberg, H. A. J. P. Kluit, W. L Driessen, J. Reedijk, H. Oevering, W. Buijs, N. Veldman, M. T. Lakin, A. L. Spek, *Inorg. Chim. Acta*, 1998, **267**, 183-192

14) a) H Oshio, M. Yamamoto, T. Ito, *Inorg. Chem.* **2002**, 41, 5817-5820, b) I. O. Fritsky, R. Ott, H. Pritzkow, R. Kramer, *Chem. –Eur. J.* **2001**, 7, 1221-1231

Chapter 4

Effects of counter anions on dimer-of-dimer structures of platinum(II)-copper(II) hetero dinuclear complexes

4-1 Introduction

There has been attracted attention of a sires of complexes displaying weak, non-covalent metal-metal interaction[1]. In these systems, formation of dimeric or oligomeric assemble structures between two or more metal complexes provide characteristic photophysical properties. Since these interactions are based on the assemble structures, the small perturbation such as the counter anion, solvated molecules afford the distinct photopysical properties[2].

In previous chapter, platinum(II)-copper(II) heterodinuclear complexes, *syn*-[PtCu(guest)(μ-pyt)$_2$(bpy)$_2$]$^{2+}$ complexes *syn*-[**PtCu-G**]. (pyt = pyridine-2-thilate, bpy = 2,2'-bipyridine, guest = CH_3CN for *syn*-[**PtCu-CH$_3$CN**]; acetone for *syn*-[**PtCu-acetone**]; MeOH for *syn*-[**PtCu-MeOH**]) were discussed. Under various recrystallization conditions, I obtained three crystals which include solvent molecules as an axial ligands of copper ion and found that these complexes form the dimer-of-dimer structures with different crystal packings. On the other hand, the counter ions are utilized as secondary building block in coordination polymers[3]. In addition, the Lewis acid copper(II) ion are known to interact with Lewis base molecules of counter anions even including PF_6^- anion with weak coordinating ablitiy. Mixing Taking advanteage of these interactions, , the use of the counter anions as additional ligands in *syn*-[**PtCu**] motif would be effective to arrange the different dimer-of-dimer structure.

In this chapter, copper(II)-platinum(II) hetero dinuclear complexes *syn*-[PtCu(X)(μ-pyt)$_2$(bpy)$_2$]$^+$ (*syn*-[**PtCu-X**]) containing different counter anion are discussed (X = PF_6^- for *syn*-[**PtCu-Cl**]; SCN^- for *syn*-[**PtCu-SCN**]; Cl^- for *syn*-[**PtCu-Cl**], Scheme 4-1). The combination of *syn*-[**PtCu**] molecular motif and three counter anion afford the *syn*-[**PtCu-X**] complexes containing one of the counter aninons coordinated to hetero metal ions. In crystal structure, two *syn*-[**PtCu-X**] units form dimer-of-dimer structure and the intermolecular Pt···Pt distances show the elongation in the order of donor numbers(DNs), indicating that the the intermolecular Pt···Pt interaction affect the axial ligand of counter anion even separated by copper(II) ion. Herein, the syntheses of syn-[**PtCu-X**] and their structures were discussed.

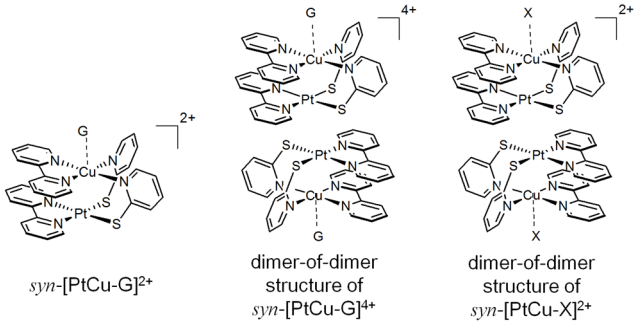

Scheme 4-1. Schematic motif of heterodinuclear motif

Experimental

Materials and syntheses. All starting materials were used as received from commercial sources, and the solvents were used without any purification. 2,2'-bipyridine (bpy), pyridine-2-thiol (Hpyt), and $CuCl_2$ were purchased from Wako. K_2PtCl_4 was purchased from Tanaka Kikinzoku. $[PtCl_2(bpy)]$[4], $[CuCl_2(bpy)]$[5] and $[Pt(pyt)_2(bpy)]$[6] were prepared according to the method previously reported. Elemental analyses were performed by a MICRO CORDER JM 10 analyzer at the Analysis Center, Hokkaido University.

[PtCu (μ-pyt)$_2$(bpy)$_2$](PF$_6$)$_2$ (*syn*-[**PtCu-PF$_6$**]): $[CuCl_2(bpy)]$ (29.0 mg, 0.1 mmol) was dissolved in 10 mL of H_2O and $[Pt(pyt)_2(bpy)]$ (57.1 mg, 0.1 mmol) in 5 mL of H_2O was added. The reaction mixture was stirred for 2 h at room temperature, and then filtered off to remove unreacted compounds. The resulting brown filtrate was treated with NH_4PF_6 (81.5 mg, 0.5 mmol) in 2 mL of water. The brown precipitate produced immediately was filtered and dried under reduced pressure. Yeild 78.9 mg (84.0%). Single crystals suitable for X-ray analysis were prepared from crude *syn*-[**PtCu**]by the diffusion method using hexane/acetone with crude of *syn*-[**PtCu**] at RT. Anal. Calcd for $C_{30}H_{24}CuF_{12}N_6S_2P_2Pt$: C, 33.32; H, 2.24; N, 7.77. Found: C, 33.16 H, 2.15; N, 7.74.

[PtCu(NCS)(μ-pyt)$_2$(bpy)$_2$](NCS) ([**PtCu-NCS**]): [**PtCu-NCS**] was synthesized by similar procedure using KSCN (97.1, 1.0 mmol) instead of NH_4PF_6. Yeild 62.2 mg (68.5%). The crystal for X-ray analysis was obtained prepared from crude by diffusion method using Et_2O/MeOH at 4 °C. Anal. Calcd. for $C_{32}CuH_{28}N_4O_2PtS_4$: C, 40.74; H, 2.99; N, 11.88. Found: C, 40.82; H, 2.86; N, 11.83

[PtCuCl(μ-pyt)$_2$(bpy)$_2$]Cl ([**PtCu-Cl**]): $[CuCl_2(bpy)]$ (58.1 mg, 0.2 mmol) was dissolved in 10 mL of H_2O and $[Pt(pyt)_2(bpy)]$ (114.2 mg, 0.2 mmol) in 20 mL of H_2O was added. The reaction mixture was stirred for 2 hr at room temperature, and then filtered off to remove unreacted compound. The brown filterate was evapotrated about 1 mL and 25 mL of acetone was added. The brown precipitate was then filtered and dried in vaquo. Yeild 78.9 mg (84.0%). The crystal for X-ray analysis was prepared from crude by diffusion method using Et_2O/MeOH at 4 °C. Anal. Calcd. for $C_{30}CuH_{30}Cl_2N_6O_3PtS_2$: C, 39.33; H, 3.30; N, 9.17, Found: C, 39.20; H, 3.36; N, 9.13.

X-ray diffraction measurements and structure analyses

A summary of the crystallographic data of the single-crystal X-ray diffraction for the *syn*-[**PtCu-PF$_6$**], *syn*-[**PtCu-SCN**], *syn*-[**PtCu-Cl**] complexes is given in Table 4-1. Each crystal was mounted on a glass fibre with silicon grease. All measurements for the three crystals were made on a

Rigaku AFC-7R diffractometer with Mercury CCD area detector, graphite monochromated Mo-$K\alpha$ radiation (λ = 0.71069 Å) and a rotating anode generator. The data were corrected for Lorentz and polarization effects. Diffraction data were collected and processed using CrystalClear[7]. The structures were solved using direct methods (SIR92)[8] and expanded using Fourier techniques (DIRDIF99)[9]. Full-matrix least-squares structural refinement based on F^2 was employed. The non-hydrogen atoms were refined anisotropically. The hydrogen atoms were refined using a riding model.

Table 4- 1 . Crystallographic data of of [**PtCu-X**]

	syn-[**PtCu-PF$_6$**](PF$_6$) ·2C$_3$H$_6$O	*syn*-[**PtCu-NCS**](NCS)• 3H$_2$O	*syn*-[**PtCu-Cl**]Cl•3MeOH
Formula	$C_{36}H_{36}CuF_{12}N_6O_2P_2PtS_2$	$C_{32}H_{24}CuN_8O_3PtS_4$	$C_{33}H_{36}Cl_2CuN_6O_3PtS_2$
Formula weight	1197.40	955.47	958.35
Crystal system	Monoclinic	Monoclinic	Triclinic
Space group	$P2_1/c$ (#14)	$P2_1/n$ (#14)	P-1 (#2)
a (Å)	13.622(1)	11.701(2)	11.248(4)
b (Å)	20.267(2)	12.936(3)	11.488(5)
c (Å)	16.082(2)	24.091(5)	14.988(6)
α (°)	90	90	77.26(1)
β (°)	106.2898(5)	97.393(1)	68.39(1)
γ (°)	90	90	88.15(1)
V (Å^3)	4262.0(8)	3616(1)	1753(1)
Z	4	4	2
T (K)	150	150	150
D_{calcd} (g cm^{-3})	1.866	1.755	1.815
μ (Mo $K\alpha$) (cm^{-1})	40.32	47.13	48.90
R_1 [a] ($F^2>2\sigma(F^2)$)	0.0497	0.0610	0.0342
wR_2 [b] (all data)	0.0812	0.1710	0.0959

[a] $R_1 = \Sigma||F_o| - |F_c||/\Sigma|F_o|$. [b] $wR_2 = [\Sigma w(F_o^2 - F_c^2)/\Sigma w(F_o)^2]^{1/2}$, $w = [\sigma_c^2(F_o^2) + (xP)^2 + yP]^{-1}$, $P = (F_o^2 - 2F_c^2)/3$.

4-3 Results and Discussions

4-3-1 Syntheses

The synthetic procedure of *syn*-[**PtCu-X**] is shown in Scheme 4-2. In previous chapter, the systematic introduction of hetero metal ions into the *syn*-[**PtM**] motif utilizing the affinity of coordinating atoms to metal ions were discribed. As in the case, a series of *syn*-[**PtCu-X**] complexes have been constructed from $[Pt(pyt)_2(bpy)]$ and $[CuCl_2(bpy)]$. Using different counter anions, hexafluoro- phospate, thiocyanate and chloride ions, three salts of *syn*-[**PtCu-X**] were obtained.

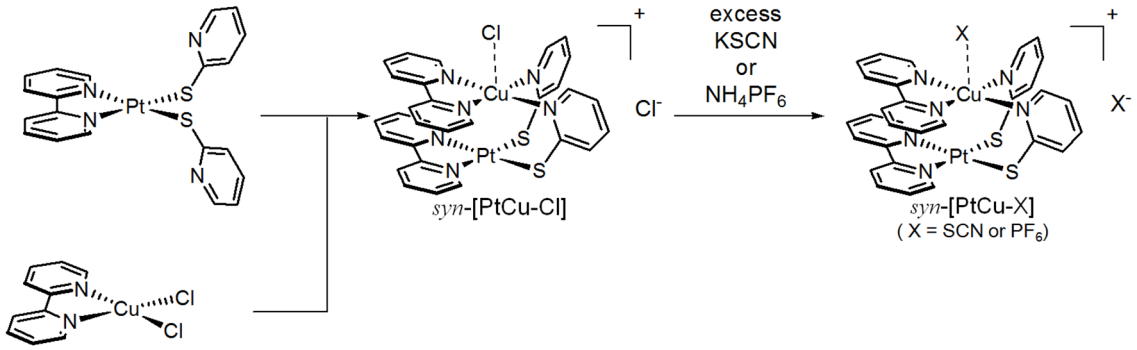

Scheme 4-2. Systematic introductions of *syn*-[**PtCu-X**]

4-3-2 Crystal structure

The selected bond distances and angles of *syn*-[**PtCu-X**] are shown in Table 4-2. All of cations have similar structural motifs *syn*-[**PtM**] basically. Platinum (II) ion and copper (II) ions are bridged by two pyt ligands adopt a *head-to-head* orientation. Two pyt ligands coordinate to the platinum ion with the thiol ion and to the copper ion with the nitrogen atom. The coordination spheres of platinum ion and copper ion in plane were completed by bpy ligand respectively. In all crystals, copper ion had an additional anionic ligand X^- on axial site to form monocationic *syn*-[**PtCu-X**]$^+$ motif. Therefore the coordination mode of platinum ion and copper ion is N_2S_2 for platinum ion and N_4X for copper ion. In all crystals, interestingly, two *syn*-[**PtCu-X**] units were arranged so that the Pt ions are closely located to form dimer-of-dimer structure.

The single crystal of *syn*-[**PtCu-PF_6**] was obtained from slow diffusion method of hexane to acetone solution. Figure 4-1a shows the structures of hexafluorophosphate salt of *syn*-[**PtCu-PF_6**]. *Syn*-[**PtCu-PF_6**] crystallized in monoclinic $P2_1/c$ space group. The copper ion has a PF_6^- anion at the axial site. Although PF_6^- anion is a weak coordinating ligand, Cu(1)-F(1) distance 2.740(3) Å is shorter than the sum of Van der Waals radius of Cu and F(2.87 Å), and P(1)-F(1) distance 1.612(3) Å is longer than those between phosphine and non-coordinating fluorine (1.585 – 1.604 Å), suggesting coordination of PF_6^- anion. The Cu···Pt distance is 2.7435(4) Å and the intermolecular

Pt···Pt distance in dimer-of-dimer structure (Figure 1b) is 3.3772(2) Å shorter than twice the van der Waals radius of Pt (3.50 Å), suggesting a Pt···Pt interaction between two *syn*-[**PtCu-PF$_6$**].

An ORTEP view of cation of *syn*-[**PtCu**-SCN] is depicted in Figure 4-2a. In *syn*-[**PtCu**-SCN] crystal, copper ion has an thiocyanate ion on the axial site with N-coordination mode. The thicyanate ion coordinates slightly bending from Cu···Pt axis with Cu-N-C bond angle 163.8°, and Cu-N bond distance is 2.287(7) Å. The intramolcular Cu···Pt bond distance is 2.8727(7) Å. In packing structure, another thiacyanate ion were located in void space and disordered. In the dimer-of-dimer structure, intermolecular Pt···Pt distance is 3.5268(3) Å, slightly longer than twice the van der Waals radius of Pt (3.50 Å), suggesting a little or no Pt-Pt interaction between two *syn*-[**PtCu-SCN**] (Figure 4-2b).

Figure 4-3a shows the cation of *syn*-[**PtCu**-Cl]. *Syn*-[**PtCu**-Cl] crystallized in $P\bar{1}$ space group. On the axial site of copper ion, Cl^- anion coordinates with Cu-Cl distance 2.285(8) Å. The intramolecular Cu···Pt distance is 2.9313(4) Å. In crystal, dimer-of-dimer structure was constructed by π-π stacking between thiol ligand and bpy plane (shortest thiol···bpy distance; 3.429 Å) instead of the intermolecular Pt···Pt interactions (intermolecular Pt···Pt distance: 4.4893(2) Å, Figure 4-3b). The bpy ligand coordinating copper ion also form the π-π stacking with neighboring another bpy ligand coordinating copper ion (shortest bpy···bpy distance; 3.385(4) Å).

In three crystals, one of anions coordinated to copper ion of *syn*-[**PtCu**]. Interestingly, axial ligands of anions affect the intramolecular Cu···Pt distances. The Lewis acid copper(II) ion are known to interact with Lewis base molecules[10]. The donor numbers (DNs) of PF_6^-, $SCN^-$and Cl^- anions are 2.18, 31.9 and 36.2[11] , respectively. and intermolecular Cu···Pt distances increase in this order (2.7435(4) Å for *syn*-[**PtCu**-PF_6] < 2.8727(7) Å for *syn*-[**PtCu**-SCN] < 2.9313(4) Å for *syn*-[**PtCu**- PF_6]). Notably, the intermolecular Pt···Pt distances in dimer-of-dimer structures also exhibit elongation in the order of DNs for axiali ligans (3.3772(2) Å for *syn*-[**PtCu**-PF_6] < 3.5268(3) Å for *syn*-[**PtCu**-SCN] < 4.4893(2) Å for *syn*-[**PtCu**- PF_6]). Doerrer and co-workers reported that dimer-of-dimer structure for [PtCo(tba)$_4$(OH_2)] have dimorphism and some of the electoron density from Co···Pt interactions is transferred to the intermolecular Pt···Pt interactions[12]. These results, therefore, suggest that the electron density from axial ligand in *syn*-[**PtCu**-X] affects not only intramolecular Cu···Pt interactions but also intermolecular Pt···PT interactions.

Table 4-2 Selected interatomic distances (Å) and dihedral angles (°) for three *syn*-[**PtCu-X**] complexes.

	syn-[**PtCu-PF_6**](PF_6) •$2C_3H_6O$	*syn*-[**PtCu-NCS**](NCS) •$3H_2O$	*syn*-[**PtCu-Cl**](Cl) •3MeOH
Selected distance(Å)	X = PF_6^-	X = NCS^-	X = Cl^-
Pt–S	2.298(1), 2.278(2)	2.282(2), 2.265(2)	2.2914(8), 2.2870(9)
Pt–N(bpy)	2.053(4), 2.067(3)	2.072(6), 2.068(6)	2.072(3), 2.069(2)
Cu–N(bpy)	1.999(4), 2.026(3)	2.019(6), 2.030(6)	2.028(3), 2.025(2)
Cu–N(pyt)	1.985(3), 1.995(4)	2.028(6), 2.042(7)	2.034(2), 2.047(3)
Cu-X	2.743(2)	2.285(8)	2.6658(9)
Cu···Pt (intramolecular)	2.7437(4)	2.8727(7)	2.9313(4)
Pt···Pt (intermolecular)	3.3775(2)	3.5268(3)	4.4893(2)

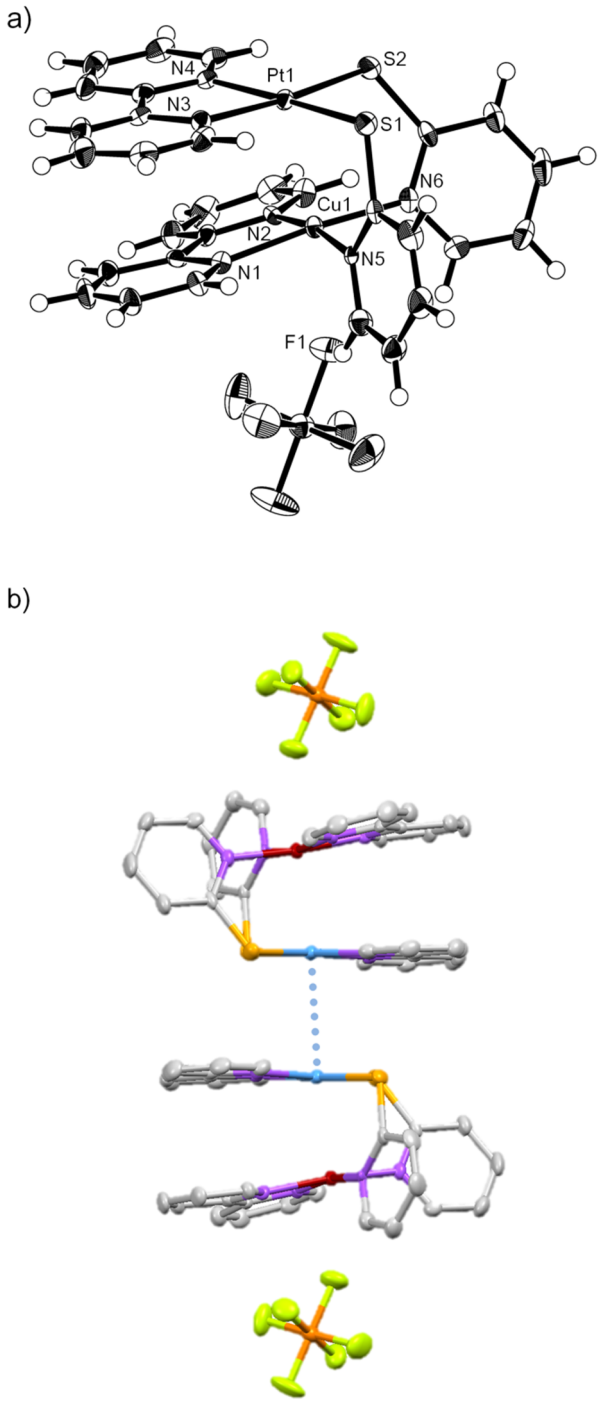

Figure 4-1. a) Molecular structure of *syn*-**[PtCu-PF$_6$]** (50% probability ellipsoids). b) The dimer-of-dimer structure of *syn*-**[PtCu-PF$_6$]**. The PF_6^- ions located at the top and bottom of the dimer-of-dimer motif are also included. The intermolecular Pt···Pt contact is shown by the dotted line.

a)

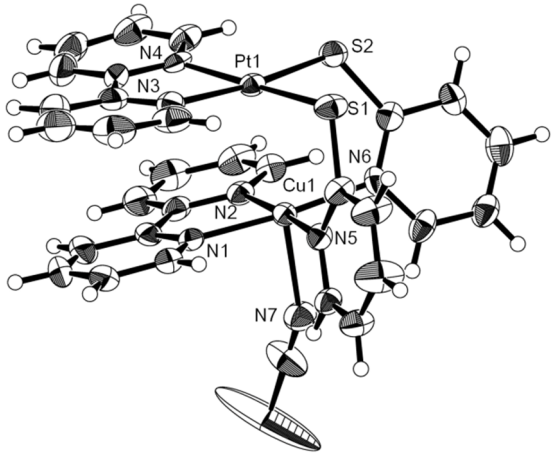

b)

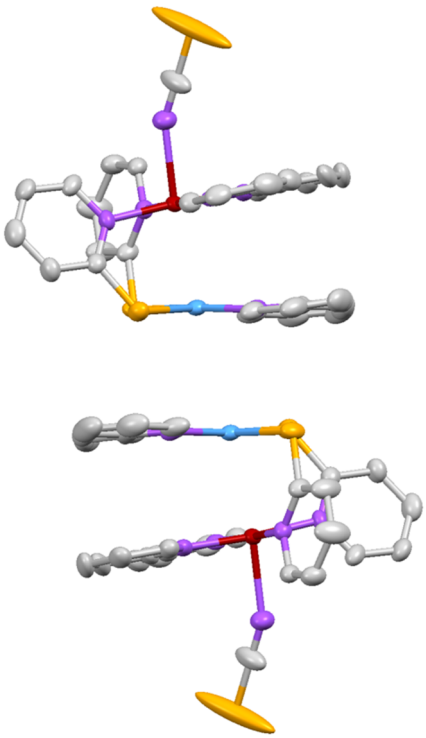

Figure 4-2. a) Molecular structure of *syn*-**[PtCu-SCN]** (50% probability ellipsoids). b) The dimer-of-dimer structure of *syn*-**[PtCu-SCN]**.

a)

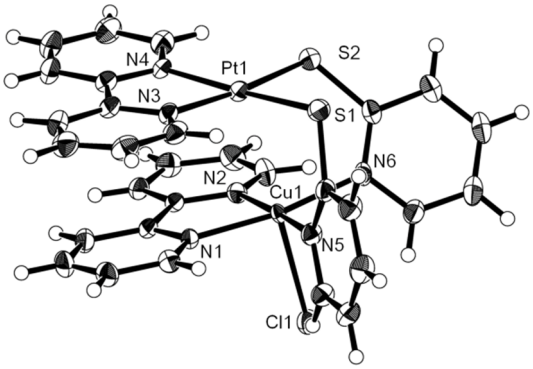

b)

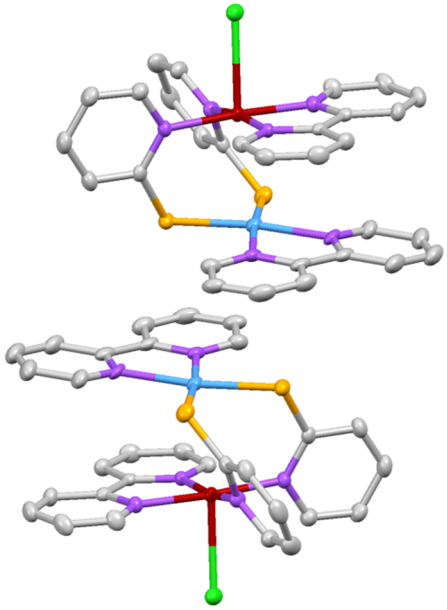

Figure 4-3. a) Molecular structure of *syn*-**[PtCu-Cl]** (50% probability ellipsoids). b) The dimer-of-dimer constructed by π-π stacking structure of *syn*-**[PtCu-Cl]**.

4-3-3 EPR spectra

Figure 4-4 and 4-5 depicted electron paramagnetic resonance (EPR) spectra of *syn*-[**PtCu-X**] complexes at 123K. In CH_3CN solution (Figure 4-4), all *syn*-[**PtCu-X**] complexes show similar spectra and the $g_{||}$ absorption (split into four components by copper nuclear hyperfine interaction) is lower field than the $g_{\perp}$ absorption band, displaying an axially symmetric EPR pattern. These feature of *syn*-[**PtCu-X**] complexes suggest that the spin states of monomer of *syn*-[**PtCu-X**] show little or no difference to each other. In powder sample (Figure 4-5), on the other hand, EPR spectra of *syn*-[**PtCu-X**] complexes show the different g value and anisotropic line width. This result imply that spin interaction and electronic state was purtabated based on the intermolecular interactions.

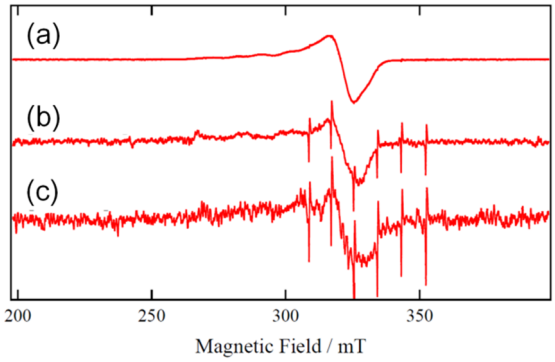

Figure 4-4. X-band EPR spectrum in CH_3CN solution of a) *syn*-[**PtCu-PF_6**], b) *syn*-[**PtCu-SCN**] and c) *syn*-[**PtCu-Cl**].

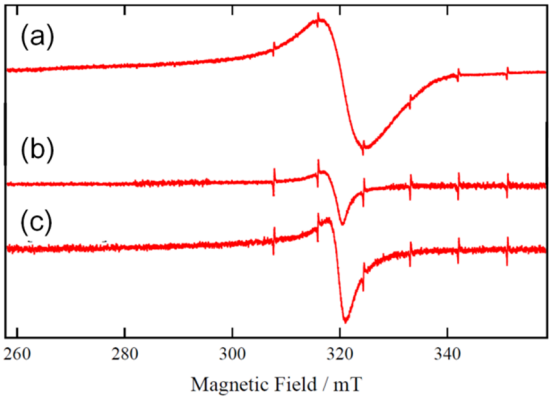

Figure 4-5. Powder X-band EPR spectrum of a) *syn*-[**PtCu-PF_6**], b) *syn*-[**PtCu-SCN**] and c) *syn*-[**PtCu-Cl**]

4-4 Conclusion

The introduction of one of the counter anions as additional ligands into *syn*-[**PtCu**] motif at the axial site of copper(II) ion give three copper(II)-platinum(II) complexes. The X-ray analyses revealed that all of complexes have one of the counter anions coordinated to copper ion and form the dimer-of-dimer structure. In dimer-of-dimer structure, the DNs of counter anions of axial ligands show correlations of not only intramolecular Cu···Pt distances but also intermolecular Pt···Pt distances, suggesting that the that the the intermolecular Pt···Pt interaction affect the axial ligand of counter anion even separated by copper(II) ion.

4-5 Refernces

1) a) M. Kato, *Bull. Chem. Soc. Jpn.*, 2007, **80**, 284-294, b) K. Matsumoto, M. Ochiai, *Coord. Chem. Rev.*,2002, **234**, 229-238, c) V.-W. W. Yam, K. K.-W. Lu, Chem. Soc. Rev., 1999, **28**, 323-334, d) L. H. Doerrer, Dalton. Trans., 2010, **39**, 3543-3553.

2) a) M. Saitoh, A. L .Barich, J. Yuassa, T. Kawai, *Inorg. Chem.*, 2010, 49, 7129-7134, b) V. Phillips, F. G. Baddour, T. Lasanta, J. M Lopez,-de-Luzuriaga, J. W. Bacon, J. A. Golen, A. L. Rheingold, L. H. Doerrer, *Inorg. Chim. Acta.*, 2010, 195-204, c) D. C. Powers, T. Ritter, *Organoteallics*. 2013, **32**, 2042-2045.

3) a) S. –I. Noro, N. Yanai, S. Kitagawa, T. Akutagawa, T. Nakamura, *Inorg.Chem.* **2008**, 47, 7360-7365, b) S. –I. Noro, R. Kitaura, M. Kondo, S. Kitagawa, T. Ishii, H. Matsuzaka, M. Yamashita, *J. Am. Chem. Soc.* **2002**, 2568-2583, c) K. Fukuhara, S.-I. Noro, K. Sugimoto, T. Akutagawa, K. Kubo, T. Nakamura, *Inorg. Chem.*, 2013, **52**, 4229–4237.

4) T. J. Egan, K. R. Koch, P. L. Swan, C. Clarkson, D. A. V. Schalkwyk, and P. J. Smith, *J. Med. Chem.,* 2004, **47**, 2926.

5)M. Hernández-Molina, J. Gonzálaias-Platas, C. Ruiz-Pérez, F. Llore and M. Julve, Inorg. Chim. Acta, 1999, **284**, 258-265

6) B.-C. Tzeng, W.-F Fu, C.-M. Che, H.-Y. Chao, K.-K. Cheung, and S.-M. Peng, *J. Chem. Soc., Dalton Trans.,* **1999**, 1017.

7) *CrystalClear*, Molecular Structure Corporation, Orem, UT, 2001.

8) *SIR92*: A. Altomare, G. Cascarano, C. Giacovazzo, A. Guagliardi, M. Burla, G. Polidori, and M. Camalli, *J. Appl. Cryst.,* 1994, **27**, 435.

9) *DIRDIF99*, P. T. Beurskens, G. Admiraal, G. Beurskens, W. P. Bosman, R. de Gelder, R. Israel, and J. M. M. Smits (1999).

10) W. Linert, Y. Fukuda, A. Camard, *Coord. Chm. Rev.*, 218, 113-152

11) S.-I. Noro, N. Yanai, S. Kitagawa, T. Akutagawa, T. Nakamura, *Inorg. Chem.*, 2008, **47**, 7360-7365

12) E. W. Dahl, F. G. Baddour, S. B. Fiedler, W. A. Hoffert, M. P. Shores, G. T. Yee, J. –P. Djukic, J. W. Bacon, A. L. Rhcingold, L. H. Doerrer, *Chem. Sci.*, 2012, **3**, 602-609

Chapter 5

Syntheses and Structures of platinum(II)-cobalt(II) and platinum(II)-nickel(II) hetero dinuclear complexes

5-1 Introduction

The metal-metal interaction between closed chell metal toms have been widely recognized, and attracted much attention to charactreristic properties such as catalyst[1)], photophysical properties[2)], electric conductivity[3)]. These interactions is often found the complexes containing d^8 or d^{10} metal ions such as Pt^{2+} [4)],Pd^{2+} [5)], Au^{+} [6)] and Cu^{+} [7)] ions. In addition, the heterometal complexes are also promising precursors in developing nanostructured materials including molecular scale electronic, optical and chemical devics[8),9)].

In previous chapter, the hetero dinuclear copper(II)–platinum(II) complexes *syn*-$[PtCu(\mu\text{-pyt})_2(bpy)_2]^{2+}$ (*syn*-[**PtCu**]) were described (pyt = pyridine-2-thilate, bpy = 2,2'-bipyridine). In *syn*-[**PtCu**], various recrystallization conditions and different counter anions afford a sires of the structures which include solvent molecules or counter anions as axial ligands of copper(II) ion at the axial site. The introduction of 3d metal ion into *syn*-[**PtM**] molecular motif, thus, would be effective to construction of different molecular arrangement including the solvent molecules as an axial ligand of 3d metal ion.

In this chapter, the heterodinuclear complexes *syn*-$[PtM\text{-}(CH_3CN)(\mu\text{-pyt})_2(bpy)_2]^{2+}$, *syn*-[**PtM-$CH_3$CN**] consisting of platinum(II) and 3d metal(II) ions (M = Co^{2+} for *syn*-[**PtCo-CH_3CN**]; Ni^{2+} for *syn*-[**PtNi-CH_3CN**] have been newly synthesized. The X-ray structure analyses revealed that each *syn*-[**PtM-CH_3CN**] complex has dimorphism and all of structures have one of CH_3CN solvated molecules as an axial ligand on the 3d metal ions. The structures of dimorphism both in *syn*-[**PtCo-CH_3CN**] and *syn*-[**PtNi-CH_3CN**] complex are isostructural each other and form the dimer-of-dimer structure. Herein, the syntheses and the structure of *syn*-[**PtM-CH_3CN**] complex were discussed..

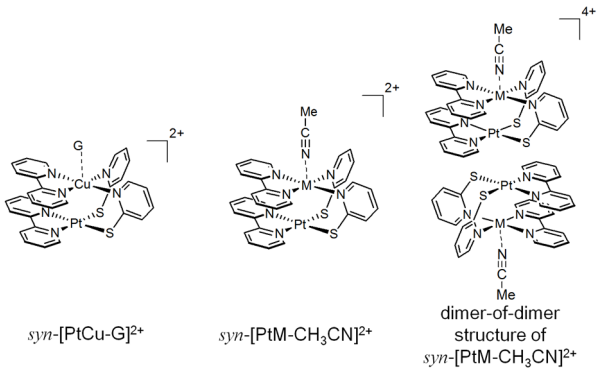

Scheme 5-1. Hetero dinuclear *syn*-[**PtM**] motifs.

5-2 Experimental

5-2-1 Materials and syntheses. All starting materials were used as received from commercial sources, and the solvents were used without any purification. 2,2'-bipyridine (bpy), pyridine-2-thiol (Hpyt), and $NiCl_2$, $CuCl_2$, $CoCl_2$ were purchased from Wako. K_2PtCl_4 was purchased from Tanaka Holdings. $[PtCl_2(bpy)]$[10], $[NiCl_2(bpy)]$[11], $[CoCl_2(bpy)]$[12] and $[Pt(pyt)_2(bpy)]$[13] were prepared according to the method previously reported. Elemental analyses were performed by a MICRO CORDER JM 10 analyzer at the Analysis Center, Hokkaido University.

syn-$[PtCo(CH_3CN)(pyt)_2(bpy)_2](PF_6)_2$ (α- and β–*syn*-[**PtCo-CH$_3$CN**]): $[CoCl_2(bpy)]$ (57.2 mg, 0.2 mmol) was dissolved in H_2O 10 mL and $[Pt(pyt)_2(bpy)]$ (114.2 mg, 0.1 mmol) in 10 mL of EtOH was added. The reaction mixture was stirred for 12 hr at room temperature, and then filtered off to remove unreacted compound. The bright red filtrate was treated with NH_4PF_6 (326.0 mg, 2.0 mmol) in 2 mL of water. The brown precipitate was immediately emerged and then filtered and dried under reduced pressure. Yield 95.7 mg (44.4%). Dark red crystals suitable for X-ray diffraction were obtained by diffusion method using Et_2O / CH_3CN at 4 °C. Anal. Calcd. for $C_{30}H_{26}CuF_{12}N_8OP_2PtS_2$: C, 32.92; H, 2.39; N, 7.68. Found: C, 32.85; H, 2.42; N, 7.74

syn-$[PtNi(CH_3CN)(pyt)_2(bpy)_2](PF_6)_2$ (α- and β-*syn*-[**PtNi-CH$_3$CN**]): *syn*-[**PtNi-CH$_3$CN**] was synthesized by a similar procedure as α- and β-*syn*- [**PtCo-CH$_3$CN**], but using $[NiCl_2(bpy)]$ instead of $[CoCl_2(bpy)]$. Yield 61.0 mg (56.8%). Dark red crystals suitable for X-ray diffraction were obtained by diffusion method using Et_2O / CH_3CN at 4 °C. Anal. Calcd. for $C_{30}H_{26}F_{12}NiN_8OP_2PtS_2$: C, 32.92; H, 2.38; N, 7.68. Found: C, 32.66; H, 2.52; N, 7.64.

5-2-2 X-ray diffraction measurements and structure analyses

A summary of the crystallographic data of the single-crystal X-ray diffraction for the both form of *syn*-[**PtCo-CH$_3$CN**] and *syn*-[**PtNi-CH$_3$CN**] complexes is given in Table 1. Each crystal was mounted on a glass fibre with silicon grease. All measurements for the three crystals were made on a Rigaku AFC-7R diffractometer with Mercury CCD area detector, graphite monochromated Mo-*K*α radiation (λ = 0.71069 Å) and a rotating anode generator. The data were corrected for Lorentz and polarization effects. Diffraction data were collected and processed using CrystalClear.[14] The structures were solved using direct methods (SIR92)[15] and expanded using Fourier techniques (DIRDIF99).[16] Full-matrix least-squares structural refinement based on F^2 was employed. The non-hydrogen atoms were refined anisotropically. The hydrogen atoms were refined using a riding model.

Table 5-1. . Crystallographic data of of [**PtM-CH_3CN**]

	α-*syn*-[**PtCo-CH_3CN**] $(PF_6)_2 \cdot 2CH_3CN$	α-*syn*-[**PtNi-CH_3CN**]($PF_6)_2 \cdot 2CH_3CN$	β-*syn*-[**PtCo-CH3CN**] $(PF_6)_2 \cdot 2CH_3CN$	β-*syn*-[**PtNi-CH3CN**]($PF_6)_2 \cdot 2CH_3CN$
Formula	$C_{36}H_{33}CoN_9F_{12}P_2PtS_2$	$C_{36}H_{33}N_9NiF_{12}P_2PtS_2$	$C_{36}H_{33}CoN_9F_{12}P_2PtS_2$	$C_{36}H_{33}N_9NiF_{12}P_2PtS_2$
Formula weight	1145.33	1113.24	1145.33	1145.33
Crystal system	Monoclinic	Monoclinic	Monoclinic	Monoclinic
Space group	$P2_1/n$ (#14)	$P2_1/c$ (#14)	$P2_1/c$ (#14)	$P2_1/c$ (#14)
a (Å)	11.923(3)	11.928(2)	11.609(4)	11.651(2)
b (Å)	13.584(3)	13.630(2)	19.091(5)	19.250(3)
c (Å)	27.258(7)	27.094(5)	19.727(6)	19.875(3)
α (°)	90	90	90	90
β (°)	102.608(3)	102.1480(8)	100.758(4)	100.990(3)
γ (°)	90	90	90	90
V (Å^3)	4308(1)	4306(1)	4295(2)	4376(1)
Z	4	4	4	4
T (K)	150	150	150	200
D_{calcd} (g cm^{-3})	1.849	1.850	1.855	1.855
μ (Mo $K\alpha$) (cm^{-1})	38.79	39.33	38.91	38.67
R_1 [a] ($F^2>2\sigma(F^2)$)	0.0482	0.0428	0.0402	0.0386
wR_2 [b] (all data)	0.1184	0.1108	0.1156	0.1027

[a] $R_1 = \Sigma||F_o| - |F_c||/\Sigma|F_o|$. [b] $wR_2 = [\Sigma w(F_o^2 - F_c^2)/\Sigma w(F_o)^2]^{1/2}$, $w = [\sigma_c^2(F_o^2) + (xP)^2 + yP]^{-1}$, $P = (F_o^2 - 2F_c^2)/3$

5-3 Results and Discussions

5-3-1 Syntheses

The synthetic procedure of *syn*-[**PtM-CH$_3$CN**] is shown in Scheme 5-2. In previous chapter, the syntheses of hetero dinuclaer complexes *syn*-[**PtPd**], *syn*-[**PtAu**], *syn*-[**PtCu**] by stepwise introduction of metal ion into *syn*-[**PtM**] motifs were discribed. As in the case, *syn*-[**PtM-CH$_3$CN**] have been obtained from the reaction of [Pt(pyt)$_2$(bpy)] and [MCl$_2$(bpy)] utilizing the differences of affinities of coordinating atoms to metal ion, suggesting that systematic introduction of metal ion from 3d metal ions to 5d metal ion were succeeded. A number of hetero metal complexes containing Pt(II) and 3d or 4d metal ions linked by N,O-bridigng ligand have been reported[17], however, systematic introduction from 3d to 5d metal ions in same molecular motif were limited. In *syn*-[**PtM**] motifs, the pyt lingad with N,S-coordinating atoms could lead the syntheses of dinuclar *syn*-[**PtM**] motifs.

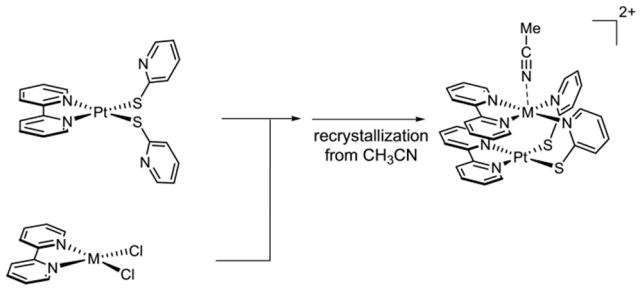

Scheme 5-2. Systematic introductions of *syn*-[**PtM-CH$_3$CN**]

5-3-2 Crystal structure

The recrystallization from the diffusion method of Et$_2$O into CH$_3$CN solution of *syn*-[**PtCo**] and *syn*-[**PtNi**] have been yielded the two dimorphism, α-form and β-form, while the compositions of these form of are comparable to each other. The selected bond distances and angles of α-form and β-form in *syn*-[**PtCo-CH$_3$CN**], *syn*-[**PtNi-CH$_3$CN**] as well as α-form of *syn*-[**PtCu-CH$_3$CN**] are shown in Table 5-2. The α-forms of *syn*-[**PtCo-CH$_3$CN**] and *syn*-[**PtNi-CH$_3$CN**] are found to be isostructural to that of *syn*-[**PtCu-CH$_3$CN**] reported in chapter 3, and β-*syn*-[**PtCo-CH$_3$CN**] and β-*syn*-[**PtNi-CH$_3$CN**] also are found to be isostructural. This result suggests that the valence of metal ion is superior to the number of d electron and ion radius of metal ion in assemble structure of *syn*-[**PtM**] motif including 3d metal ions.

The structure of α-form and β-form of *syn*-[**PtCo-CH$_3$CN**] was depicted in Figure 5-1 and 5-2, and those of *syn*-[**PtNi-CH$_3$CN**] was also shown in Figure 5-3 and 5-4, respectively. All of cations have similar structural motifs *syn*-[**PtM**] basically. Platinum(II) ion and metal(II) ions are bridged by two

pyt ligands adopt a *head-to-head* orientation. Two pyt ligands coordinate to the platinum ion with the thiol ion and to another ion with the nitrogen atom. The coordination spheres of platinum ion and metal ion in plane were completed by bpy ligand respectively. The bond distance between M ion and Pt ion are similar to each other. (α-*syn*-[**PtCo-CH_3CN**]; 2.8023(4) Å, α-*syn*-[**PtNi-CH_3CN**]; 2.7657(6) Å, α-*syn*-[**PtCu-CH_3CN**]; 2.8089(8) Å, β-*syn*-[**PtCo-CH_3CN**]; 2.8078(8) Å, β-*syn*-[**PtNi-CH_3CN**]; 2.7752(4) Å). In two forms of *syn*-[**PtCo-CH_3CN**], the bond distances between cobalt(II) ion and nitrogen atoms of pyt and bpy ligand are range from 2.005(3)-2.054(5) Å, suggesting low spin state of cobalt(II) ion. Interestingly, one of the acetonitrile molecules solvated in the crystals coordinates to metal ions as an additional axial ligand, while no additional acetonitrile was coordinated to the hetero metal ions in the cryastals of *syn*-[**PtPt**], *syn*-[**PtPd**] and *syn*-[**PtAu**]. This is thought to be due to the variety of coordination number of 3d metal ions of cobalt(II), nickel(II), copper(II) ions in comparison to the square-planer coordination mode of palladium(II), platinum(II), gold (III) ions with d^8 electron configuration.

In botn forms of *syn*-**[PtCo-CH_3CN]** and *syn*-**[PtNi-CH_3CN]** crystals, interestingly, two *syn*-[**PtM**] units are arranged so that the Pt ions are closely located to adopt the dimer-of-dimer structure (M = Co^{2+}, Figures 5-1b) and 5-2b); M = Ni^{2+}, Figures 5-3b) and 5-4b)). In α-form, dimer-of-dimer structure form the π-π stacking with adjacent dimer-of-dimer structure each other to arrange linearly in *bc* plane (Figures 5-5a), 5-6a) and 5-7). On the other hand, in β-form, the lack of the π-π stacking of bpy ligand between dimer-of-dimer structure give zigzag alignment of dimer-of-dimer structure in *bc* plane(Figures 5-5b) and 5-6b)). The intermolecular Pt···Pt distances in α-form is shorter than those of b-form (*α-syn*-[**PtCo-CH_3CN**]; 3.5444(1) Å< β-*syn*-[**PtCo-CH_3CN**]; 3.5934(8) Å, α-*syn*-[**PtNi-CH_3CN**]; 3.5763(2) Å< β-*syn*-[**PtNi-CH_3CN**]; 3.6816(5) Å), suggesting that the intermolrculra the π-π stacking of bpy ligand with adjacent dimer-of-dimer structure force the tight packing to shorten the intermolecular Pt···Pt distances.

Table 5-2 Selected interatomic distances (Å) and dihedral angles (°) for α-*syn*-[**PtCo-CH_3CN**]$_2$ and α-*syn*-[**PtNi-CH_3CN**] complexes as well as α-*syn*-[**PtCu-CH_3CN**], and β-*syn*-[**PtCo-CH_3CN**] and β-*syn*-[**PtNi-CH_3CN**]

	α-*syn*-[**PtCo-CH_3CN**]$(PF_6)_2 \cdot 2CH_3CN$	α-*syn*-[**PtNi-CH_3CN**]$(PF_6)_2 \cdot 2CH_3CN$	α-*syn*-[**PtCu-CH_3CN**]$(PF_6)_2 \cdot 2CH_3CN$	β-*syn*-[**PtCo-CH_3CN**]$(PF_6)_2 \cdot 2CH_3CN$	β-*syn*-[**PtNi-CH_3CN**]$(PF_6)_2 \cdot 2CH_3CN$
Selected distance(Å)	M = Co	M = Ni	M = Cu	M = Co	M = Ni
Pt–S	2.2694(9), 2.286(1)	2.286(1), 2.271(1)	2.293(2), 2.272(2)	2.282(1), 2.271(1)	2.272(1), 2.282(1)
Pt–N(bpy)	2.060(3), 2.060(3)	2.054(3), 2.070(3)	2.067(6), 2.061(7)	2.071(4), 2.067(4)	2.065(4), 2.066(4)
M–N(bpy)	2.014(3), 2.005(3)	2.060(3), 2.071(3)	2.026(6), 2.011(7)	2.042(5), 2.018(4)	2.066(4), 2.094(4)
M–N(pyt)	2.034(3), 2.054(3)	2.098(3), 2.089(3)	2.029(7), 2.020(6)	2.052(4), 2.054(5)	2.083(3), 2.090(4)
M-N (CH_3CN)	2.197(3)	2.098(3)	2.558(8)	2.168(5)	2.085(4)
M···Pt (intra-molecular)	2.8023(4)	2.7657(6)	2.8084(8)	2.8078(8)	2.7754(6)
Pt···Pt (inter-molecular)	3.5444(1)	3.5763(2)	3.5109(3)	3.5934(8)	3.6816(5)

a)

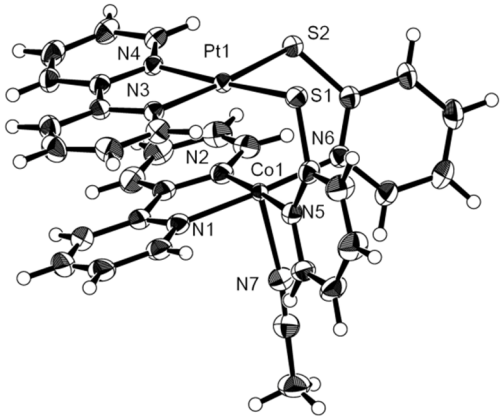

b)

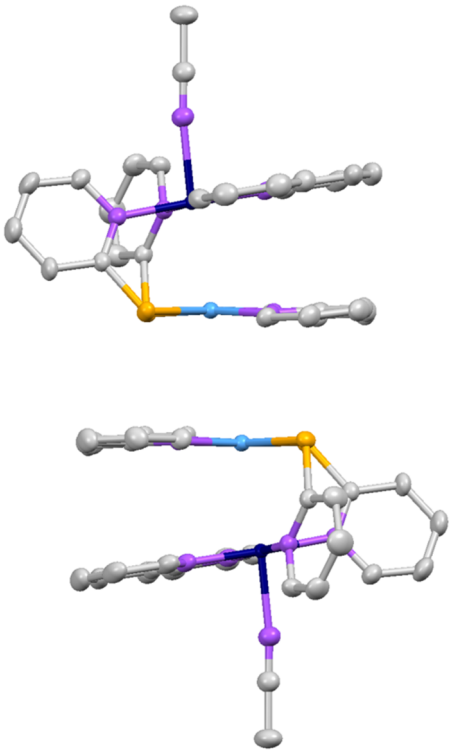

Figure 5-1. a) Molecular structure of α-*syn*-**[PtCo-CH$_3$CN]** (50% probability ellipsoids). b) The dimer-of-dimer structure of α-*syn*-**[PtCo-CH$_3$CN]**..

a)

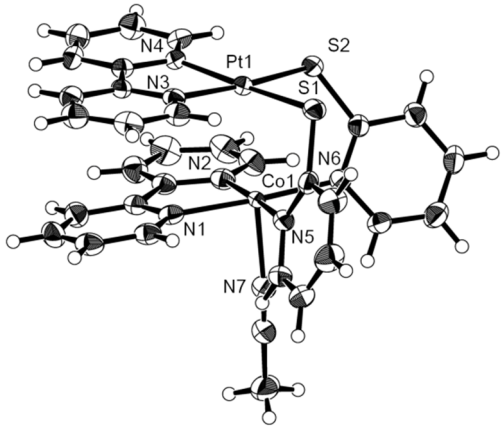

b)

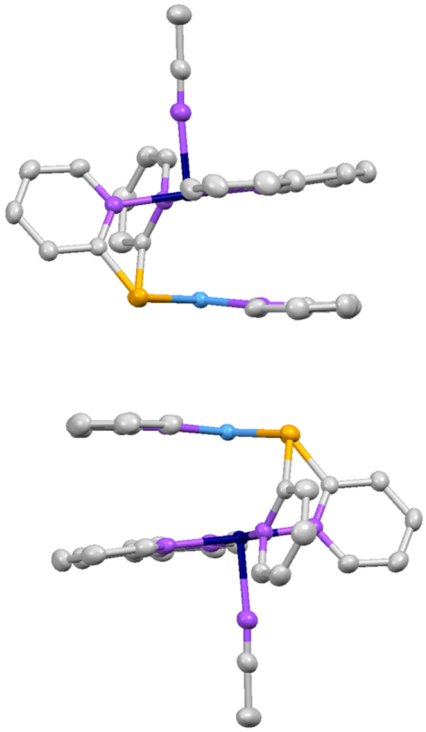

Figure 5-2. a) Molecular structure of β-*syn*-**[PtCo-CH$_3$CN]** (50% probability ellipsoids). b) The dimer-of-dimer structure of β-*syn*-**[PtCo-CH$_3$CN].**

a)

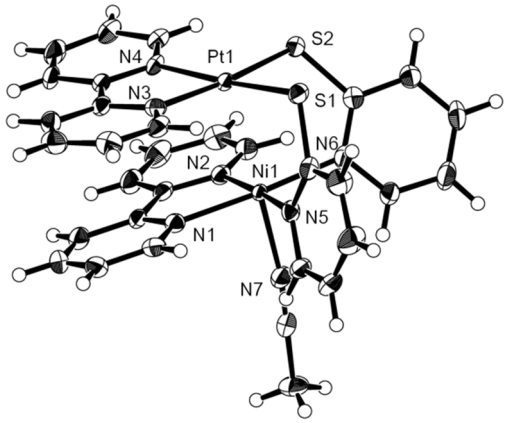

b)

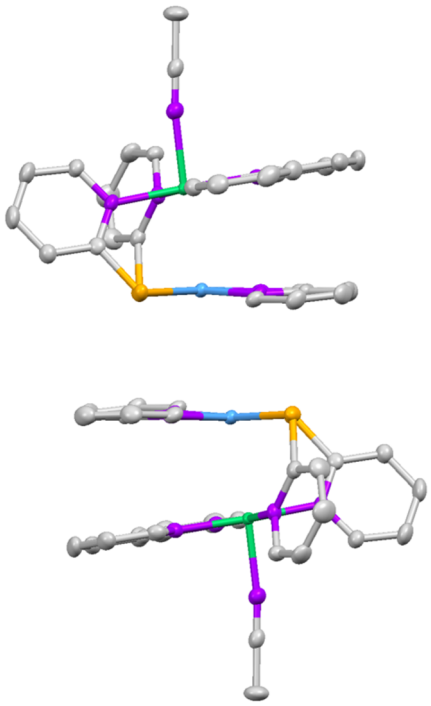

Figure 5-3. a) Molecular structure of α-*syn*-**[PtNi-CH$_3$CN]** (50% probability ellipsoids). b) The dimer-of-dimer structure of α-*syn*-**[PtNi-CH$_3$CN].**

a)

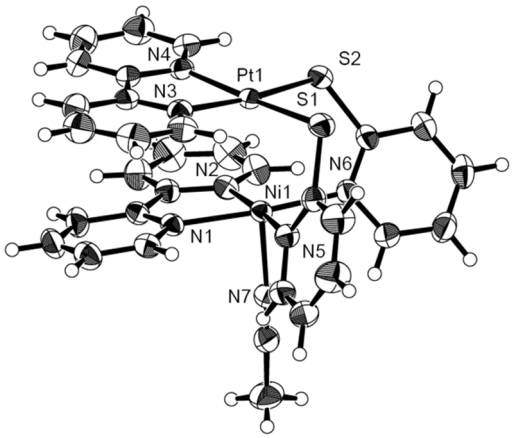

b)

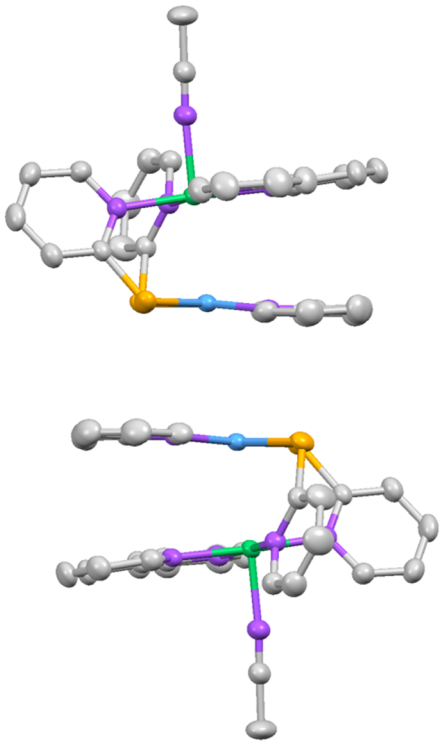

Figure 5-4. a) Molecular structure of β-*syn*-**[PtNi-CH$_3$CN]** (50% probability ellipsoids). b) The dimer-of-dimer structure of β-*syn*-**[PtNi-CH$_3$CN].**

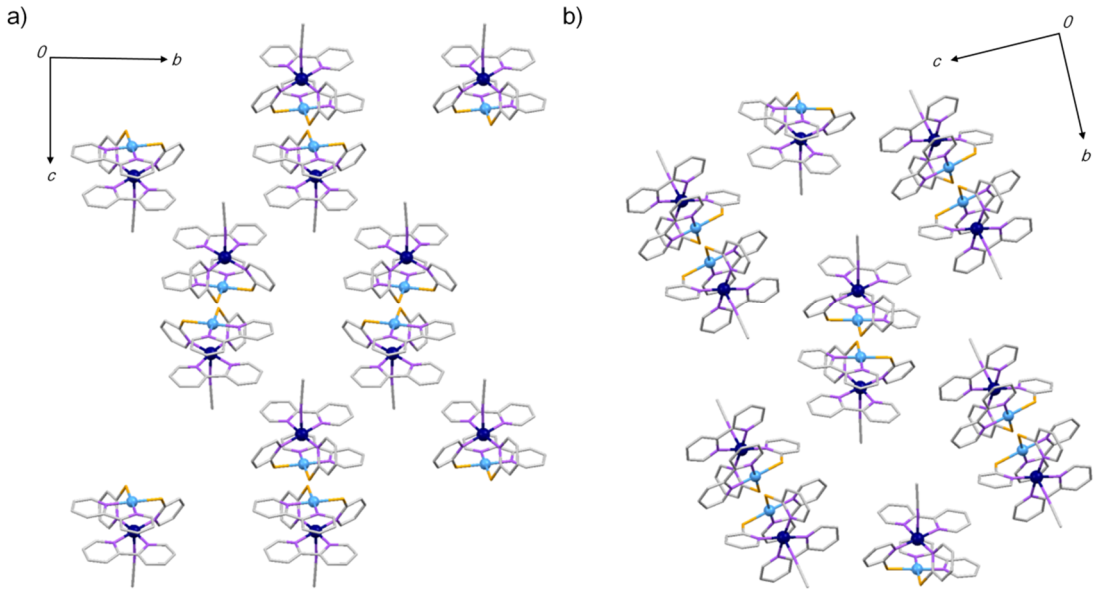

Figure 5-5. Comparison of the packing of dimer-of-dimer structure in a) α-*syn*-**[PtCo-CH$_3$CN]** and b) β-*syn*-**[PtCo-CH$_3$CN]**.

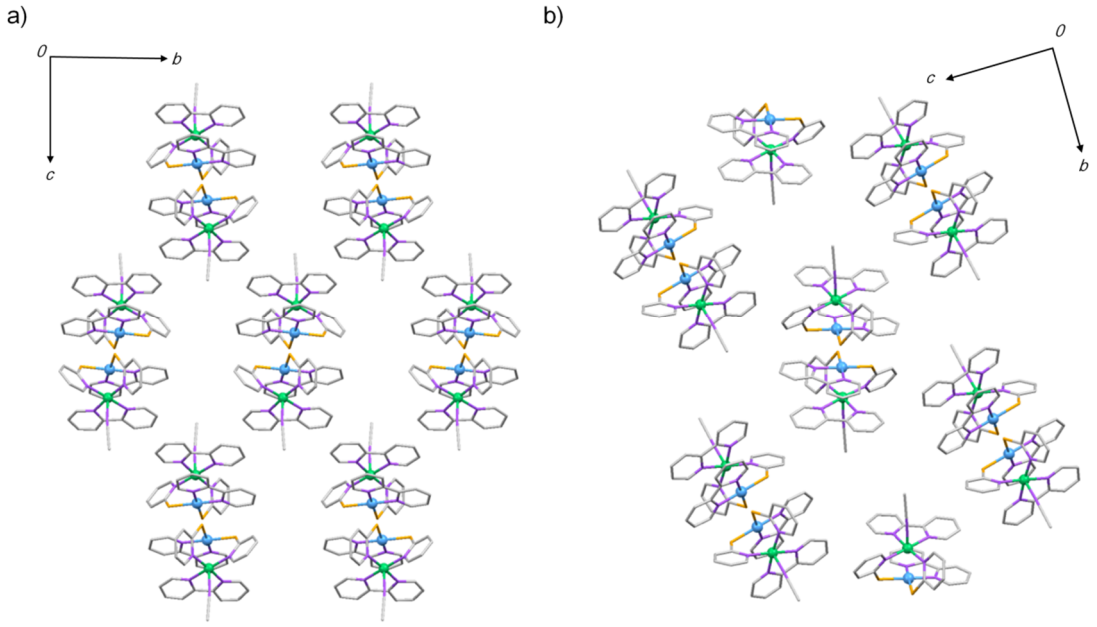

Figure 5-6. Comparison of the packing of dimer-of-dimer structure in a) α-*syn*-**[PtNi-CH$_3$CN]** and b) β-*syn*-**[PtNi-CH$_3$CN]**.

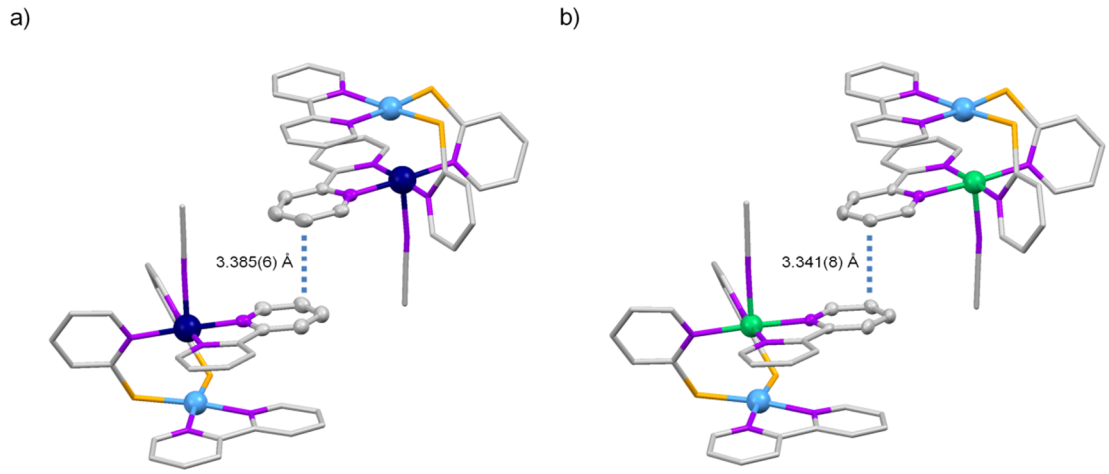

Figure 5-7. The π-π stacking structure in a) α-*syn*-**[PtCo-CH_3CN]** and. b) α-*syn*-**[PtNi-CH_3CN].**

5-4 Conclusion

The introduction of 3d metal ion into *syn*-[PtM] motif were systematically succeeded to obtained two forms of *syn*-[**PtCo-CH_3CN**] and *syn*-[**PtNi-CH_3CN**]. Each complexes has one of the acetonitrile molecule solvated in packing as axial ligands on 3d metal ions. In α-form, the dimer-of-dimer structures were arranged linearly in bc plane due to the π-π stacking of bpy ligand between neghbouring dimer-of-dimer structure. The intermolecular Pt···Pt distances of a-forms are shorter than that of β-form which does not have π-π stacking of bpy ligand, suggesting that that the intermolrculra the π-π stacking of bpy ligand with adjacent dimer-of-dimer structure force the tight packing to shorten the intermolecular Pt···Pt distances.

.

Refernces

References

1) a) D. C. Powers, T. Ritter, *Nature Chem.*, 2009 1, 302-309. b) D. C. Powers, T. Ritter, *Acc. Chem. Res.*, 2012, **45**, 840-850, c) K. Matsumoto, M. Ochiai, *Coord. Chem. Rev.*, 2002, **231**, 229-238,

2) a) V. W.-W. Yam, K. K.-W. Lu, *Chem. Soc., Rev.*, 1999, **28**, 323-334, b) X. Zhang, B. Li, Z.-H. Chen, Z.-N. Chen, *J. Mat. Chem.*, 2012, 22, 11427-11441, c) M. Kato, *Bull. Chem. Soc. Jpn.*, **80**, 287-294, d) L. H. Doerrer, Dalton Trans., 2010, **39**, 3544-3553, eD. M. Roundhill, H. B. Gray, C.-M. Che, *Acc. Chem. Res.*, 1989, **29**, 55-61.

3) a) I. P.-C. Liu, W.-Z. Wang, S.-M. Peng, *Chem. Commun.*, **2009**, 4323-4331, b) B. Ma, J. Li, P. I. Djurovich, M. Yousufuddin, R. Bau, M. E. Thompson, *J. Am. Chem. Soc.*, 2005, **127**, 28-29, c) J. Ni, Y. –H. Wu, Xu. Zhang, B. Li, L. –Y. Zhang, Z. –N. Chen, *Inorg. Chem.*, 2009, **48**, 10202-10210,

4) a) W. Lu, M. C. W. Chan. K. –K. Cheung, C. –M. Chi., *Organometallics*, 2001, **20**, 2477-2488, b) T. J. Wadas, Q. –M. Wang, Y. -j. Kim, C.Flaschenreim, T. N. Bianton, R. Eisenberg, *J. Am. Chem. Soc.*, 2004, **126**, 16841-16849, c) A. Kobayashi, H. Hara, T. Yonemura, H. –C. Chang, M. Kato, *Dalton Trans.*, 2012, **41**, 1876-1888, d) A. Kobayashi, Y. Fukuzawa, H. –C. Chang, M. Kato, *Inorg. Chem.*, 2012, **51**, 7508-7519, e) V. W-W. Yam, K. M. Chung, N. Zhu, *J. Am. Chem. Soc.*, 2002, **124**, 8506-8507.

5) a) D. C. Powers, T. Ritter, *Organometallics*, 2013, **32**, 2042-2045, b) C.-L. Yao, L. P. He, J. D. Korp, J. L. Bear, *Inorg. Chem,*, 1989, **27**, 4389-4395.

6) a) C.-M. Che, S.-W. Lai, *Coord. Chem. Rev.*, 2005, **249**, 1296-1309, b) M. Saitoh, A. L. Balch, J. Yuasa, T. Kawai, 2010, **49**, 7129-7134, c) Y.-A. Lee, R. Eisenberg, *J. Am. Chem. Soc.*, 2003, **125, 7778-7779, d)** H. Ito, T. Saito, N. Oshima, N. Kitamura, S. Ishizaka, Y. Hinatsu, M. Wakeshima, M. Kato, K. Tsuge, M. Sawamura, *J. Am. Chem. Soc.*, 2008, **130**, 10044-10045.

7) a) R. G. Raptis, J. P. Rackler, Jr, *Inorg. Chem.*,1988, **27** , 4179 – 4182, b) H. V. R. Dias, H. V. K. Diyabalanage, M. G. Eldabaja, O. Elbjeirami, M. A. Rawashdeh-Omary, M. A. Omary, *J. Am. Chem. Soc.,* 2005*,* **127**, 7489-7501

8) a) M.-M. Rohmer, I. P.-C. Lin, J. –C. Lin, M. -J. Chin, C.-H. Lee, G. –H. Lee, M. Bènard, Z. López, S. –M. Peng, *Angew. Chem. Int. Ed.*, 2007, **46**, 3533-2536, b) M. Kiguchi, J. Inatomi, Y. Takahashi, R. Tanaka, T. Osuga, T. Murase, M. Fujita, T. Tada, S. Watanabe, *Angew. Chem. Int. Ed.* , 2013, **52**, 6202 –6205, c) K. Uemura, K. Fukuki, K. Yamasaki, K. Matsumoto, M. Ebihara, *Inorg. Chem.*, 2010, **49**, 7323-7330.

9) a) F. G. Baddour. S. R. Fiedler, M. P. Shores, J. A. Golen, A. L. Rheingold, L. H. Doerrer, Inorg Chem., 2013, **52**, 4926–4933, b) E. W. Dahi, E. G. Baddour, S. R. Fiedler, W. A. Hoffert, M. P. Shores, G. L. Yee, J. –P. Djukie, W. Bacon, A. L. Rheingold, L. H. Doerrer, *Chem. Sci.*, 2012, **3**, 602-609.

10) T. J. Egan, K. R. Koch, P. L. Swan, C. Clarkson, D. A. V. Schalkwyk, and P. J. Smith, *J. Med. Chem.,* 2004, **47**, 2926.

11) D. G. Yakhvarov,_ E. H._Hawkins, R. M. Kagirov, Y. H. Budnikova, Y. S. Ganushevich, O. G. Sinyashina, *Russian Chem. Bull. Int. Ed.*, 2007. **56**, 935-942.

12) Boone Brewer, Neil R. Brooks, S. Abdul-Halim, A. G. Sykes, *J. Chem. Cryst.*,2003, **33**, 651-662.

13) B.-C. Tzeng, W.-F Fu, C.-M. Che, H.-Y. Chao, K.-K. Cheung, and S.-M. Peng, *J. Chem. Soc., Dalton Trans.,* **1999**, 1017.

14) *CrystalClear*, Molecular Structure Corporation, Orem, UT, 2001.

15) *SIR92*: A. Altomare, G. Cascarano, C. Giacovazzo, A. Guagliardi, M. Burla, G. Polidori, and M. Camalli, *J. Appl. Cryst.,* 1994, **27**, 435.

16) *DIRDIF99*, P. T. Beurskens, G. Admiraal, G. Beurskens, W. P. Bosman, R. de Gelder, R. Israel, and J. M. M. Smits (1999).

17) a) W. Zhen, K. Matsumoto, *E. J. Inorg. Chem.*, **2002**, 2661-2670, b) W. Chen, F. Liu, T. Nishioka, K. Matsumoto, *E. J. Inorg. Chem.*, 2003, 3244-4241.

Chapter 6

General Conclusion

General conclusion

In this thesis, the systematic introduction of hetero metal ion into *syn*-[**PtM**] for control of vapochromismic behaviour were described. The molecular motif *syn*-[**PtM**] were effective to introduction of heteromatl ion due to the different coordination sphere of metal(II) ion and platinum(II) ions.

In chapter I, general introduction and remarkable noticed in this thesis such as vapochromism, metal-metal interaction, hetero dinuclear complxes were briefly summarized.

In chapter II, the introduction into *syn*-[**PtM**] of Pd^{2+} and Au^{3+} ions with d^8 electron configuration and properties of their hetero metal dinuclear complexes *syn*-[$MPt(\mu\text{-pyt})_2(bpy)_2](PF_6)_n$ (*syn*-[**PtM**]) were described. Utilizing the different affinity (-N and -S atoms) of pyt ligand, Pd^{2+} and Au^{3+} ions were systematically introduced into *syn*-[**PtM**] motif. *Syn*-[**PtPd**] was isostructural with *syn*-[**PtPt**], forming the dimer-of-dimer structure so that two *syn*-[**PtPd**] were arranged close to Pt ion, while *syn*-[**PtAu**] was not, indicating that the charge of heteromatl ion affects the dimer-of-dimer structure. The structural transformations and vapour responsibilities of *syn*-[**PtPt**] were elucidated and the origin of vapochromicm of *syn*-[**PtPt**] was the change of intermolecular Pt···Pt interaction based on formation / disruption induced by the absorption / desorption of solvent molecules. The *syn*-[**PtPd**] exhibited the vapo- and mechanochromic behaviour as well as that of *syn*-[**PtPt**], and these chromic behaviors were observed in higher energy region than that of *syn*-[**PtPt**]. These result suggest that the choromic behaviour affected introduced hetero metal ion.

In chapter III, for introduction of guest binding site into *syn*-[**PtM**], copper(II) ion was introduced into *syn*-[**PtM**] motif. The introduction of copper(II) ion into *syn*-[**PtM**] motif and recrystallizations of various solvent afford the *syn*-[**PtCu-G**] which have one of the solvated molecules as an additional ligand on the axial site of copper(II) ion. Each complex form the dimer of dimer structure, but the crystal packings of dimer-of-dimer structures of these complexes were different to afford the. In all complexes, the absorption / desorption behaviour were found to be reversible, but the structure of desorbed form of *syn*-[**PtCu-G**] are completely different each other despite the same composition. In these absorption / desorption behaviours, the chromic shift of *syn*-[**PtCu-G**] were different, suggesting that the use of copper(II) ion as guset binding site make different chromic behaviour.

In chapter IV, the effects of counter anions on dimer-of-dimer structures in *syn*-[**PtCu**] were described. Three counter anions give three complexes *syn*-[**PtCu-X**] which have one of the counter anions as axial ligands of copper(II) ions in crystal. In spite of the counter anions, two *syn*-[**PtCu-X**] motifs are arranged so that close to each other to form dimer-of-dimer structures. The intermolecular Pt···Pt in dimer-of-dimer structure show the elongation in the order of donor numbers of axial ligands, suggesting that the intermoledular Pt···Pt interaction affects the donating abilities of axial ligands even separated by copper(II) ions.

In chapter V, the introduction of 3d metal ions into *syn*-[**PtM**] motifs are described. *Syn*-[**PtCo**] and

syn-[**PtNi**] were successfully synthesized utilizing stepwise introduction of hetero metal ions. The recrystallization from CH_3CN solutions, two forms of *syn*-[**PtM-CH_3CN**] were obtained and each form of *syn*-[**PtM**] is isostructural to each other. In α-form the inter molecular Pt···Pt distance are shorter than that of β-form due to the tigtht packing in α–form base on the π-π stacking of bpy ligand, which was not formed in β-form.

Finally, I have shown in this thesis that molecular motif of *syn*-[**PtM**] is good candidate of forming the dimer-of-dimer structure to exhibit multi stimuli responsive chromic behaviours. The engneering of vapochromism are still difficult, however, the *syn*-[**PtM**] complexes with dimer-of-dimer structure provide some knowledge about design of vapochromic behaviours.

Acknowledgement

This study on this thesis has been carried out under the direction of Professor Masako Kato during April 2007-September 2013 at the Department of Chemistry Graduate School of Scienece, Hokkaido University.

I would like to express the deepest appreciation to Professor Masako Kato for her earnest guidance and proper suggestions. Without her guidance and persistent help, this thesis would not have been possible. I wish to express my gratitude to Professor Ho-Chol Chang (present address, Chuo University), and Dr. Atsushi Kobayashi for invaluable suggestions and discussions. I am deeply thankful to Professor Kiyoshi Tsuge (present address, Toyama University) for helpful suggestions. I would like to offer my special thanks to Professor Tatsuhisa Kato for EPR measurements. I am deeply grateful to Professor Takanori Suzuki and Professor Sadamu Takeda for reviewing this thesis.

I am thankful to Ms. Mayu Shimizu and Mariko Sugwara for her succretarial works. I would like to thank Dr. Takeshi Matusmoto, Dr. Mee Chang for helpful advice. I am indebted to Dr. Rie Aoki, Mr. Hiroki Ohara for fruitful discussions and kind comments. Special thanks also to all members of the group of Professor Kato for their friendship during the time in the laboratory.

I am much imbedted for the financial support of Global COE program for doctoral students.

Finally, I would like to express special thanks to my parents, sister, and friends for their supports and encouragement.

Tadashi Ohba

Department of Chemistry
Graduate School of Science, Hokkaido University